DYNAMICS OF A SEMI-ACTIVE IMPACT DAMPER: REGULAR AND CHAOTIC MOTIONS

Thesis by

Michael P. Karyeaclis

In Partial Fullfillment
of the Requirements for the Degree of
Doctor of Philosophy

California Institute of Technology
Pasadena, California

1988
(Submitted July 29, 1987)

to my mother

and in memory of my father

Acknowledgements

I wish to take this opportunity to thank my advisor, Professor T. K. Caughey, for his inspiring guidance and support, as well as the freedom he allowed me in research. His valuable insights, and discussions on a broad range of subjects, from the Hula-Hoop and the rattleback to homoclinic oscillations, have greatly enriched my studies, and are deeply appreciated.

I also wish to thank Professor S. F. Masri of USC for suggesting the problem of the impact damper.

The financial support of the California Institute of Technology is greatfully acknowledged.

I would especially like to thank my friend Nick Vasilakos for his invaluable support and encouragement throughout my studies, and my sister Eleni and Kathleen for being there.

Finally, I would like to express my deepest gratitude to my mother for her love, understanding and unconditional support throughout my life.

Abstract

A study is made of the general behavior of a semi-active impact damper. The system consists of an undamped forced torsional oscillator, and a flywheel which can be locked to the oscillator through a clutch. Clutch engagement takes place instantaneously when the two rotors move in opposite directions. The resulting impact is effective in reducing the vibration amplitude level of the oscillator when it is subjected to bounded excitation.

All solutions of the system are shown to be bounded when the input is bounded. Emphasis is placed on 2 impacts/cycle periodic solutions. Exact symmetric and nonsymmetric solutions are derived analytically and the region of asymptotic stability is determined. The stability analysis leads to the definition of a transition matrix which determines the state of the system immediately after impact from its state after the previous impact. It also leads to the definition of a nonlinear map associated with the impact damper so that periodic solutions of the system correspond to fixed points of the map. The region of stability is defined as the region in parameter space where the eigenvalues of the transition matrix have modulus less than unity.

In the region of instability solutions are quasiperiodic or chaotic. As the parameter of the problem varies, the fixed points of the associated map undergo Hopf bifurcation which results in an invariant circle. Breakdown of the invariant circle leads to chaotic motions by the impact damper. Time histories, phase plane portraits, power spectra and Poincaré maps are used as descriptors to observe the evolution of chaotic motions. Computation of the largest Lyapunov exponent verifies the fact that when the structure of the invariant circle in resonance breaks down motions of the system are indeed chaotic.

It is found that under practically realizable conditions the mechanism is an effective damper. Applications include rotating shafts, and numerical simulations of a two-degree- of-freedom torsion bar were also carried out to observe the effects and effectiveness of impact in a multidegree of freedom primary system.

Contents

List of Figures

1

Introduction

The idea of dissipating energy in a vibrating mechanical system by allowing internal parts to collide with each other is not new, and its developement spans the last four decades [9][1].

Early investigations centered on determining the motion of a particle constrained to move in a container and which collided with the walls of the container. The fundamental assumption was that the motion involved two impacts per cycle and methods for determining such motion were developed. Estimates of the dissipated energy were also made for these undamped single degree of freedom oscillators. Moreover, theoretical investigations were complemented by experiments involving a variety of applications [9]. These investigations confirmed the fact that the predominant motion is that which involves two impacts per cycle.

Due to the impacts involved, the equation of motion is only piecewise linear, the resulting solution is piecewise continuous and, as a result, the stability of the periodic solutions was not investigated until 1966, when Masri and Caughey [7,8] developed a suitable method for analyzing a 4th order model. Their method is based on the idea of determining how initial perturbations evolve between impacts and is applicable not only to impact dampers, but also to any system governed by piecewise linear/nonlinear differential equations as long as the solution between

[1] Numbers in brackets designate references at the end of the thesis.

impacts is known.

Recently, Shaw [11,12] and Shaw and Holmes [13] employed bifurcation theory to study a second order forced system with rigid amplitude constraints, and they observed that periodic motion is not the only possible, but that in the appropriate range of system parameters the motion may be chaotic.

The objective of this investigation is to introduce a new element in the study of impact dampers, namely, the idea of actively controlling the time of impact and, in addition, to complement earlier studies by providing information on the global behavior of impacting systems. The system studied consists of two rotating masses which are locked together by energizing a fast-acting clutch at selected times, but the idea is not necessarily restricted to rotating masses. In the next chapter we develop a model for the system and show that all solutions are ultimately bounded to a region around the origin in phase plane.

In chapter 3 we determine all 2 impacts/cycle periodic solutions and in chapter 4 the stability of these solutions is analyzed.

In chapter 5 we focus on the behavior of the system when parameters are outside the stability region. These solutions are chaotic and are studied by a variety of methods. From the engineering point of view, the study of chaotic motion may appear superfluous. However, such motions have been observed in such a wide variety of phenomena ranging from population dynamics to meteorology [3,7,10,12,13], that their study has become a necessity. Moreover, the idea that perhaps chaos or noise is an intrinsic system property rather than externally generated [7], is sufficient in itself to justify the study of chaotic motions within the context of any engineering discipline.

Finally, in chapter 6 we state conclusions drawn from this investigation and provide recommendations for future work on this subject.

2

Global Behavior

In this chapter we present general results regarding the global behavior of the semi-active impact damper. First, we give a brief description of the system under consideration. Then we show that for a fairly wide class of inputs, the response of the system is bounded.

2.1 System Description

The system under consideration is shown in fig. 2.1. It consists of two parts. The primary system is an undamped forced torsional oscillator while the secondary system consists of a flywheel which is free to rotate with respect to the main rotor. The two can be linked together by energizing a fast-acting clutch. It is assumed that there is no slip between the rotors when the clutch is engaged and, as a result, they both have the same angular velocity during and immediately after engagement.

Let I and J be the moments of inertia of the primary and secondary rotors respectively, and k the stiffness of the torsional spring. Let $F(x, \dot{x}, v)$ represent the torque acting between the rotors when the clutch is engaged and $x(t)$, $y(t)$ be the angular displacements of the two rotors. Then, the equations of motion for the

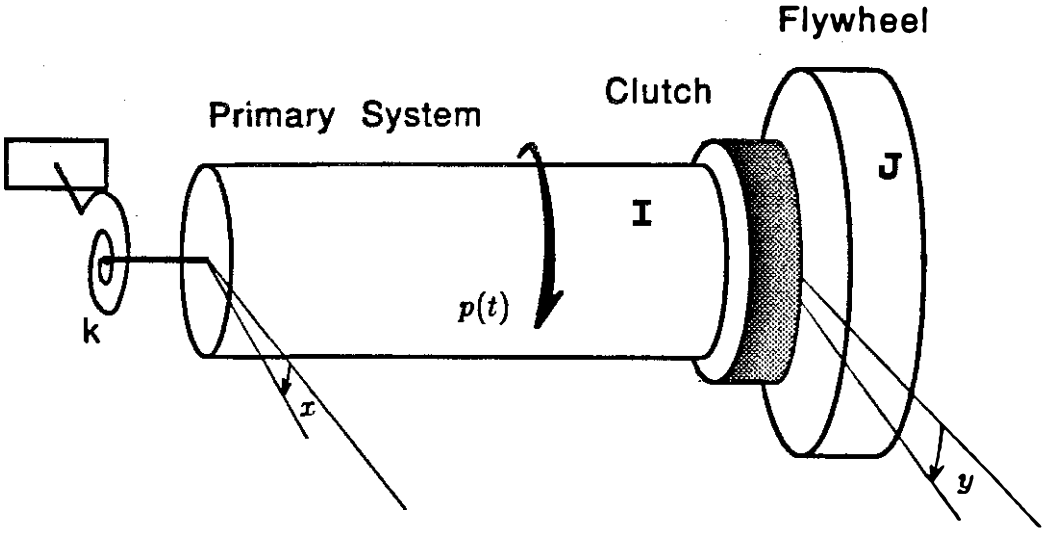

Figure 2.1: Schematic representation of the impact damper.

system are:

$$\left.\begin{aligned} I\ddot{x} + kx + F(x,\dot{x},v) &= p(t) \\ J\dot{v} - F(x,\dot{x},v) &= 0 \\ \dot{y} &= v \\ x(0),\ \dot{x}(0),\ v(0) &\text{ given} \end{aligned}\right\} \tag{2.1}$$

Assumptions:

1. $p(t)$ is bounded with zero mean.

2. The period of time during which the clutch is engaged is very short. During that time, $x(t)$ and $y(t)$ do not change significantly.

3. Clutch actuation is instantaneous.

Under the above assumptions, the functional form of $F(x,\dot{x},v)$ may be determined. The active aspect of the damper refers to the triggering mechanism for

the clutch. In a fully active arrangement, a feedback control law would be determined and the clutch would engage accordingly. In this formulation, actuation is determined a priori and remains fixed during operation.

The purpose of the mechanism desribed is to provide damping for the torsional oscillator. To determine what instant in time clutch actuation would be most beneficial, suppose that the primary and secondary rotors are locked and then released. The secondary rotor will continue to rotate with constant angular velocity in a given direction while the primary rotor will reach maximum displacement and then begin to rotate in the opposite direction. It has maximum velocity as it crosses the equilibrium position $x = 0$. Impact time t_i is therefore chosen such that the velocity difference between the two rotors is maximum, i.e., when $x(t_i) = 0$. It follows then that

$$F(x, \dot{x}, v) = \delta(x)\dot{x}g(\dot{x}, v) \tag{2.2}$$

Adding the two equations (2.1) we obtain

$$I\ddot{x} + J\dot{v} + kx = p(t) \tag{2.3}$$

Let t be the time of impact. Integrating (2.3) over the infinitesimal time interval during which the clutch is engaged we get

$$I[\dot{x}(t^+) - \dot{x}(t^-)] + J[v(t^+) - v(t^-)] = 0$$

since both $x(t)$ and $p(t)$ are continuous.

Rearranging

$$I\dot{x}(t^+) + Jv(t^+) = I\dot{x}(t^-) + Jv(t^-) \tag{2.4}$$

which is simply a statement of conservation of angular momentum.

Moreover, at $t = t^+$ the rotors are locked and therefore have the same angular velocity. Hence $v(t^+) = \dot{x}(t^+)$. Using (2.4) we obtain an expression for the velocity after impact in terms of the velocities just before as follows:

$$\dot{x}(t^+) = v(t^+) = \frac{I}{I+J}\dot{x}(t^-) + \frac{J}{I+J}v(t^-) \tag{2.5}$$

or

$$\dot{x}(t^+) = v(t^+) = a\dot{x}(t^-) + bv(t^-), \quad t \text{ such that } x(t) = 0 \tag{2.6}$$

where

$$a = \frac{I}{I+J}, \quad b = \frac{J}{I+J}, \quad a+b=1 \tag{2.7}$$

Expression (2.6) represents the impact condition and will be used extensively in this analysis.

2.2 Ultimate Boundedness

The main result of this section is that if $p(t)$ is bounded, then so are all solutions of the impact damper. Before proving this, we need some facts concerning the following autonomous auxiliary system:

$$\left.\begin{aligned} I\ddot{x} + kx + F(x,\dot{x},v) &= T\text{sgn}(\dot{x}) \\ J\dot{v} - F(x,\dot{x},v) &= 0 \\ x(0) = -C_x; \quad \dot{x}(0) = 0; \quad v(0^+) = -C_v; & \qquad C_x > 0, \quad C_v > 0 \end{aligned}\right\} \tag{2.8}$$

where T is a positive constant and $F(x,\dot{x},v)$ is as before.

Lemma 1 *The auxiliary system (2.8) possesses a unique limit cycle $\mathcal{L}(T,\beta)$, where $\beta = I/(I+2J)$.*

PROOF: We prove the existence of the limit cycle by finding initial conditions C_x and C_v such that the orbit of the system in the $x - \dot{x}$ phase plane is closed. Uniqueness then follows from the fact that the solution of the initial value problem is unique.

A typical trajectory is shown in fig. 2.2. Due to the symmetry of the system, it suffices to consider only semi-trajectories.

Let t_1 be such that $x(t_1) = 0$ and suppose that $x(t) \leq 0$, $\dot{x} \geq 0 \quad \forall t \in [0, t_1]$. Then, equations (2.8) become:

$$I\ddot{x} + kx = T \tag{2.9}$$

$$J\dot{v} = 0 \tag{2.10}$$

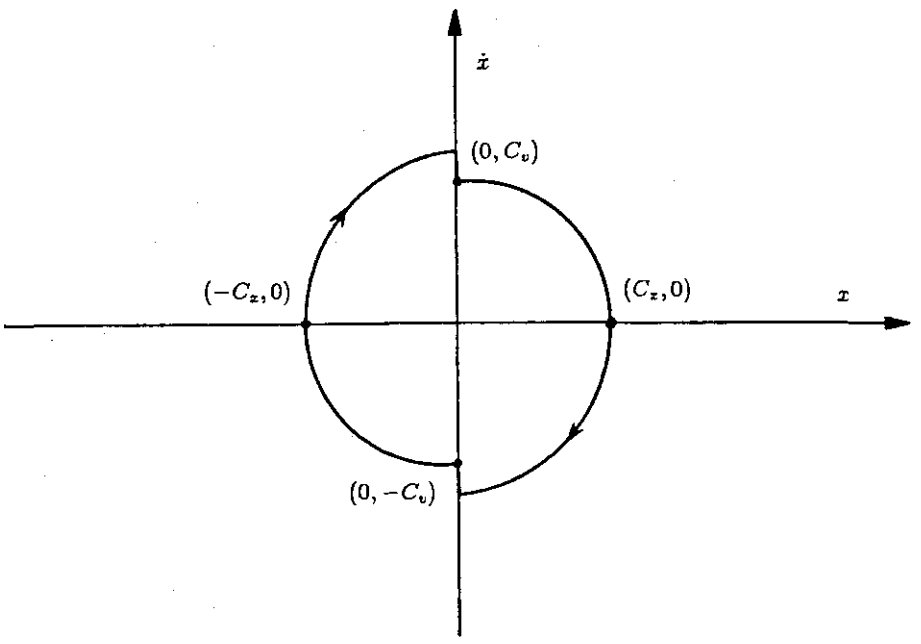

Figure 2.2: The limit cycle of auxiliary system (2.8).

Multiplying (2.9) by $\dot{x}$ and integrating

$$\int I\ddot{x}\dot{x}dt + \int k\dot{x}xdt = \int T\dot{x}dt$$

$$\Longrightarrow H(t) = I\dot{x}^2(t) + kx^2(t) - 2Tx(t) = \text{constant} \tag{2.11}$$

The constant of integration is evaluated using the initial conditions. Thus

$$I\dot{x}^2(t) + kx^2(t) - 2Tx(t) = kC_x^2 + 2TC_x; \quad t \in [0, t_1) \tag{2.12}$$

Since at $t = t_1 \quad x(t_1) = 0$, equation (2.12) can be solved for the velocity of the primary mass just prior to impact. Thus

$$\dot{x}(t_1^-) = \sqrt{\frac{kC_x^2 + 2TC_x}{I}} \tag{2.13}$$

$$v(t_1^-) = -C_v \tag{2.14}$$

If the solution is to satisfy the symmetry conditions, then $\dot{x}(t_1^+) = C_v = -v(t_1^-)$. Substituting in the expression for the impact condition we get

$$\dot{x}(t_1^+) = \frac{I}{I+J}\dot{x}(t_1^-) - \frac{J}{I+J}\dot{x}(t_1^+) \Longrightarrow \dot{x}(t_1^+) = \frac{I}{I+2J}\dot{x}(t_1^-)$$

Using (2.13) it follows that

$$\dot{x}(t_1^+) = C_v = \beta\sqrt{\frac{kC_x^2 + 2TC_x}{I}}, \quad \beta = \frac{I}{I+2J} \tag{2.15}$$

To determine C_x, we continue the solution in the interval $t_1 < t \leq t_2$ where t_2 is such that $\dot{x}(t_2) = 0$. From symmetry $x(t_2) = C_x$. Evaluating the integral of the motion $H(t)$ at t_1^+ and at t_2 we find

$$\begin{aligned} H(t_1^+) = &\quad I\dot{x}^2(t_1^+) + kx^2(t_1^+) - 2Tx(t_1^+) &= I\beta^2(kC_x^2 + 2TC_x) \\ H(t_2) = &\quad I\dot{x}^2(t_2) + kx^2(t_2) - 2Tx(t_2) &= kC_x^2 - 2TC_x \end{aligned}$$

Setting the above expressions equal, we obtain a relationship which can be solved for C_x. The solution is

$$C_x = 0; \quad C_x = \frac{2T}{k}\frac{1+\beta^2}{1-\beta^2}$$

Thus, the initial conditions are

$$C_x = \frac{2T}{k}\frac{1+\beta^2}{1-\beta^2} \tag{2.16}$$

$$C_v = \beta\sqrt{\frac{kC_x^2 + 2TC_x}{I}} \tag{2.17}$$

and they specify the limit cycle which is unique and consists of elliptical arcs passing through the four points $(-C_x, 0)$, $(0, C_v)$, $(C_x, 0)$, and $(0, -C_v)$ as shown in fig. 2.2. We denote this limit cycle by $\mathcal{L}(T, \beta)$. ∎

It is evident from expressions (2.16) and (2.17) that both C_x and C_v are monotone increasing functions of T and the parameter β. As a result, for $0 < \beta_1 < \beta_2$ the curve $\mathcal{L}(T, \beta_1)$ lies entirely inside $\mathcal{L}(T, \beta_2)$. Let $S(T, \beta)$ be the set enclosed by the limit cycle $\mathcal{L}(T, \beta)$.

Once the existence of the limit cycle is established, the question of its stability must be addressed. Thus we have the following:

Lemma 2 *The limit cycle $\mathcal{L}(T, \beta)$ of system (2.8) is globally asymptotically stable.*

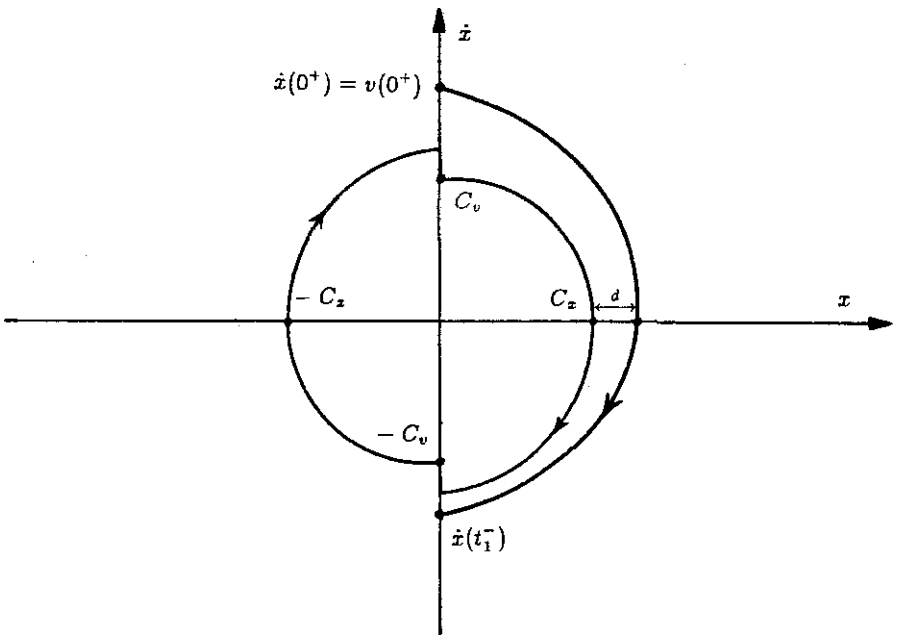

Figure 2.3:

PROOF: Clearly we need not consider completely arbitrary initial conditions. For if we do so, after the first impact we will have $x(t_0) = 0$, $\dot{x}(t_0^+) = v(t_0^+)$ where t_0 is the first impact time.

Thus, without loss of generality, we assume that at $t = 0$ $x(0) = 0$ and $\dot{x}(0^+) = v(0^+)$. Now let $\{t_n\}_{n=1}^{\infty}$ be the sequence of instants in time that impacts occur. Then $t_n < t_{n+1}$ and $x(t_n) = 0$. Let $\dot{x}_n = \dot{x}(t_n^+)$. We will show that $\lim_{n\to\infty} |\dot{x}_n| = C_v$.

Consider a semi-trajectory starting at $(0, \dot{x}(0^+))$ in the $x - \dot{x}$ projection of the phase plane as shown in fig. 2.3. Suppose that $v(0^+) = \dot{x}(0^+) \neq C_v$. Let t' be such that $\dot{x}(t') = 0$ and suppose that the next impact occurs at $t = t_1 \Rightarrow x(t_1) = 0$. Then

$$H(t) = \begin{cases} I\dot{x}^2(t) + kx^2(t) - 2Tx(t) = I\dot{x}^2(0^+) = kx^2(t') - 2Tx(t') & \text{for } \dot{x} > 0 \\ I\dot{x}^2(t) + kx^2(t) + 2Tx(t) = I\dot{x}^2(t_1^-) = kx^2(t') + 2Tx(t') & \text{for } \dot{x} < 0 \end{cases}$$

Solving for the velocities we find

$$\dot{x}(0^+) = \sqrt{\frac{kx^2(t') - 2Tx(t')}{I}} \tag{2.18}$$

$$\dot{x}(t_1^-) = -\sqrt{\frac{kx^2(t') + 2Tx(t')}{I}} \tag{2.19}$$

The impact condition (2.5) at $t = t_1$ gives:

$$\begin{aligned} \dot{x}(t_1^+) &= \frac{I}{I+J}\dot{x}(t_1^-) + \frac{J}{I+J}\dot{x}(0^+) \\ \Rightarrow \frac{\left|\dot{x}(t_1^+)\right|}{\dot{x}(0^+)} &= \frac{I}{I+J}\frac{\left|\dot{x}(t_1^-)\right|}{\dot{x}(0^+)} - \frac{J}{I+J} \end{aligned}$$

Let $R = \frac{\left|\dot{x}(t_1^+)\right|}{\dot{x}(0^+)}$ and substitute for $\dot{x}(t_1^-)$ and $\dot{x}(0^+)$ above to get:

$$\begin{aligned} R &= \frac{I}{I+J}\sqrt{\frac{kx(t') + 2T}{kx(t') - 2T}} - \frac{J}{I+J} \\ &= 1 - \frac{I+J}{I+J} + \frac{I}{I+J}\sqrt{\frac{kx(t') + 2T}{kx(t') - 2T}} - \frac{J}{I+J} \end{aligned} \tag{2.20}$$

Let $x(t') = C_x + d$ where C_x is given by (2.16). Substituting above for $x(t')$ and C_x, we obtain after rearrangement the following expression for R:

$$R = \frac{\left|\dot{x}(t_1^+)\right|}{\dot{x}(0^+)} = 1 - \left(\frac{I+2J}{I+J}\right)\left[1 - \sqrt{\frac{1+\beta^2 qd}{1+qd}}\right] \tag{2.21}$$

where

$$q = \frac{k}{T}\frac{J(I+J)}{I^2} > 0, \quad \beta = \frac{I}{I+2J} \leq 1 \tag{2.22}$$

Clearly, if $d > 0$, then $R < 1$ and the trajectory is closer to the limit cycle than it was at 0^+. If $d < 0$, i.e., if the trajectory lies in $S(T, \beta)$, then $R > 1$ and $\dot{x}(t_1^+)$ is closer to the limit cycle than $\dot{x}(0^+)$. The same argument holds for the other half of the trajectory. Thus, as $t_n \longrightarrow \infty$, $d \longrightarrow 0$ and $R \longrightarrow 1$ and therefore the trajectory approaches the limit cycle asymptotically. If $d = 0$, then $R = 1$, i.e., the orbit is on the limit cycle. Moreover, this is true for all initial conditions and therefore the region of attraction is the entire phase plane. ∎

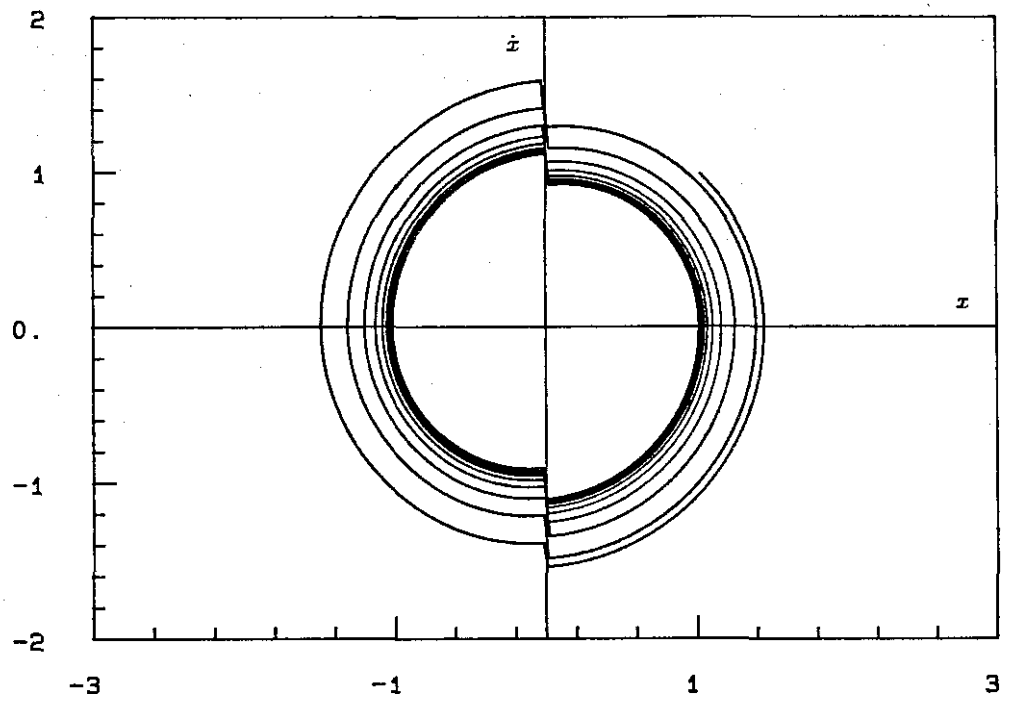

Figure 2.4: Convergence to the limit cycle from the outside.

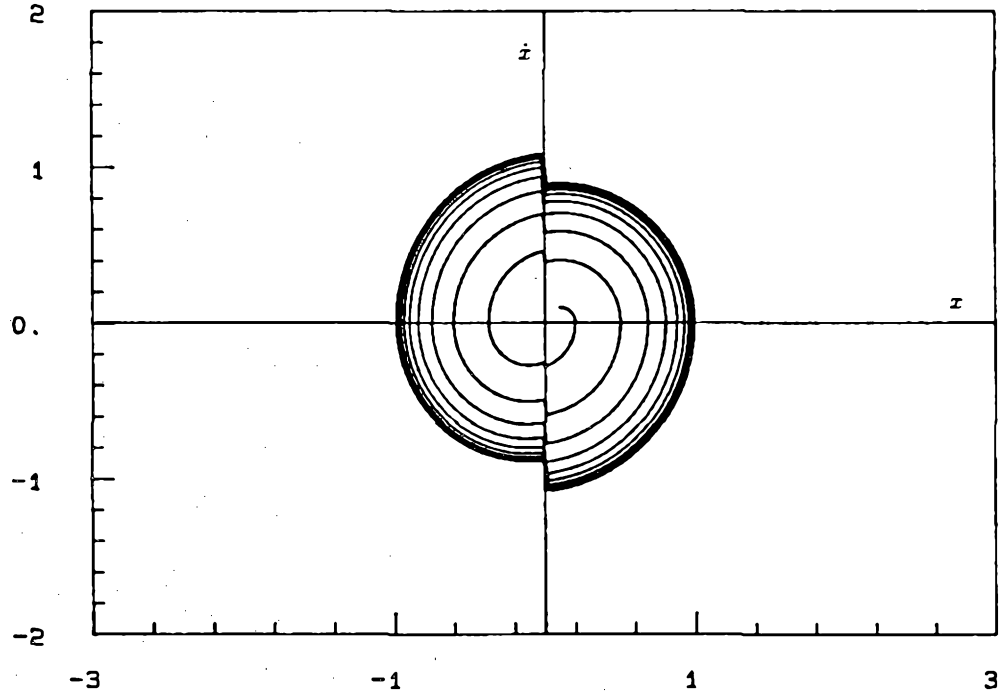

Figure 2.5: Convergence to the limit cycle from the inside.

The stability characteristics of the limit cycle are shown in fig. 2.4 and 2.5 for the case $T = 0.1,\ k = 1,\ I = 1,\ a = 0.9$.

The next lemma makes the connection between the impact damper and the auxiliary system.

Lemma 3 *All solutions of the impact damper (2.1) which start outside the limit cycle $\mathcal{L}(T,\beta)$ are ultimately bounded in the set $S(T,\beta)$ where $T = \sup_t |p(t)| + \epsilon$, $\epsilon > 0$.*

PROOF: Since the excitation torque $p(t)$ in (2.1) is bounded, let $T = \sup_t |p(t)| + \epsilon$, $\epsilon > 0$. Suppose that $x(0^+) = 0$ with $\dot{x}(0^+) = v(0^+) > 0$ and outside the limit cycle. Define

$$V(t) = I\dot{x}^2(t) + kx^2(t) - 2Tx(t) > 0 \tag{2.23}$$

Differentiating

$$\dot{V}(t) = 2I\dot{x}\ddot{x} + 2kx\dot{x} - 2T\dot{x} \tag{2.24}$$

Using (2.1), the derivative of $V(t)$ along the trajectories of the impact damper is

$$\begin{aligned} \dot{V}(t) &= 2p(t)\dot{x} - 2kx\dot{x} + 2kx\dot{x} - 2T\dot{x} \\ &= -2\left(T - p(t)\right)\dot{x} \end{aligned}$$

Therefore

$$\dot{V}(t) \leq -2\epsilon\dot{x} \leq 0 \tag{2.25}$$

Consider the trajectory of the auxiliary system starting with the same initial conditions. Then, along that trajectory, the derivative of the same Lyapunov function is

$$\dot{V}(t) = -(2T - 2T)\dot{x} = 0 \tag{2.26}$$

Hence, the trajectory of (2.1) lies closer to the origin than the trajectory of the autonomous system.

Similar arguments apply to each of the other four quadrants. Therefore, the trajectories of the damper must approach the interior of the limit cycle, since by Lemma

2, the autonomous system approaches $\mathcal{L}(T,\beta)$. Moreover, once inside $S(T,\beta)$ they can never escape. ∎

The ultimate boundedness of solutions of the impact damper is an immediate consequence of the three lemmas. Thus we have the

Theorem 2.1 *All solutions of (2.1) are ultimately bounded in the set $S(T,\beta)$, the interior of the limit cycle $\mathcal{L}(T,\beta)$.*

PROOF: Lemma 1 establishes the existence of the limit cycle, lemma 2 proves that the limit cycle is stable and lemma 3 proves that all solutions of (2.1) must enter the region bounded by the set $\mathcal{L}(T,\beta)$. Once in $S(T,\beta)$, the solutions can never escape. ∎

The proof of the theorem also provides weak bounds for the maximum velocity and displacement of the impact damper through the expressions for C_x and C_v. Note that even though the solutions are shown to be bounded, the theorem does *not* guarantee that the response is *always* smaller than that which would be obtained had the damper not been used.

The implications of the theorem are depicted in fig. 2.6 and 2.7 where it is seen that solutions starting far from the origin end up in $S(T,\beta)$ and remain in that region. Figures 2.8 and 2.9 show similar results for $a = I/(I+J) = 0.99$ and $\omega = 7$, $\omega_0 = \sqrt{k/T} = 1$. The second figure shows traces of the trajectory for $170 \leq t \leq 190$. In all cases $p(t) = \cos(\omega t)$.

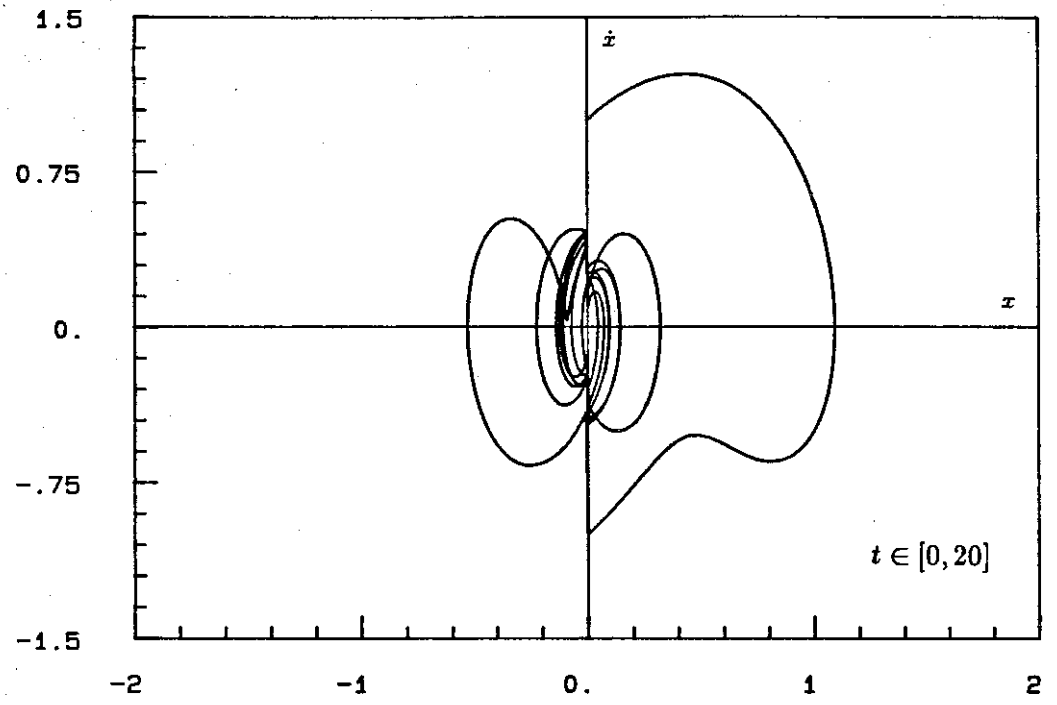

Figure 2.6: Ultimate boundedness of solutions. $\omega = 3,\ \omega_0 = 1,\ a = 0.7$

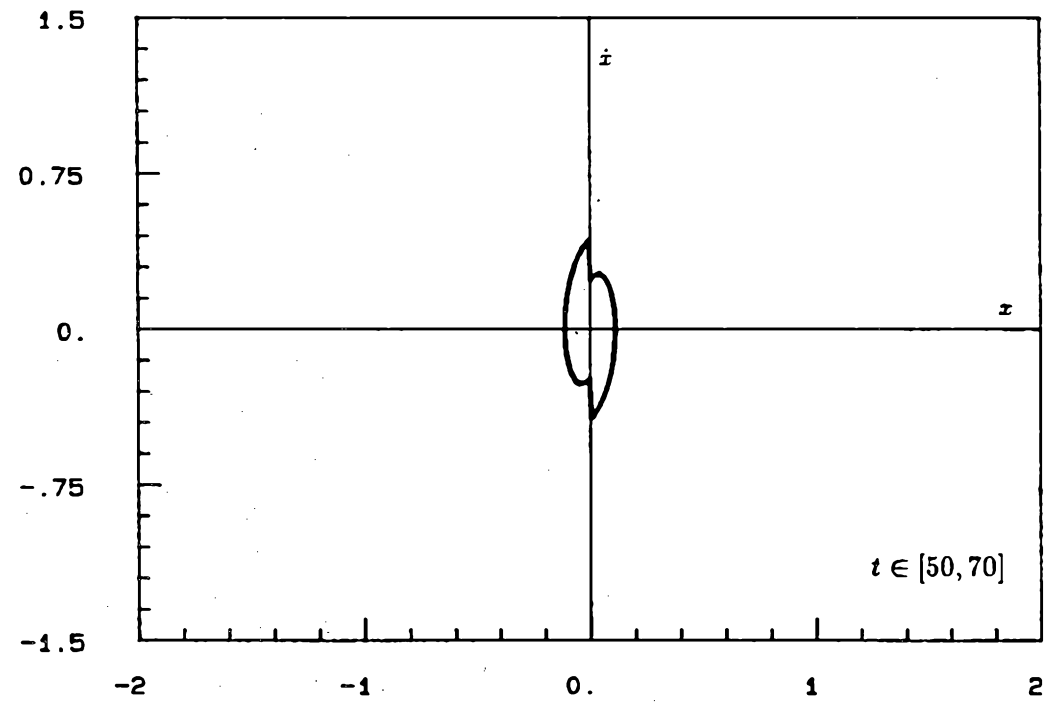

Figure 2.7: Ultimate boundedness. $\omega = 3,\ \omega_0 = 1,\ a = 0.7,\ 50 \leq t \leq 70.$

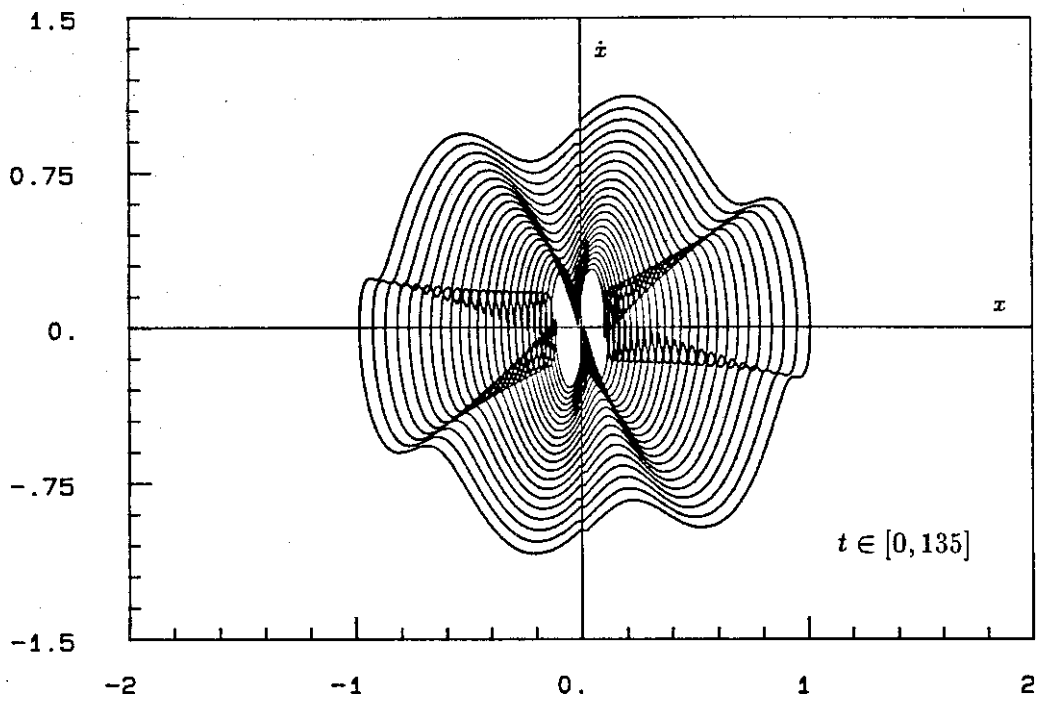

Figure 2.8: Ultimate boundedness. $\omega = 7,\ \omega_0 = 1,\ a = 0.99.$

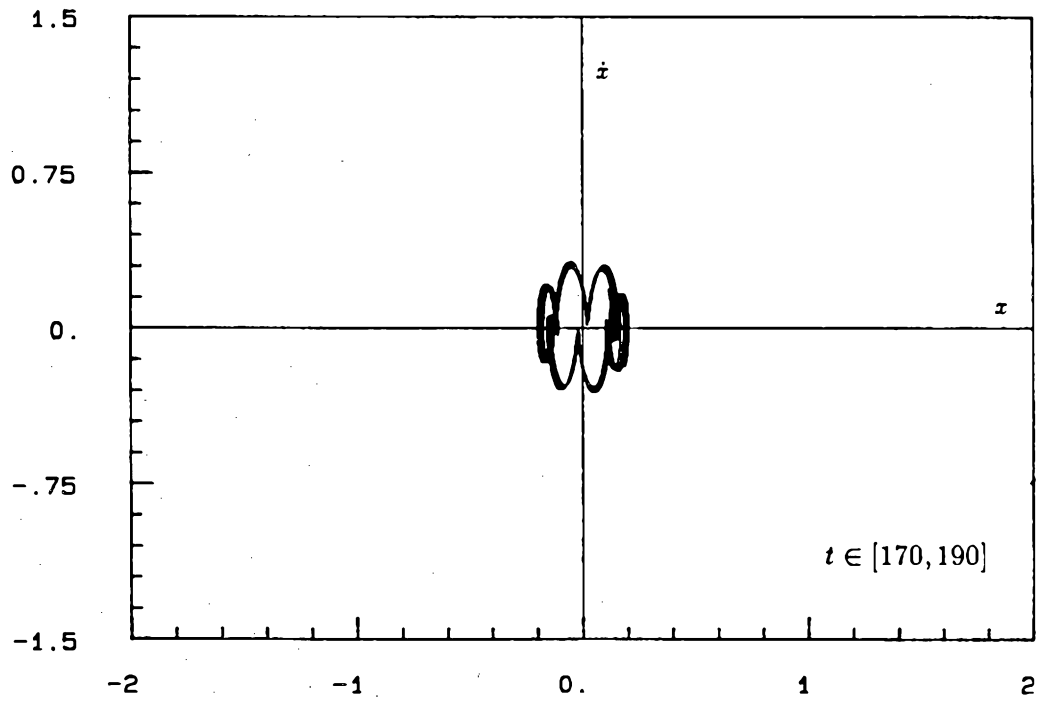

Figure 2.9: Ultimate boundedness. $\omega = 7,\ \omega_0 = 1,\ a = 0.99,\ 170 \leq t \leq 190.$

3

Periodic Solutions

Having established the fact that all solutions of the impact damper are bounded, we proceed to find periodic solutions. Experiments and analytical work by Masri [8,9] and Shaw [11,12,13] on similar systems suggest the existence of 2-impact per cycle periodic solutions when the excitation is periodic. Simulation of the behavior of system (2.1) also support this behavior as shown in fig. 2.7. We distinguish between two types of periodic solutions, namely symmetric and nonsymmetric.

For convenience we put equations (2.1) in standard form with $\omega_0 = \sqrt{k/I}$ and rewrite the pertinent equations here in a form more suitable to the present analysis. Let the excitation torque

$$p(t) = P\cos(\omega t + \theta)$$

Then we have:

$$\left.\begin{array}{lll} \text{Equation of motion:} & \ddot{x} + \omega_0^2 x = P\cos(\omega t + \theta);\ \dot{v} = 0; & x(t) \neq 0 \\ \text{Impact condition:} & \dot{x}(t_1^+) = v(t_1^+) = a\dot{x}(t_1^-) + bv(t_1^-); & x(t_1) = 0 \\ & a + b = 1 & \end{array}\right\} \quad (3.1)$$

3.1 Symmetric Solutions

A typical symmetric solution is shown in fig. 3.1 and is referred to as such because the $x - \dot{x}$ projection of the trajectory is symmetric with respect to the origin. Solutions which do not satisfy this property are the so called nonsymmetric.

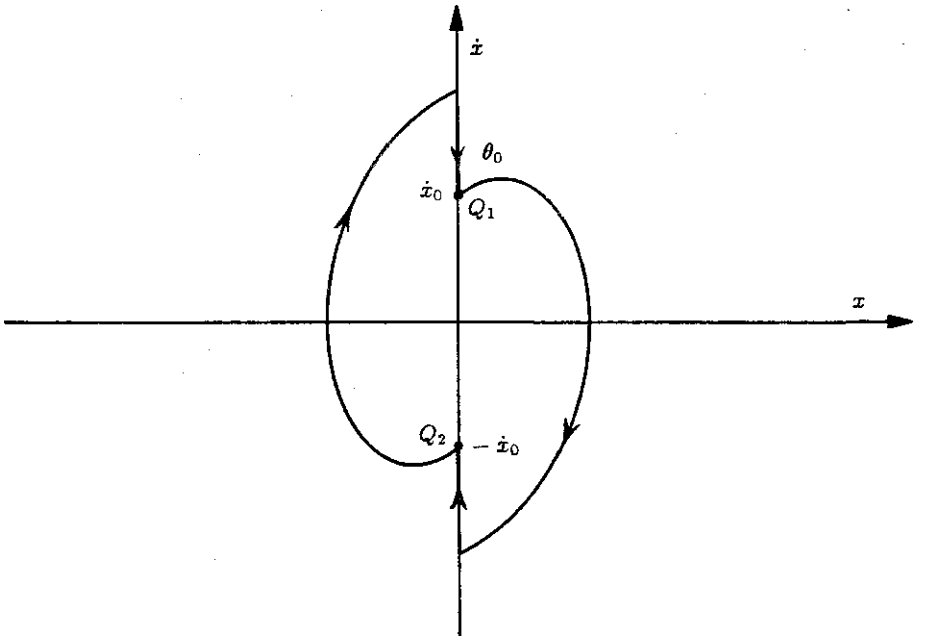

Figure 3.1: Symmetric periodic solution.

The construction of solutions is based on the observation that equation (3.1) is linear in each of the half-planes $x > 0$ and $x < 0$. We start the solution at point Q_1 where $x(0) = 0$ and determine the phase angle θ and initial velocity $\dot{x}(0^+) = v(0^+)$ such that the orbit is closed. Because of symmetry, only one arc of the orbit need be considered.

Let $\dot{x}(0^+) = \dot{x}_0 = v(0^+)$ and $\theta = \theta_0$ at $t = 0$. Then, for $x > 0$

$$\ddot{x} + \omega_0^2 x = P\cos(\omega t + \theta_0) \tag{3.2}$$

and the solution for $\omega \neq \omega_0$ is

$$\begin{aligned} x(t) &= \frac{P}{\omega^2 - \omega_0^2}\cos\theta_0\cos\omega_0 t + \left[\frac{\dot{x}_0}{\omega_0} - \frac{P\left(\frac{\omega}{\omega_0}\right)}{\omega^2 - \omega_0^2}\sin\theta_0\right]\sin\omega_0 t - \\ &\quad - \frac{P}{\omega^2 - \omega_0^2}\cos(\omega t + \theta_0) \end{aligned} \tag{3.3}$$

$$\begin{aligned} \dot{x}(t) &= -\frac{P\omega_0}{\omega^2 - \omega_0^2}\cos\theta_0\sin\omega_0 t + \omega_0\left[\frac{\dot{x}_0}{\omega_0} - \frac{P\left(\frac{\omega}{\omega_0}\right)}{\omega^2 - \omega_0^2}\sin\theta_0\right]\cos\omega_0 t + \\ &\quad + \frac{P\omega}{\omega^2 - \omega_0^2}\sin(\omega t + \theta_0) \end{aligned} \tag{3.4}$$

Let t_1 be the time that the first impact occurs, at point Q_2 in fig. 3.1. For an harmonic periodic solution, the period of oscillation is $2\pi/\omega$. Due to symmetry, it follows that $t_1 = \pi/\omega$. Thus, at Q_2

$$x\left(\frac{\pi}{\omega}\right) = 0 \tag{3.5}$$

$$\dot{x}\left(\frac{\pi^+}{\omega}\right) = v\left(\frac{\pi^+}{\omega}\right) = -\dot{x}_0 \tag{3.6}$$

Using (3.6), the impact condition gives:

$$-\dot{x}_0 = a\dot{x}\left(\tfrac{\pi}{\omega}^-\right) + b\dot{x}_0 \implies$$

$$\implies -\tfrac{(1+b)}{a}\dot{x}_0 = \dot{x}\left(\tfrac{\pi}{\omega}^-\right) \tag{3.7}$$

The velocity $\dot{x}(\frac{\pi}{\omega}^-)$ is evaluated from (3.4). Thus, (3.5) and (3.7) after rearrangement are as follows:

$$-\frac{\dot{x}_0}{\omega_0}\sin(\tfrac{\omega_0}{\omega}\pi) = \frac{P}{\omega^2-\omega_0^2}\left[1+\cos(\tfrac{\omega_0}{\omega}\pi)\right]\cos\theta_0 - \frac{P\left(\frac{\omega}{\omega_0}\right)}{\omega^2-\omega_0^2}\sin(\tfrac{\omega_0}{\omega}\pi)\sin\theta_0 \tag{3.8}$$

$$\frac{\dot{x}_0}{\omega_0}\left[\frac{1+b}{a}+\cos(\tfrac{\omega_0}{\omega}\pi)\right] = \frac{P}{\omega^2-\omega_0^2}\sin(\tfrac{\omega_0}{\omega}\pi)\cos\theta_0 + \frac{P\left(\frac{\omega}{\omega_0}\right)}{\omega^2-\omega_0^2}\left[1+\cos(\tfrac{\omega_0}{\omega}\pi)\right]\sin\theta_0 \tag{3.9}$$

Equations (3.8) and (3.9) are linear in $\sin\theta_0$ and $\cos\theta_0$ and can be solved easily. Substitution in $\sin^2\theta_0 + \cos^2\theta_0 = 1$ then provides an expression which involves only the velocity $\dot{x}_0$ and which can be solved. Once $\dot{x}_0$ is known, expressions for $\cos\theta_0$ and $\sin\theta_0$ give the solution for the phase angle. The solution of these equations is given in appendix A. The case of resonance ($\omega = \omega_0$) must be treated separately because the solution for $x > 0$ in this case is given by:

$$x(t) = \left[\frac{\dot{x}_0}{\omega_0} - \frac{P}{2\omega_0^2}\sin\theta_0\right]\sin\omega_0 t + \frac{1}{2}P\frac{t}{\omega_0}\sin(\omega_0 t+\theta_0) \tag{3.10}$$

$$\dot{x}(t) = \omega_0\left[\frac{\dot{x}_0}{\omega_0} - \frac{P}{2\omega_0^2}\sin\theta_0\right]\cos\omega_0 t + \frac{1}{2}\frac{P}{\omega_0}\sin(\omega_0 t+\theta_0) + \frac{1}{2}Pt\cos(\omega_0 t+\theta_0) \tag{3.11}$$

The procedure however for solving (3.5) and (3.7) in this case is the same.

To ensure that the system (3.8)-(3.9) is nonsingular, special consideration must be given to the cases where the frequency ratio ω_0/ω is such that the coefficients $1+\cos(\frac{\omega_0}{\omega}\pi)$ and $\sin(\frac{\omega_0}{\omega}\pi)$ vanish. This gives rise to two special cases, in addition to resonance: (i) $\sin(\frac{\omega_0}{\omega}\pi)=0,\ \cos(\frac{\omega_0}{\omega}\pi)=1$ and (ii) $\sin(\frac{\omega_0}{\omega}\pi)=0,\ \cos(\frac{\omega_0}{\omega}\pi)=-1$. In the first case the ratio ω_0/ω is an even integer while in the second case ω_0/ω is odd. For these two cases the analysis simplifies considerably, but for the sake of completeness it is also included in appendix A. It turns out, as might be expected, that the stability characteristics of these special cases differ considerably from those of the generic case.

The solutions of equations (3.8)-(3.9) are summarized below for each case separately.

CASE I: (Generic) $\cos(\frac{\omega_0}{\omega}\pi)\neq -1,\ \sin(\frac{\omega_0}{\omega}\pi)\neq 0.$

$$\tan\theta_0=\frac{1+\cos(\frac{\omega_0}{\omega}\pi)}{b\left(\frac{\omega}{\omega_0}\right)\sin(\frac{\omega_0}{\omega}\pi)} \tag{3.12}$$

$$\dot{x}_0=\frac{Pa\omega}{|\omega^2-\omega_0^2|}\frac{1}{\sqrt{1+\left[\frac{\left(\frac{\omega}{\omega_0}\right)b\sin(\frac{\omega_0}{\omega}\pi)}{1+\cos(\frac{\omega_0}{\omega}\pi)}\right]^2}}=\frac{Pa\omega}{|\omega^2-\omega_0^2|}\sin\theta_0 \tag{3.13}$$

CASE II: $\sin(\frac{\omega_0}{\omega}\pi)=0,\ \cos(\frac{\omega_0}{\omega}\pi)=1 \iff \frac{\omega_0}{\omega}=2l,\ l=1,2,\ldots$

$$\theta_0 = -\frac{\pi}{2} \tag{3.14}$$

$$\dot{x}_0 = \frac{Pa\omega}{\omega_0^2-\omega^2} \tag{3.15}$$

In this case $x(t)$ simplifies considerably and we have:

$$x(t) = (1-a)\frac{P\left(\frac{\omega}{\omega_0}\right)}{\omega^2-\omega_0^2}\sin\omega_0 t + \frac{P}{\omega^2-\omega_0^2}\sin\omega t, \quad x \geq 0 \tag{3.16}$$

CASE III: $\sin(\frac{\omega_0}{\omega}\pi) = 0, \ \cos(\frac{\omega_0}{\omega}\pi) = -1 \iff \frac{\omega_0}{\omega} = 2l+1, \ l = 1,2,\ldots$

$$\theta_0 = -\frac{\pi}{2} \tag{3.17}$$

$$\dot{x}_0 = 0 \tag{3.18}$$

and

$$x(t) = \frac{P\left(\frac{\omega}{\omega_0}\right)}{\omega^2-\omega_0^2}\sin\omega_0 t + \frac{P}{\omega^2-\omega_0^2}\sin\omega t, \quad x \geq 0 \tag{3.19}$$

CASE IV:(Resonance) $\omega = \omega_0$.

$$\theta_0 = 0 \tag{3.20}$$

$$\dot{x}_0 = \left(\frac{a}{b}\right)\frac{P\pi}{4\omega_0} \tag{3.21}$$

The solution is

$$x(t) = \frac{P}{2\omega_0}\left[\left(\frac{a}{b}\right)\frac{\pi}{2\omega_0} + t\right]\sin\omega_0 t, \quad x \geq 0 \tag{3.22}$$

Typical solutions are shown in figures 3.2, 3.3, 3.4 and 3.5. Observe that case III is singular in the sense that it involves no impacts at all. The secondary rotor remains at rest while the velocity of the primary system is zero at the equilibrium position. The impact damper in this case degenerates to a simple harmonic oscillator

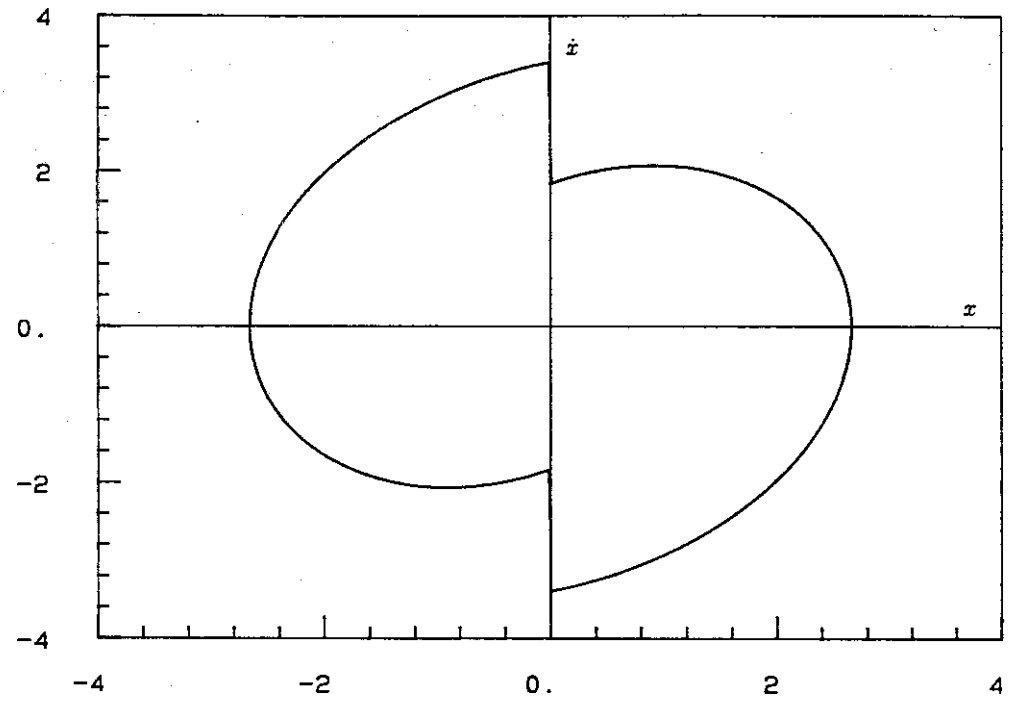

Figure 3.2: Periodic solution, resonance, $a = 0.7,\ P = 1,\ \dot{x}_0 = 1.8326,\ \theta_0 = 0.$

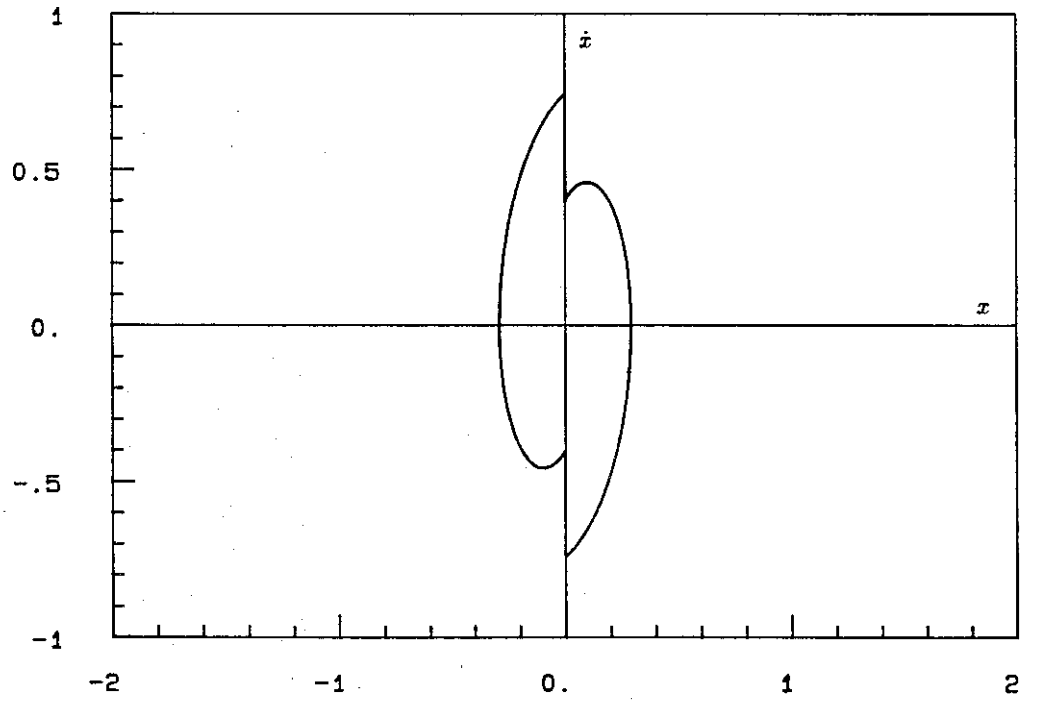

Figure 3.3: Periodic solution, $\frac{\omega_E}{\omega} = 0.5,\ a = 0.7,\ P = 1,\ \dot{x}_0 = 0.40016,\ \theta_0 = 1.03038.$

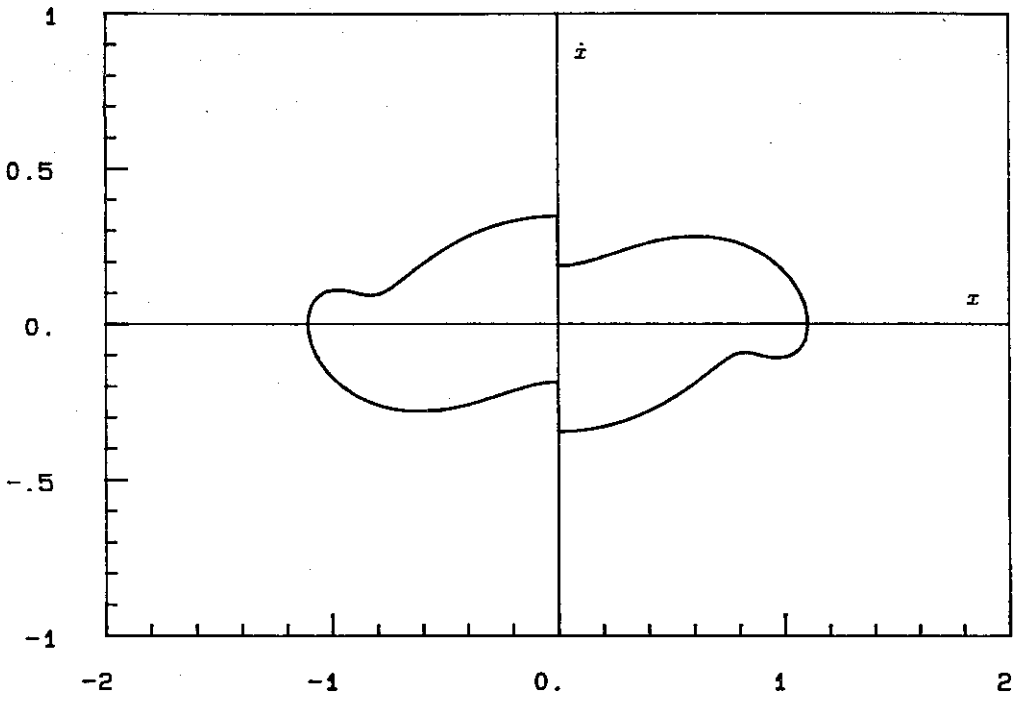

Figure 3.4: Periodic solution, $\frac{\omega_0}{\omega} = 4,\ a = 0.7,\ P = 1,\ \dot{x}_0 = 0.18667,\ \theta_0 = -\frac{\pi}{2}$.

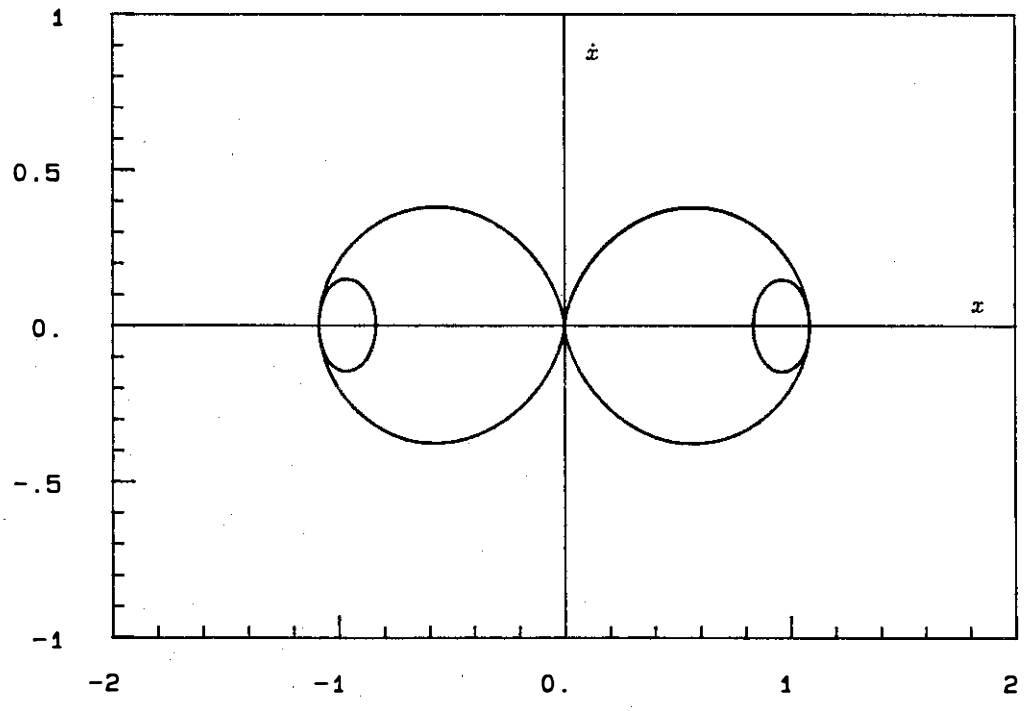

Figure 3.5: Periodic solution, $\frac{\omega_0}{\omega} = 5,\ a = 0.7,\ P = 1,\ \dot{x}_0 = 0,\ \theta_0 = -\frac{\pi}{2}$.

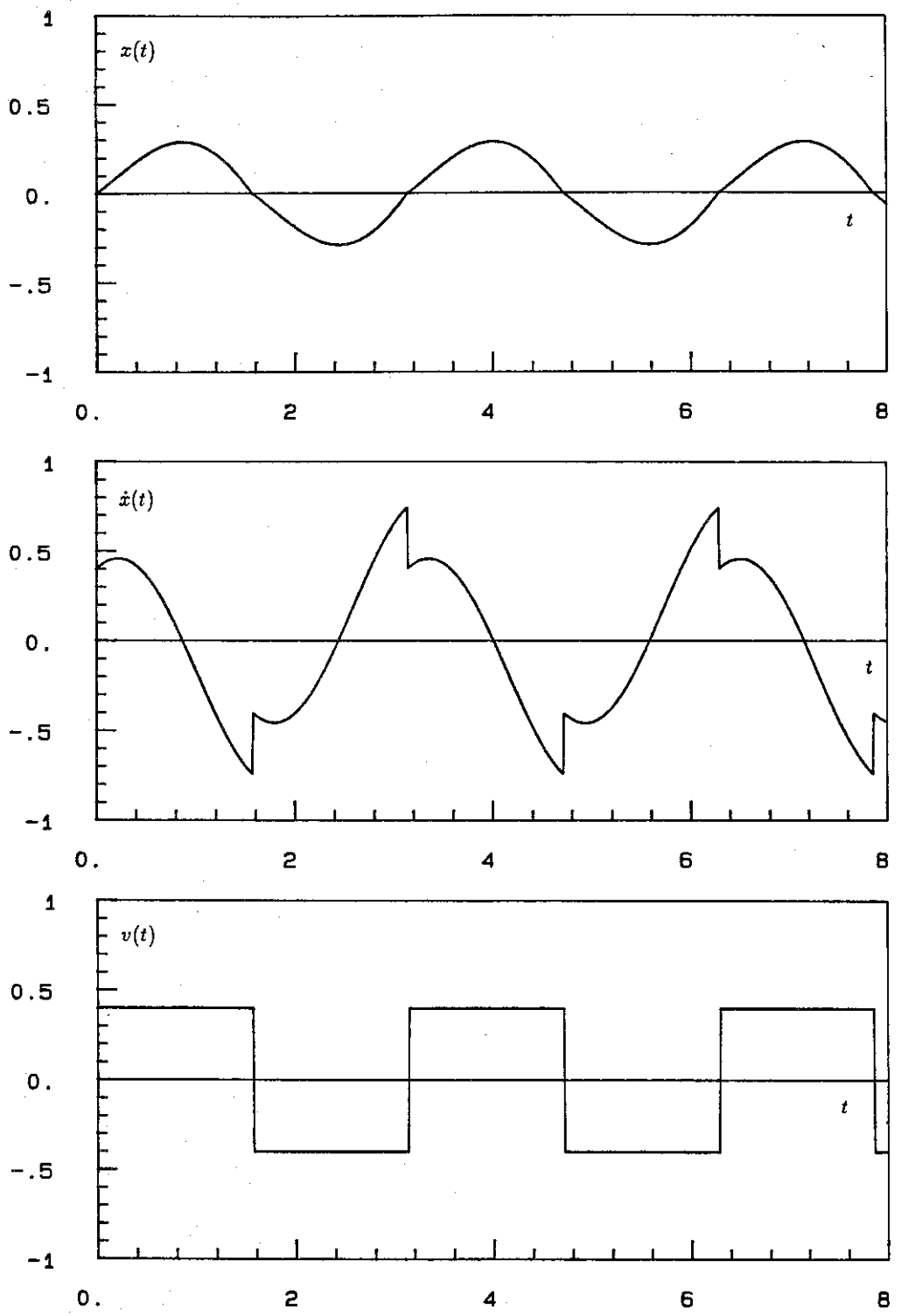

Figure 3.6: Periodic solution for $\frac{\omega_0}{\omega} = 0.5,\ a = 0.7,\ P = 1.$

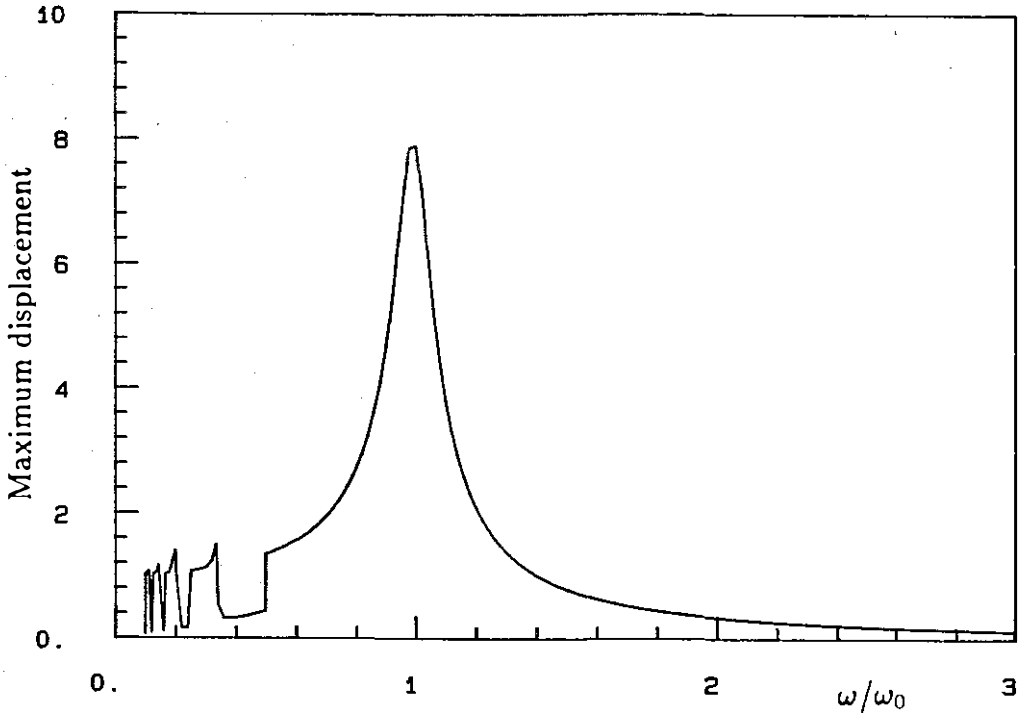

Figure 3.7: Frequency response, $a = 0.9$, $P = 1$.

subjected to periodic excitation. The response of the system is also shown as a function of time in figure 3.6

As the trajectory crosses the $x-$ axis, $\dot{x} = 0$ and therefore displacement has a stationary value. Typical solutions show only a maximum, while the singular frequency ratios $\frac{\omega_u}{\omega} = 5, 6, 7, \ldots$ exhibit multiple loops and therefore have multiple crossings of the $x-$ axis. The maximum displacement can be found by setting the velocity to zero and determining the time t of the crossing. However, analytical solution of this transcendental equation is not possible. Rather than solving this equation numerically, the equations of motion are integrated starting at the proper initial conditions and maximum displacement is recorded. Thus, we can plot the maximum displacement as a function of the frequency ratio. The results for $a = 0.9$ and $a = 0.7$, $P = 1$ are shown in figures 3.7 and 3.8 respectively. The effect of the relative size of the rotor inertias on damping effectiveness is evident.

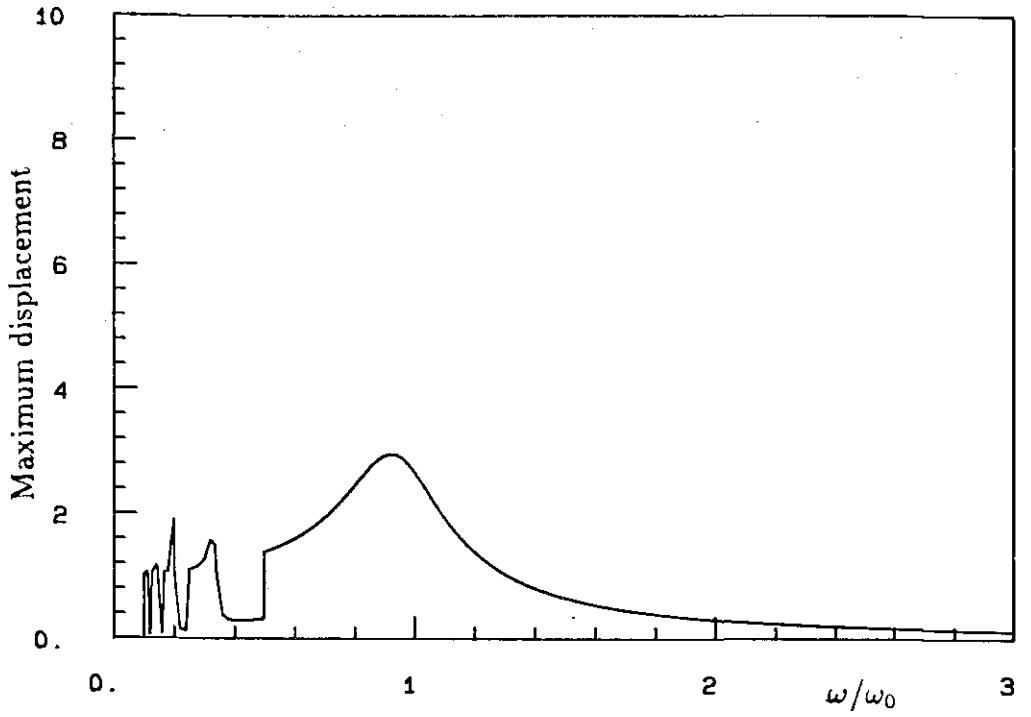

Figure 3.8: Frequency response, $a = 0.7$, $P = 1$.

3.2 Nonsymmetric Periodic Solutions

The existence of nonsymmetric periodic solutions is not immediately obvious. In simulation of the system behavior, solutions originating from different initial conditions converge to the symmetric periodic loops. Moreover, the analysis of possible solutions without any symmetry is considerably more complicated than that of the symmetric case.

Consider a possible nonsymmetric periodic solution as shown in figure 3.9. As before, let $t = 0$ be the time at Q_1 and t_1 be the time of impact at Q_3. While in the symmetric case $t_1 = \pi/\omega$, in this case, due to lack of symmetry, there is no reason to expect the same timing for the second impact. As a result, determination of the initial conditions $\dot{x}_0$ and θ_0 for a closed loop involves the determination of the time of impact as well. Moreover, if $\dot{x}_1 = \dot{x}(t_1^+) = v(t_1^+)$, then $\dot{x}_1 \neq \dot{x}_0$. Thus, the additional complication arises due to the fact that two distinct impacts must

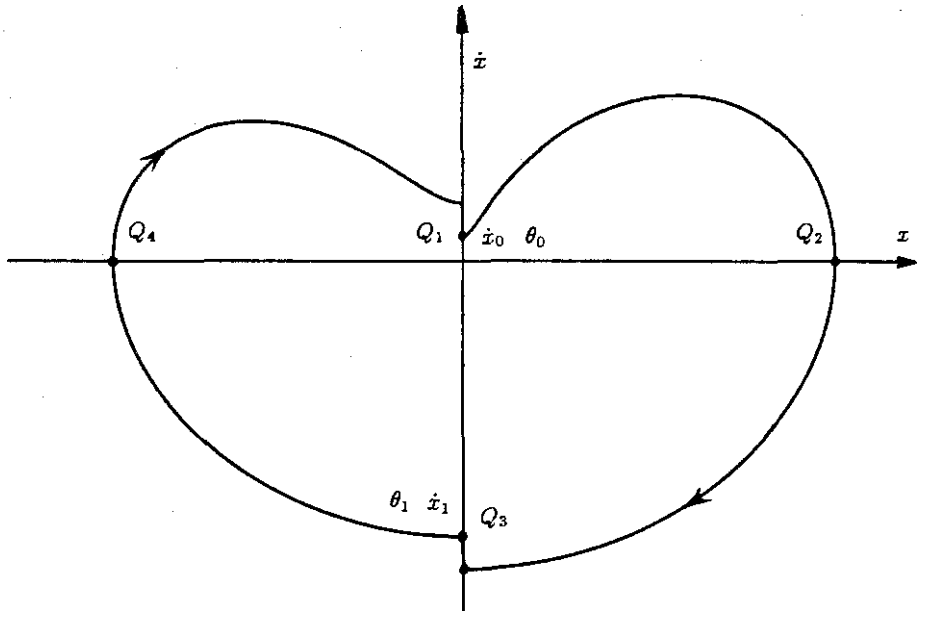

Figure 3.9: Nonsymmetric Solution.

be considered in the nonsymmetric case.

For the arc $Q_1Q_2Q_3$ we have the following:

at Q_1:

$$x(0) = 0, \quad \dot{x}(0^+) = v(0^+) = \dot{x}_0, \quad \theta = \theta_0$$

at Q_3:

$$x(t_1) = 0 \tag{3.23}$$

$$\dot{x}(t_1^+) = v(t_1^+) = \dot{x}_1 \tag{3.24}$$

$$\theta_1 = \theta_0 + \omega t_1 \tag{3.25}$$

The impact condition at Q_3 gives:

$$\dot{x}_1 = a\dot{x}(t_1^-) + b\dot{x}_0 \tag{3.26}$$

For the second arc $Q_3Q_4Q_1$ of the trajectory we have:

at Q_3:

$$x(0) = 0, \quad \dot{x}(0^+) = v(0^+) = \dot{x}_1, \quad \theta = \theta_1$$

at Q_1:

$$t_2 = \frac{2\pi}{\omega} - t_1 \tag{3.27}$$

$$x(t_2) = 0 \tag{3.28}$$

$$\dot{x}(t_2^+) = v(t_2^+) = \dot{x}_0 \tag{3.29}$$

and the impact condition

$$\dot{x}_0 = a\dot{x}(t_2^-) + b\dot{x}_1 \tag{3.30}$$

In principle equations (3.23), (3.26), (3.28) and (3.30) can be solved for the four unknowns $\dot{x}_0$, θ_0, $\dot{x}_1$ and t_1. In practice the most substantial obstacle comes from the solution of the transcendental equation (3.23).

At first, we investigate the possibility of $t_1 = \frac{\pi}{\omega} \implies \theta_1 = \theta_0 + \pi$. Then, for the arc $Q_1Q_2Q_3$ we have that

$$x(\frac{\pi}{\omega}) = 0$$

Since the solution is known, we obtain from (3.3) the following expression for zero displacement at Q_3 $(\omega \neq \omega_0)$:

$$\frac{P}{\omega^2 - \omega_0^2}\cos\theta_0\left[1 + \cos(\tfrac{\omega_0}{\omega}\pi)\right] + \left[\frac{\dot{x}_0}{\omega_0} - \frac{P\left(\frac{\omega}{\omega_0}\right)}{\omega^2 - \omega_0^2}\sin\theta_0\right]\sin(\tfrac{\omega_0}{\omega}\pi) = 0 \tag{3.31}$$

A similar condition at Q_1 can be obtained for the second arc from (3.31) by substitution of $\theta_1 = \theta_0 + \pi$ and $\dot{x}_1$ in place of θ_0 and $\dot{x}_0$ respectively. We get

$$-\frac{P}{\omega^2 - \omega_0^2}\cos\theta_0\left[1 + \cos(\tfrac{\omega_0}{\omega}\pi)\right] + \left[\frac{\dot{x}_1}{\omega_0} + \frac{P\left(\frac{\omega}{\omega_0}\right)}{\omega^2 - \omega_0^2}\sin\theta_0\right]\sin(\tfrac{\omega_0}{\omega}\pi) = 0 \tag{3.32}$$

Adding (3.31) and (3.32)

$$\left[\frac{\dot{x}_0}{\omega_0} - \frac{P\left(\frac{\omega}{\omega_0}\right)}{\omega^2 - \omega_0^2}\sin\theta_0 + \frac{\dot{x}_1}{\omega_0} + \frac{P\left(\frac{\omega}{\omega_0}\right)}{\omega^2 - \omega_0^2}\sin\theta_0\right]\sin(\tfrac{\omega_0}{\omega}\pi) = 0$$

$$\Longrightarrow \quad \frac{1}{\omega_0}\left[\dot{x}_1 + \dot{x}_0\right]\sin\left(\frac{\omega_0}{\omega}\pi\right) = 0 \tag{3.33}$$

Thus, either $\dot{x}_1 = -\dot{x}_0$ which gives the symmetric solution, or $\sin(\frac{\omega_0}{\omega}\pi) = 0 \Rightarrow \frac{\omega_0}{\omega} = l,\ l = 2,3,\ldots$

The case of resonance will be treated below and it will be shown that only the symmetric solution is possible. Thus, the only existing possibilities are those for which the frequency ratio ω_0/ω is an integer.

Consider first $\frac{\omega_0}{\omega} = 2m, \quad m = 1,2,\ldots$. Then, expressions for position and velocity at first impact are as follows:

$$x(t_1) \;=\; x(\frac{\pi}{\omega}) = \frac{2P}{\omega^2 - \omega_0^2}\cos\theta_0 = 0 \tag{3.34}$$

$$\dot{x}(t_1^-) \;=\; \dot{x}_0 - \frac{2P\omega}{\omega^2 - \omega_0^2}\sin\theta_0 \tag{3.35}$$

From (3.34) we conclude that $\theta_0 = \pm\frac{\pi}{2}$.

Substituting for the velocity in (3.26) we find

$$\dot{x}_1 = a\left[\dot{x}_0 - \frac{2P\omega}{\omega^2 - \omega_0^2}\sin\theta_0\right] + b\dot{x}_0$$

$$\Longrightarrow \quad \dot{x}_1 = \dot{x}_0 - \frac{2Pa\omega}{\omega^2 - \omega_0^2}\sin\theta_0 \tag{3.36}$$

For the second arc of the trajectory we make again the substitutions $\theta_0 \longrightarrow \theta_1 = \theta_0 + \pi;\ \dot{x}_0 \longrightarrow \dot{x}_1$. Condition (3.28) is satisfied identically with this choice for the phase angle while

$$\dot{x}(t_2^-) = \dot{x}_1 + \frac{2P\omega}{\omega^2 - \omega_0^2}\sin\theta_0$$

Substituting in (3.30) we get

$$\begin{aligned}
\dot{x}_0 \;&=\; a\left[\dot{x}_1 + \frac{2P\omega}{\omega^2 - \omega_0^2}\sin\theta_0\right] + b\dot{x}_1 \\
&=\; (a+b)\dot{x}_1 + \frac{2Pa\omega}{\omega^2 - \omega_0^2}\sin\theta_0 \\
&=\; \dot{x}_0 - \frac{2Pa\omega}{\omega^2 - \omega_0^2}\sin\theta_0 + \frac{2Pa\omega}{\omega^2 - \omega_0^2}\sin\theta_0 \\
&=\; \dot{x}_0
\end{aligned}$$

Thus, the closure conditions are satisfied identically and θ_0 as well as $\dot{x}_0$ have not been determined. Note however that $\dot{x}_1$ must be negative. Morever, since $\dot{x}_0 > 0$ and $\omega^2 - \omega_0^2 < 0$, it follows that $\sin\theta_0 < 0$

$$\Longrightarrow \quad \theta_0 = -\frac{\pi}{2} \tag{3.37}$$

Substituting into (3.36) we get

$$\dot{x}_1 = \dot{x}_0 - \frac{2Pa\omega}{\omega_0^2 - \omega^2} \leq 0$$

Hence, the only restriction on the initial velocity of the primary mass is

$$0 \leq \dot{x}_0 \leq \frac{2Pa\omega}{\omega_0^2 - \omega^2} \tag{3.38}$$

The above inequality indicates that there is an infinity of solutions of this type which lie arbitrarily close to each other. Note that the symmetric solution $\dot{x}_0 = \frac{Pa\omega}{\omega_0^2-\omega^2}$ is a special case of the one above. Specifically, any solution starting in the interval specified by (3.38) above with $\theta_0 = -\pi/2$ is a periodic solution.

Three of the solutions specified above are shown in figures 3.10, 3.11 and 3.12 for the frequency ratio $\frac{\omega_n}{\omega} = 2$. The one shown in figure 3.12 is the symmetric solution. Note that for each nonsymmetric solution with $\dot{x}_0 \in [0, \frac{Pa\omega}{\omega_0^2-\omega^2})$ there is a "conjugate" one which is its symmetric image about the origin and for which $\dot{x}_0 \in (\frac{Pa\omega}{\omega_0^2-\omega^2}, \frac{2Pa\omega}{\omega_0^2-\omega^2}]$ A pair of these "conjugate" solutions is shown in the other two figures.

In the case $\frac{\omega_n}{\omega} = 2m + 1$, $m = 1, 2, \ldots$ the position is zero at $t_1 = \pi/\omega$ and this is independent of the phase angle θ_0. Moreover, the velocity prior to impact is $\dot{x}(t_1^-) = -\dot{x}_0$. After impact

$$\begin{aligned} \dot{x}_1 &= a\dot{x}(t_1^-) + b\dot{x}_0 \\ &= -a\dot{x}_0 + b\dot{x}_0 \\ &= (b-a)\dot{x}_0 \end{aligned} \tag{3.39}$$

Repeating for the second arc we find

$$\dot{x}_0 = (b-a)\dot{x}_1 \tag{3.40}$$

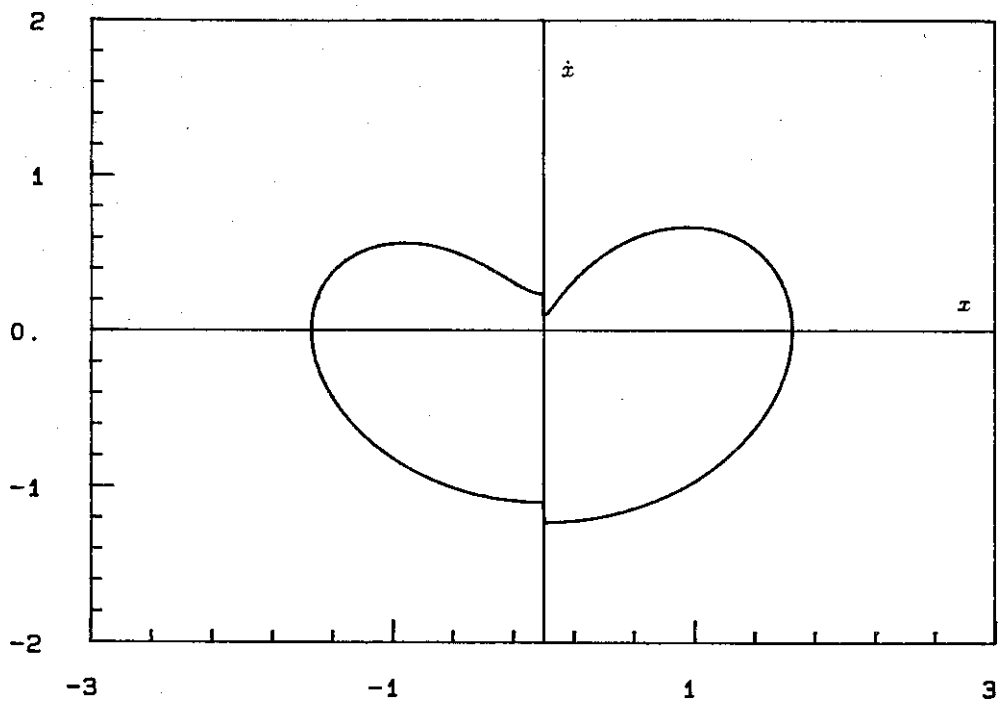

Figure 3.10: Nonsymmetric solution, $\frac{\omega_0}{\omega} = 2,\ a = 0.9,\ \dot{x}_0 = 0.1,\ P = 1.$

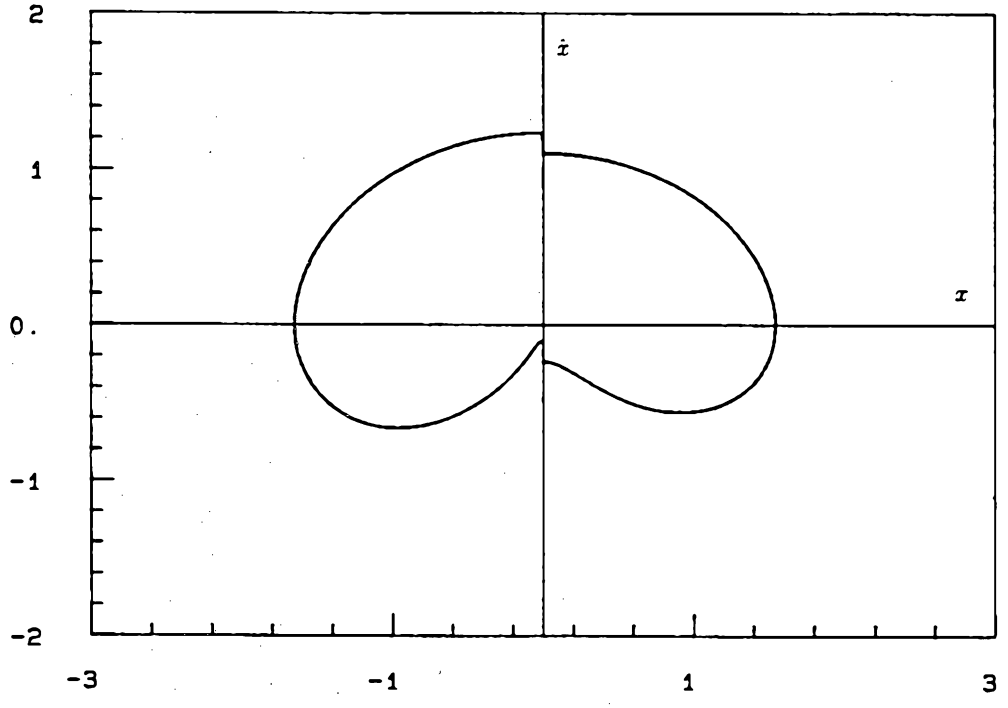

Figure 3.11: Nonsymmetric solution, $\frac{\omega_0}{\omega} = 2,\ a = 0.9,\ \dot{x}_0 = 1.1,\ P = 1.$

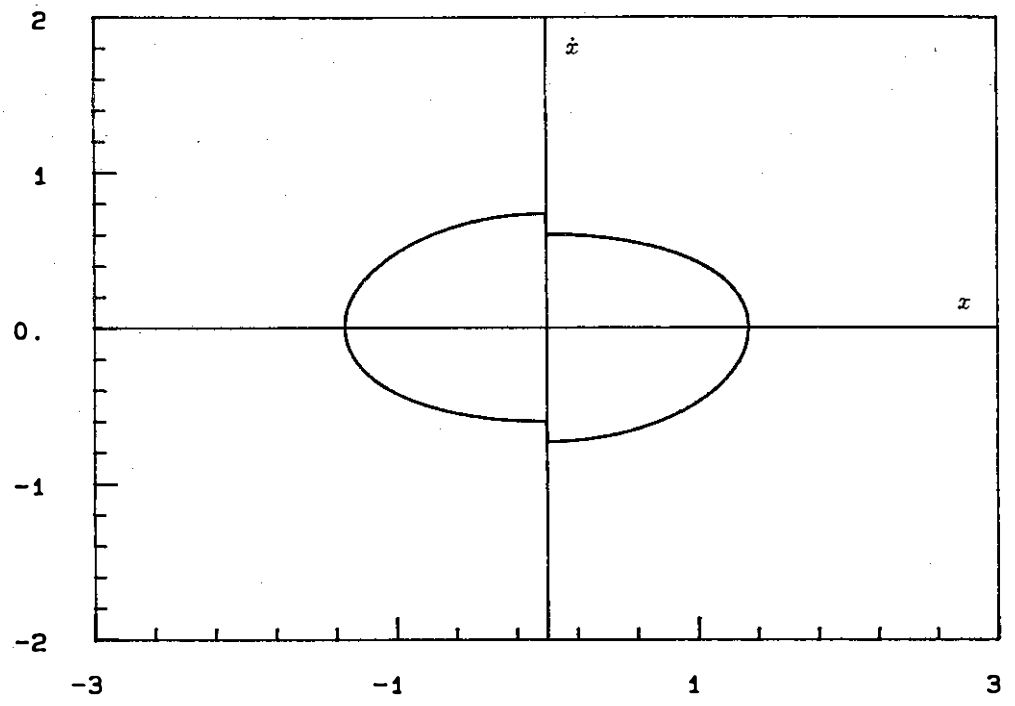

Figure 3.12: Symmetric solution belonging to the group shown in fig. 3.10 and 3.11.

The only possible solution of (3.39) and (3.40) is $\dot{x}_0 = \dot{x}_1 = 0$ which is the symmetric solution.

In the case of resonance, clearly $\theta_0 = 0$ and the velocity prior to impact is

$$\dot{x}(t_1^-) = -\left(\dot{x}_0 + \frac{P\pi}{2\omega_0}\right)$$

After impact

$$\begin{aligned} \dot{x}_1 &= a\dot{x}(t_1^-) + b\dot{x}_0 \\ &= -a\left(\dot{x}_0 + \frac{P\pi}{2\omega_0}\right) + b\dot{x}_0 \\ &= (b-a)\dot{x}_0 - \frac{Pa\pi}{2\omega_0} \end{aligned} \tag{3.41}$$

For the second arc, $\theta_1 = \theta_0 + \pi = \pi$ and $x(t_2) = x(\pi) = 0$. The velocity is $\dot{x}(t_2^-) = -\dot{x}_1 + \frac{P\pi}{2\omega_0}$. After impact

$$\dot{x}_0 = a\left(-\dot{x}_1 + \frac{P\pi}{2\omega_0}\right) + b\dot{x}_1$$

$$
\begin{aligned}
\Longrightarrow \dot{x}_0 &= (b-a)\dot{x}_1 + \frac{Pa\pi}{2\omega_0} \\
&= (b-a)\left[(b-a)\dot{x}_0 - \frac{Pa\pi}{2\omega_0}\right] + \frac{Pa\pi}{2\omega_0} \\
&= (b-a)^2\dot{x}_0 + \frac{Pa\pi}{2\omega_0}(1-b+a) \\
&= (b-a)^2\dot{x}_0 + \frac{Pa^2\pi}{\omega_0} \qquad (3.42)
\end{aligned}
$$

Solving for $\dot{x}_0$ we find $\dot{x}_0 = \left(\frac{a}{b}\right)\frac{P\pi}{4\omega_0}$ which is the symmetric solution. In summary, the only nonsymmetric periodic solutions in which the impacts occur at half period are those with $\frac{\omega_0}{\omega}$ even.

Attempts to solve the system of equations (3.23), (3.26), (3.28) and (3.30) numerically resulted in two problems. Iterative methods like Newton's method and the iteration method either converged to the symmetric solution or did not converge at all. The bisection method was also applied in order to circumvent this difficulty in the following way: we notice first that an initial guess in $\dot{x}_0$ and θ_0 determines t_1 and $\dot{x}_1$ uniquely through equation $x(t_1) = 0$ and the impact condition at Q_3. As a result, the problem is reduced to finding two unknowns θ_0 and $\dot{x}_0$ such that the trajectory is closed at Q_1. This implies that

$$
\begin{aligned}
f(\dot{x}_0, \theta_0) &= t_1 + t_2 - \frac{2\pi}{\omega} = 0 \qquad (3.43) \\
g(\dot{x}_0, \theta_0) &= \dot{x}_0 - \dot{x}(t_2^+) = 0 \qquad (3.44)
\end{aligned}
$$

Thus, the bisection method was applied to find the zeroes of $f(\dot{x}_0, \theta_0)$ and $g(\dot{x}_0, \theta_0)$.

To determine the range of values for $\dot{x}_0$ and θ_0 in which to search for possible solutions, the two fuctions were plotted. It was found that they both have discontinuities from negative to positive values, in effect never crossing the zero axis. Clearly, they both vanish at the point representing the symmetric solution, but their unusual behavior makes the search for nonsymmetric solutions impossible.

3.3 Subharmonic Periodic Solutions

Multiple-impacts-per-cycle subharmonic solutions would be expected to exist. However, analytical investigation of these solutions is not possible due to the difficulty in solving the transcendental equations $x(t_i) = 0$ for the impact times t_i. The only other alternative available, namely numerical solution of these equations, is hindered by problems similar to those encountered in the analysis of the nonsymmetric harmonic solutions. As a result, we investigate only a small subset of these solutions which, as it turns out, play important role in the analysis of chaotic behavior.

Specifically, we look for symmetric 2 impacts/cycle periodic solutions whose frequency is equal to the natural frequency of the primary system. The response of the system is given by equations (3.3) and (3.4) as before. The time of impact then is $t = t_1 = \frac{\pi}{\omega_0}$ and therefore, at Q_2 (fig. 3.1) we have:

$$\begin{aligned} x\left(\frac{\pi}{\omega_0}\right) &= 0 \\ \dot{x}\left(\frac{\pi}{\omega_0}^+\right) = v\left(\frac{\pi}{\omega_0}^+\right) &= -\dot{x}_0 \end{aligned} \tag{3.45}$$

where $\dot{x}_0$ is as before. The impact condition gives

$$-\left(\frac{1+b}{a}\right)\dot{x}_0 = \dot{x}\left(\frac{\pi}{\omega_0}^-\right) \tag{3.46}$$

Following the same procedure as in the case of harmonic solutions, (3.45) and (3.46) reduce to

$$0 = \left[1 + \cos\left(\frac{\omega}{\omega_0}\pi\right)\right]\cos\theta_0 - \sin\left(\frac{\omega}{\omega_0}\pi\right)\sin\theta_0 \tag{3.47}$$

$$\begin{aligned} -2\left(\frac{b}{a}\right)\frac{\dot{x}_0}{\omega_0} &= \frac{P\left(\frac{\omega}{\omega_0}\right)}{\omega^2 - \omega_0^2}\sin\left(\frac{\omega}{\omega_0}\pi\right)\cos\theta_0 + \\ &\quad + \frac{P\left(\frac{\omega}{\omega_0}\right)}{\omega^2 - \omega_0^2}\left[1 + \cos\left(\frac{\omega}{\omega_0}\pi\right)\right]\sin\theta_0 \end{aligned} \tag{3.48}$$

In this case additional conditions must be imposed on the forcing term to ensure that the response is symmetric, namely that

$$\cos\left(\frac{\omega}{\omega_0}\pi + \theta_0\right) = -\cos\theta_0 \tag{3.49}$$

and

$$\sin\left(\frac{\omega}{\omega_0}\pi + \theta_0\right) = -\sin\theta_0 \tag{3.50}$$

The last two conditions imply that $\frac{\omega}{\omega_0} = 2l + 1,\ l = 1, 2, \ldots$ Thus (3.47) is satisfied identically and (3.48) gives

$$\dot{x}_0 = 0 \tag{3.51}$$

This case is therefore similar to the harmonic response for $\frac{\omega_0}{\omega} = 2l + 1,\ l = 1, 2, \ldots$ Using similar arguments, we deduce that for this subharmonic solution

$$\theta_0 = -\frac{\pi}{2} \tag{3.52}$$

also.

Thus, there are subharmonic solutions which involve no impacts at all and are given by (3.51), (3.52) and

$$\frac{\omega}{\omega_0} = 2l + 1, \quad l = 1, 2, \ldots \tag{3.53}$$

The frequency of the response is the natural frequency of the primary system. The solutions for $\frac{\omega}{\omega_0} = 5$ and $\frac{\omega}{\omega_0} = 7$ are shown in figures 3.13 and 3.14 respectively.

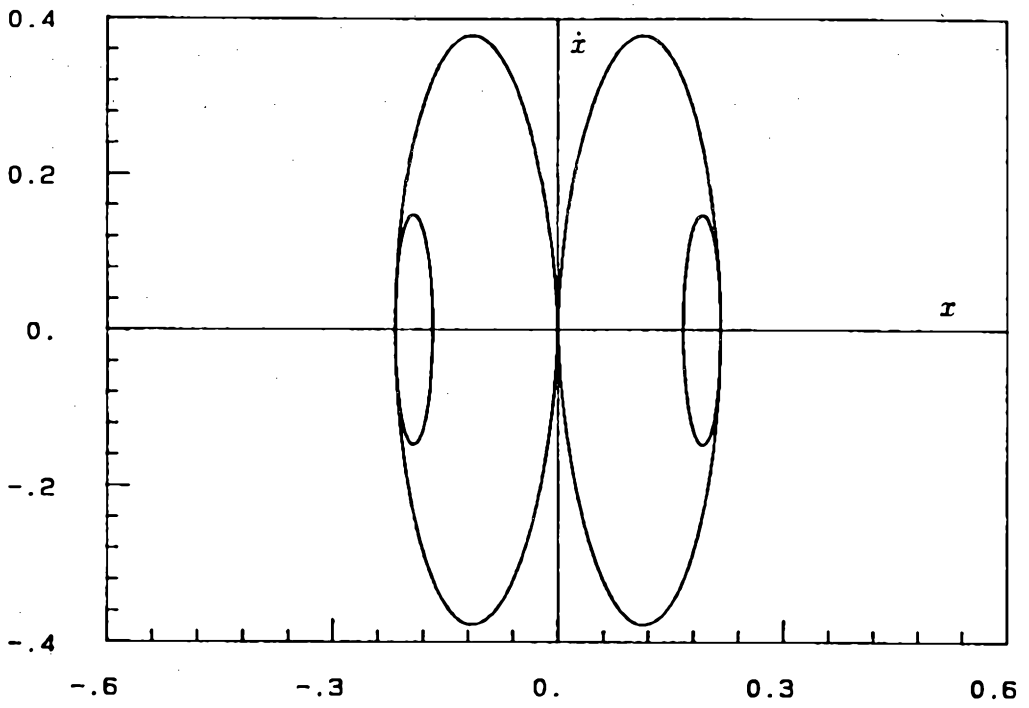

Figure 3.13: Subharmonic periodic solution, $\frac{\omega}{\omega_0} = 5, \quad P = 1.$

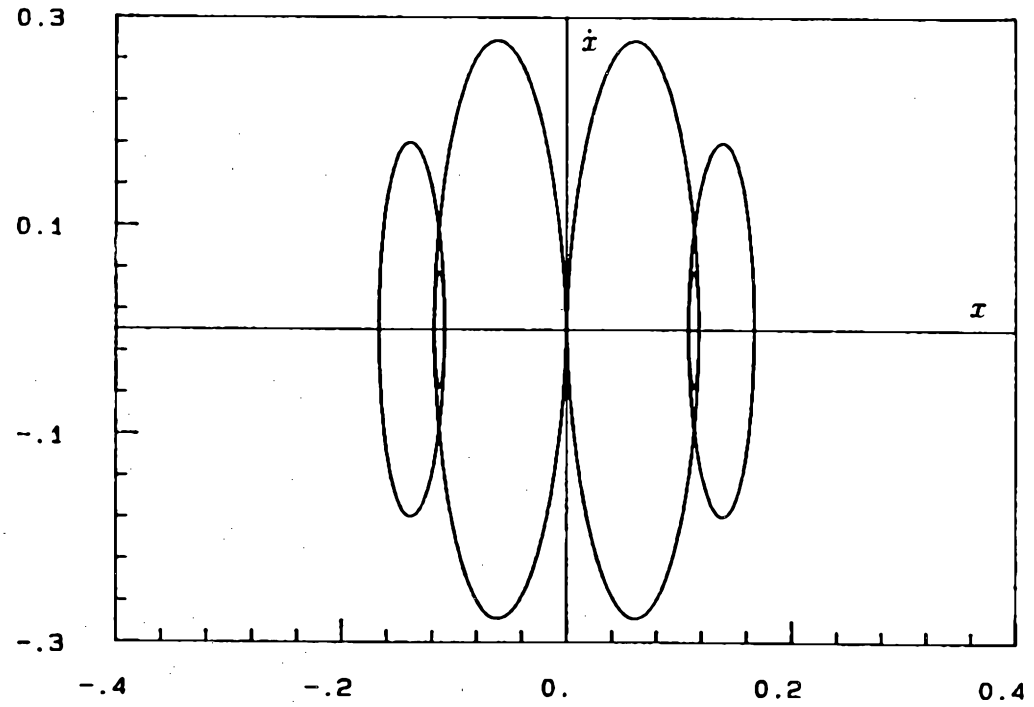

Figure 3.14: Subharmonic periodic solution, $\frac{\omega}{\omega_0} = 7, \quad P = 1.$

4

Stability

We turn now our attention to the stability of the periodic solutions found in the previous chapter. Specifically, we are interested in the asymptotic behavior of perturbations to the steady state solution of the impact damper. Because of the discontinuities in the solution of the system, the usual method of investigation does not apply and we must use an alternative approach developed by Masri and Caughey [8].

4.1 Method of Analysis

Consider the dynamical system[1]

$$\dot{\mathbf{x}} = \mathbf{f}(\mathbf{x}, t), \quad \mathbf{x} \in \mathbb{R}^n, \quad \mathbf{f} \in \mathbb{R}^n \tag{4.1}$$

with the usual assumptions on $\mathbf{f}(\mathbf{x}, t)$. Let $\mathbf{x} = \mathbf{y}(t)$ be a solution of (4.1) and suppose that this solution is perturbed so that

$$\mathbf{x}(t) = \mathbf{y}(t) + \boldsymbol{\xi}(t).$$

Then, $\mathbf{y}(t)$ is asymptotically stable if it is stable and

$$\lim_{t \to \infty} \|\boldsymbol{\xi}(t)\| = 0.$$

[1] Boldface letters denote vectors. Matrices are denoted with capital letters.

To determine the behavior of $\boldsymbol{\xi}(t)$ we substitute in the equations of motion for $\mathbf{x}(t)$ to get

$$\dot{\mathbf{y}}(t) + \dot{\boldsymbol{\xi}}(t) = \mathbf{f}(\mathbf{y}(t) + \boldsymbol{\xi}(t), t)$$

and expand $\mathbf{f}$ in a Taylor series about $\mathbf{y}(t)$ to get the variational equations for the system as

$$\dot{\boldsymbol{\xi}} = F(t)\boldsymbol{\xi} + \boldsymbol{R}(\boldsymbol{\xi}, t) \tag{4.2}$$

where $F(t)$ is an $n \times n$ matrix with

$$F_{ij} = \frac{\partial f_i(\mathbf{y}(t), t)}{\partial y_j}$$

Thus, $\mathbf{y}(t)$ is asymptotically stable if the origin is an asymptotically stable equilibrium point of (4.2). In the usual method, analysis of the linearized system

$$\dot{\boldsymbol{\xi}} = F(t)\boldsymbol{\xi}(t) \tag{4.3}$$

is often adequate for determining the stability characteristics of the solution of the complete system (4.1). Note that if $\mathbf{y}(t)$ is periodic in t, so is $F(t)$ and Floquet theory applies. However, in the present case as well as in the problem analyzed by Masri and Caughey, the solution is only piecewise continuous with discontinuities at every impact and therefore the coefficient matrix $F(t)$ cannot be computed in the usual way. We bypass this difficulty by converting the variational equation into a difference equation as follows. The steady state solution $\mathbf{y}(t)$ is perturbed immediately after impact. These initial perturbations will evolve and their new values after the next impact can be determined. The process can be repeated with the new values for the next half cycle. If the initial perturbations decrease to zero after multiple impacts, the steady state solution is asymptotically stable. Otherwise it is unstable. Note that between impacts, $\mathbf{f}(\mathbf{x}, t)$ is continuous and satisfies the Lipschitz condition. Therefore, the solution of (4.1) exists and is unique between impacts.

Now, let the initial perturbation vector be ξ_0 so that the initial conditions immediately after impact are

$$\mathbf{x}(\Delta t_0) = \mathbf{x}_0 + \xi_0$$

where $\mathbf{x}_0$ is the vector of initial conditions for steady state response. Suppose that the steady state solution is periodic with period $2\pi/\omega$ and involves 2 impacts/cycle. Then the next impact will occur at $\omega t = \pi + \Delta t_0'$ and $\Delta t_0'$ can be determined from

$$\Delta t_0' = h(\mathbf{y}, \xi_0, \Delta t_0)$$

for some function h.

Let the perturbation vector after the next impact be ξ_1. Then

$$\xi_1 = Q\xi_0 + \boldsymbol{R}(\xi_0) \tag{4.4}$$

where Q is a constant matrix and $\boldsymbol{R}$ contains all the terms in ξ_0 of second order or higher. After $m+1$ impacts we get

$$\begin{aligned} \xi_{m+1} &= Q\xi_m + \boldsymbol{R}(\xi_m) \\ &= Q^{m+1}\xi_0 + \boldsymbol{R}'(\xi_0) \end{aligned} \tag{4.5}$$

Consider the linear part of (4.5) between the mth and $(m+1)$th impacts

$$\begin{aligned} \xi_{m+1} &= Q\xi_m \\ &= Q^{m+1}\xi_0 \end{aligned} \tag{4.6}$$

If the eigenvalues of Q are distinct, it can be diagonalized using a similarity transformation so that

$$Q = S\Lambda S^{-1} \implies Q^m = S\Lambda^m S^{-1} \; ; \; \Lambda \text{ diagonal}$$

Let λ_i, $i = 1, 2, \ldots, n$ be the eigenvalues of Q. Then, the origin is an asymptotically stable equilibrium point of (4.6) if and only if the eigenvalues of Q have modulus less than one, i.e.,

$$|\lambda_i| < 1, \quad i = 1, 2, \ldots, n \tag{4.7}$$

If the eigenvalues of Q are not distinct, it can always be transformed into Jordan canonical form and the condition (4.7) still applies.

Concerning the stability of (4.4) we have the following theorem which has been proven by Masri and Caughey [8].

Theorem 4.1 (T. K. Caughey, S. Masri)
If

1. $\|\xi_0\|$ *is sufficiently small*
2. $\lim_{\|\xi\| \to 0} \frac{\|R(\xi)\|}{\|\xi\|} = 0$

and if

$$\xi_{m+1} = Q^{m+1} \xi_0 \tag{4.8}$$

is asymptotically stable, then so is the system

$$\xi_{m+1} = Q^{m+1} \xi_0 + R'(\xi_0) \tag{4.9}$$

The proof of this theorem is provided in appendix B for the sake of completeness.

Thus, the stability problem is reduced to determining the matrix Q and its eigenvalues. However, the theorem allows us to determine the stability characteristics of the nonlinear system only in "the first approximation". As a result, it provides no information at all in the case where one of the eigenvalues of Q has modulus one. To conclude stability or instability in such cases, one must analyze the full nonlinear system.

4.2 Stability of the Periodic Solutions

To put the equations of motion of the impact damper in the form of (4.1), let

$$\mathbf{x} = \begin{bmatrix} x \\ \dot{x} \\ y \end{bmatrix}, \qquad \mathbf{f}(\mathbf{x},t) = \begin{bmatrix} \dot{x} \\ -\omega_0^2 x + P\cos(\omega t + \theta) \\ v \end{bmatrix} \tag{4.10}$$

Since the system is third order, the perturbation vector ξ_0 should have three components. Rather than using the position of the primary system and the two velocities, it is convenient because of the way that the solutions have been constructed to choose the phase angle θ as the first component. Moreover, since immediately after impact the two velocities are identical, the perturbations of these velocities from their steady state value must be equal. Therefore, ξ has only two components, Q is 2×2 and the characteristic equation is quadratic. Let

$$\mathbf{x}_0 = \begin{bmatrix} \theta_0 \\ \frac{\dot{x}_0}{\omega_0} \end{bmatrix}, \qquad \xi_0 = \begin{bmatrix} \Delta\theta_0 \\ \frac{\Delta\dot{x}_0}{\omega_0} \end{bmatrix}$$

4.2.1 Symmetric Harmonic Solutions

As before, let the values of the initial conditions for steady state response be

$$\left.\begin{aligned} x(0) &= x_0 = 0 \\ \dot{x}(0) &= v(0) = \dot{x}_0 \\ \theta &= \theta_0 \end{aligned}\right\} \tag{4.11}$$

The conditions at $\omega t = \pi^+$ as well as the perturbations to these values are summarized in table 4.1. Primed quantities are those after the second impact (at half cycle). Note that because of the active nature of the system, the position at impact is always zero. Moreover, immediately after impact both rotors assume the same velocity and, therefore, $\dot{x}_0 = v_0 \implies \dot{x}_0 + \Delta\dot{x}_0 = \dot{x}_0 + \Delta v_0 \implies \Delta\dot{x}_0 = \Delta v_0$.

Steady State	Perturbed
at $\omega t = 0^+$	at $\omega t = (0 + \Delta t_0)^+$
$x = x_0 = 0$	$x = x_0 = 0$
$\dot{x} = \dot{x}_0$	$\dot{x} = \dot{x}_0 + \Delta\dot{x}_0$
$v = v_0 = \dot{x}_0$	$v = v_0 + \Delta v_0 = \dot{x}_0 + \Delta\dot{x}_0$
$\theta = \theta_0$	$\theta = \theta_0 + \Delta\theta_0$
at $\omega t = \pi^+$	at $\omega t = (\pi + \Delta t_0')^+$
$x = x_0 = 0$	$x = x_0 = 0$
$\dot{x} = -\dot{x}_0$	$\dot{x} = -\dot{x}_0 - \Delta\dot{x}_0'$
$v = -v_0 = -\dot{x}_0$	$v = -v_0 - \Delta v_0' = -\dot{x}_0 - \Delta\dot{x}_0'$
$\theta = \theta_0$	$\theta = \theta_0 + \Delta\theta_0'$

Table 4.1: Summary of initial and final conditions.

As it was shown in the previous chapter, depending on the frequency ratio ω_0/ω, there are four classes of symmetric solutions and each must be treated separately. Except for the case of resonance, the solution is

$$x(t) = A\cos\omega_0 t + B\sin\omega_0 t - \frac{P}{\omega^2 - \omega_0^2}\cos(\omega t + \theta_0) \tag{4.12}$$

$$\dot{x}(t) = -A\omega_0\sin\omega_0 t + B\omega_0\cos\omega_0 t + \frac{P\omega}{\omega^2 - \omega_0^2}\sin(\omega t + \theta_0) \tag{4.13}$$

and the coefficients A and B depend on the initial conditions.

Let A_0 and B_0 denote the values corresponding to periodic solutions, and consider first the general case where $\cos(\frac{\omega_u}{\omega}\pi) \neq \pm 1$, $\sin(\frac{\omega_u}{\omega}\pi) \neq 0$.

Then

$$A_0 = A(0) = \frac{P}{\omega^2 - \omega_0^2}\cos\theta_0 \tag{4.14}$$

$$B_0 = B(0) = \frac{\dot{x}_0}{\omega_0} - \frac{P\left(\frac{\omega}{\omega_0}\right)}{\omega^2 - \omega_0^2}\sin\theta_0 \tag{4.15}$$

For the perturbed solution $A = A(0 + \Delta t_0)$ and $B = B(0 + \Delta t_0)$. At $\omega t = \pi + \Delta t_0'$ impact occurs and the displacement is zero:

$$\begin{aligned} 0 = {} & A(0+\Delta t_0)\cos\omega_0\left(\frac{\pi + \Delta t_0' - \Delta t_0}{\omega}\right) + B(0+\Delta t_0)\sin\omega_0\left(\frac{\pi + \Delta t_0' - \Delta t_0}{\omega}\right) - \\ & - \frac{P}{\omega^2 - \omega_0^2}\cos(\pi + \Delta t_0' - \Delta t_0 + \theta_0 + \Delta\theta_0) \end{aligned}$$

$$\begin{aligned} \Rightarrow\ 0 = {} & A(0+\Delta t_0)\cos\omega_0\left(\frac{\pi + \Delta T}{\omega}\right) + B(0+\Delta t_0)\sin\omega_0\left(\frac{\pi + \Delta T}{\omega}\right) + \\ & + \frac{P}{\omega^2 - \omega_0^2}\cos(\Delta T + \theta_0 + \Delta\theta_0) \end{aligned} \tag{4.16}$$

where

$$\Delta T = \Delta t_0' - \Delta t_0 = \Delta\theta_0' - \Delta\theta_0 \tag{4.17}$$

To first order

$$A(0 + \Delta t_0) = A(0) + \frac{\partial A}{\partial \dot{x}_0}\Delta\dot{x}_0 + \frac{\partial A}{\partial \theta_0}\Delta\theta_0$$

Since

$$\begin{aligned} \frac{\partial A}{\partial \dot{x}_0} &= \frac{\partial}{\partial \dot{x}_0}\left(\frac{P}{\omega^2 - \omega_0^2}\cos\theta_0\right) = 0 \\ \frac{\partial A}{\partial \theta_0} &= -\frac{P}{\omega^2 - \omega_0^2}\sin\theta_0 \end{aligned}$$

we get

$$A(0 + \Delta t_0) = A_0 - \frac{P}{\omega^2 - \omega_0^2}\sin\theta_0\Delta\theta_0 \tag{4.18}$$

Similarly

$$\begin{aligned} B(0 + \Delta t_0) &= B(0) + \frac{\partial B}{\partial \dot{x}_0}\Delta\dot{x}_0 + \frac{\partial B}{\partial \theta_0}\Delta\theta_0 \\ &= B_0 + \frac{1}{\omega_0}\Delta\dot{x}_0 - \frac{P\left(\frac{\omega}{\omega_0}\right)}{\omega^2 - \omega_0^2}\cos\theta_0\Delta\theta_0 \end{aligned} \tag{4.19}$$

In addition

$$\cos\omega_0\left(\frac{\pi+\Delta T}{\omega}\right) \approx \cos(\tfrac{\omega_0}{\omega}\pi) - \sin(\tfrac{\omega_0}{\omega}\pi)\frac{\omega_0}{\omega}\Delta T \tag{4.20}$$

$$\sin\omega_0\left(\frac{\pi+\Delta T}{\omega}\right) \approx \sin(\tfrac{\omega_0}{\omega}\pi) + \cos(\tfrac{\omega_0}{\omega}\pi)\frac{\omega_0}{\omega}\Delta T \tag{4.21}$$

$$\cos(\Delta T + \theta_0 + \Delta\theta_0) \approx \cos\theta_0 - \sin\theta_0(\Delta T + \Delta\theta_0) \tag{4.22}$$

Note also that from the steady state solution

$$x\left(\frac{\pi}{\omega}\right) = A_0\cos(\tfrac{\omega_0}{\omega}\pi) + B_0\sin(\tfrac{\omega_0}{\omega}\pi) + \frac{P}{\omega^2-\omega_0^2}\cos\theta_0 = 0 \tag{4.23}$$

Substituting into (4.16) from (4.18), (4.19), (4.20), (4.21) and (4.22) and using (4.23) while keeping only the first order terms, we obtain, after simplification

$$d_1\Delta T + d_2\Delta\theta_0 + d_3\frac{\Delta\dot{x}_0}{\omega_0} = 0 \tag{4.24}$$

where the constants d_i, $i = 1,2,3$ are given in terms of parameters of the problem. Expressions for these constants are provided in appendix C.

The impact condition (3.1) at $\omega t = (\pi + \Delta t_0)^+$ gives

$$\begin{aligned} -(\dot{x}_0 + \Delta\dot{x}_0') &= a\dot{x}\left(\left(\frac{\pi}{\omega} + \Delta t_0'\right)^-\right) + bv(0 + \Delta t_0) \\ &= a\dot{x}\left(\left(\frac{\pi}{\omega} + \Delta t_0'\right)^-\right) + b(\dot{x}_0 + \Delta\dot{x}_0) \end{aligned} \tag{4.25}$$

The velocity $\dot{x}\left(\left(\frac{\pi}{\omega} + \Delta t_0'\right)^-\right)$ can be evaluated using (4.13) and (4.18)–(4.22). Keeping only first order terms, we obtain

$$\dot{x}\left(\left(\frac{\pi}{\omega} + \Delta t_0'\right)^-\right) = \dot{x}\left(\frac{\pi}{\omega}^-\right) + \hat{c}_1\Delta T + \hat{c}_2\Delta\dot{x}_0 + \hat{c}_3\Delta\theta_0 \tag{4.26}$$

where the coefficients $\hat{c}_i$, $i = 1,2,3$ are given in terms of parameters. The veloc-

ity $\dot{x}(\frac{\pi}{\omega}^-)$ is the velocity prior to impact in the steady state solution and can be evaluated from the known solution. Using (4.25), (4.26) and the fact that for the periodic solution $-\dot{x}_0 = a\dot{x}(\frac{\pi}{\omega}^-) + b\dot{x}_0$ we get

$$\frac{\Delta\dot{x}_0'}{\omega_0} = c_1\Delta T + c_2\Delta\theta_0 + c_3\frac{\Delta\dot{x}_0}{\omega_0} \tag{4.27}$$

The coefficients c_i, $i = 1,2,3$ are also given in appendix C. Using (4.17) ΔT can be eliminated from the problem and equations (4.24) and (4.27) can be put in matrix form as follows:

$$\begin{bmatrix} \Delta\theta_0' \\ \frac{\Delta\dot{x}_0'}{\omega_0} \end{bmatrix} = \begin{bmatrix} 1-\frac{d_2}{d_1} & -\frac{d_3}{d_1} \\ c_2 - c_1\frac{d_2}{d_1} & c_3 - c_1\frac{d_3}{d_1} \end{bmatrix} \begin{bmatrix} \Delta\theta_0 \\ \frac{\Delta\dot{x}_0}{\omega_0} \end{bmatrix} \tag{4.28}$$

Thus the transition matrix Q has the above entries for this problem. Let the characteristic polynomial of Q be

$$r(\lambda) = \lambda^2 - \alpha_1\lambda + \alpha_0 \tag{4.29}$$

Then, the stability of the steady state solution is determined by the values of the roots of this quadratic. Expressions for the coefficients α_1 and α_0 are derived in appendix C. We obtain:

$$\begin{aligned} \alpha_1 &= \frac{1}{a-2}\left\{\left[(a-1)^2\left(\frac{\omega}{\omega_0}\right)^2 - (a-1)\right] + \right. \\ &\qquad \left. + \left[(a+1) - (a-1)^2\left(\frac{\omega}{\omega_0}\right)^2\right]\cos(\tfrac{\omega_0}{\omega}\pi)\right\} \qquad (4.30) \\ \alpha_0 &= \frac{1}{a-2}\left\{\left[(a-1)^2\left(\frac{\omega}{\omega_0}\right)^2 - (1-a)\right]\cos(\tfrac{\omega_0}{\omega}\pi) - \right. \\ &\qquad \left. -(1-a)^2\left(\frac{\omega}{\omega_0}\right)^2 + 1 - 2a\right\} \qquad (4.31) \end{aligned}$$

and stability of the solution depends on the values of these coefficients.

Although the above are for the generic case, the procedure is the same for resonance and the other two special cases. The details for resonance are given in appendix C. The solutions for $\frac{\omega_0}{\omega} = l,\ l = 2,3,\ldots$ are simple enough to allow explicit evaluation of the eigenvalues of Q. In fact, for these solutions we can make statements concerning their stability which are not conditional on the values of the system parameters.

Consider first the solution for $\frac{\omega_0}{\omega} = 2l,\ l = 1,2,3,\ldots$. We find that

$$\Delta\theta_0' = \frac{a}{a-2}\Delta\theta_0 \tag{4.32}$$

$$\frac{\Delta\dot{x}_0'}{\omega_0} = -(a+b)\frac{\Delta\dot{x}_0}{\omega_0} = -\frac{\Delta\dot{x}_0}{\omega_0} \tag{4.33}$$

Thus, Q is diagonal and the two eigenvalues are

$$|\lambda_1| = \left|\frac{a}{a-2}\right| < 1 \tag{4.34}$$

$$\lambda_2 = -1 \tag{4.35}$$

The conclusion from (4.34) is that perturbations in the phase angle decrease. However, we cannot make any statement concerning perturbations of the velocity because in this case stability is *marginal* and linear theory is not adequate. Note that these solutions belong to the larger class of nonsymmetric solutions and will be discussed later.

For $\frac{\omega_0}{\omega} = 2l+1,\ l = 1,2,3,\ldots$ we find that

$$\Delta\theta_0' = \Delta\theta_0 \tag{4.36}$$

$$\frac{\Delta\dot{x}_0'}{\omega_0} = (a-b)\frac{\Delta\dot{x}_0}{\omega_0} \tag{4.37}$$

As a result

$$\lambda_1 = 1, \quad |\lambda_2| = |a-b| < 1$$

and we have another *marginal* case except that here it is the velocity perturbations that die out.

In the case of resonance we find that

$$\Delta\theta_0' = \frac{a}{1+b}\Delta\theta_0 \tag{4.38}$$

$$\frac{\Delta\dot{x}_0'}{\omega_0} = (a-b)\frac{\Delta\dot{x}_0}{\omega_0} + \frac{2Pab}{(1+b)\omega_0}\Delta\theta_0 \tag{4.39}$$

Since

$$|\lambda_1| = \left|\frac{a}{a+b}\right| < 1 \qquad \text{and} \qquad |\lambda_2| = |a-b| < 1 \tag{4.40}$$

the resonance solution is always stable.

While expressions (4.30) and (4.31) enable us to compute the eigenvalues of Q for specific cases, it is important to determine the regions in parameter space where solutions are stable. The boundaries of this region can be determined without explicit knowledge of the eigenvalues themselves. Because $r(\lambda)$ is quadratic there are two possibilities for the roots on the boundary:

1. λ_1, λ_2 are complex, $\lambda_2 = \overline{\lambda}_1$ and $|\lambda_1| = 1$.

2. λ_1, λ_2 are real, $|\lambda_1| > |\lambda_2|$ and $|\lambda_1| = 1$.

In the first case

$$\lambda_1\overline{\lambda}_1 = \alpha_0 = |\lambda_1|^2 \tag{4.41}$$

so that on the boundary $\alpha_0 = 1$

$$\Longrightarrow \cos\left(\tfrac{\omega_u}{\omega}\pi\right)\left[(1-a)^2\left(\frac{\omega}{\omega_0}\right)^2 - (1-a)\right] - (1-a)^2\left(\frac{\omega}{\omega_0}\right)^2 + 1 - 2a = a - 2$$

Solving for a we find[2]

$$a = 1 - \frac{\cos\left(\tfrac{\omega_u}{\omega}\pi\right) - 3}{\left(\tfrac{\omega}{\omega_0}\right)^2\left[\cos\left(\tfrac{\omega_u}{\omega}\pi\right) - 1\right]} \tag{4.42}$$

[2]The other root, $a = 1$, is not a possible parameter for the problem.

When the roots are real and the largest is equal to ± 1 we obtain from (4.29)

$$1 - \alpha_1 \lambda + \alpha_0 = 0 \implies 1 + \alpha_0 = \pm \alpha_1$$

Assume first that $\lambda_1 = -1$. Substituting above for α_1 and α_0 from (4.30) and (4.31) we obtain

$$2a \left[1 - \cos\left(\tfrac{\omega_0}{\omega}\pi\right)\right] = 0$$

Since the term in the brackets is different from zero, it follows that $a = 0$. However, zero is not in the range of values of a and as a result the possibility that $\lambda = -1$ does not exist. Using the positive sign we obtain

$$\left(\frac{\omega}{\omega_0}\right)^2 (a-1)^2 \left[\cos\left(\tfrac{\omega_0}{\omega}\pi\right) - 1\right] = 1 + \cos\left(\tfrac{\omega_0}{\omega}\pi\right)$$

which does not have any solution because the left hand side is always negative while the right is always positive. Thus, $\lambda = 1$ is an impossible case. The stability boundary is therefore given by (4.42).

The stability diagram is shown in figure 4.1. The lines $a = 1$ and $a = 0$ are shown as boundary lines but clearly they do not belong to the region of stability. The vertical lines at $\frac{\omega}{\omega_0} = \frac{1}{l}$, $l = 2,3,4,\ldots$ are meant to indicate that those points represent marginal stability. Near resonance, the region of practical interest, periodic solutions are stable. The right boundary, represented by (4.42) approaches a horizontal asymptote which can be found from that expression. Let $\frac{\omega}{\omega_0} = \eta$ and expand $\cos\left(\frac{\omega_0}{\omega}\pi\right)$ in a Taylor series about zero. Then we get from (4.42)

$$a = 1 - \frac{1 - \frac{1}{2!}\frac{\pi^2}{\eta^2} + \frac{1}{4!}\frac{\pi^4}{\eta^4} - \cdots - 3}{\eta^2 \left[1 - \frac{1}{2!}\frac{\pi^2}{\eta^2} + \frac{1}{4!}\frac{\pi^4}{\eta^4} - \cdots - 1\right]}$$

Thus

$$\lim_{\eta \to \infty} a = 1 - \frac{4}{\pi^2} \approx 0.595 \tag{4.43}$$

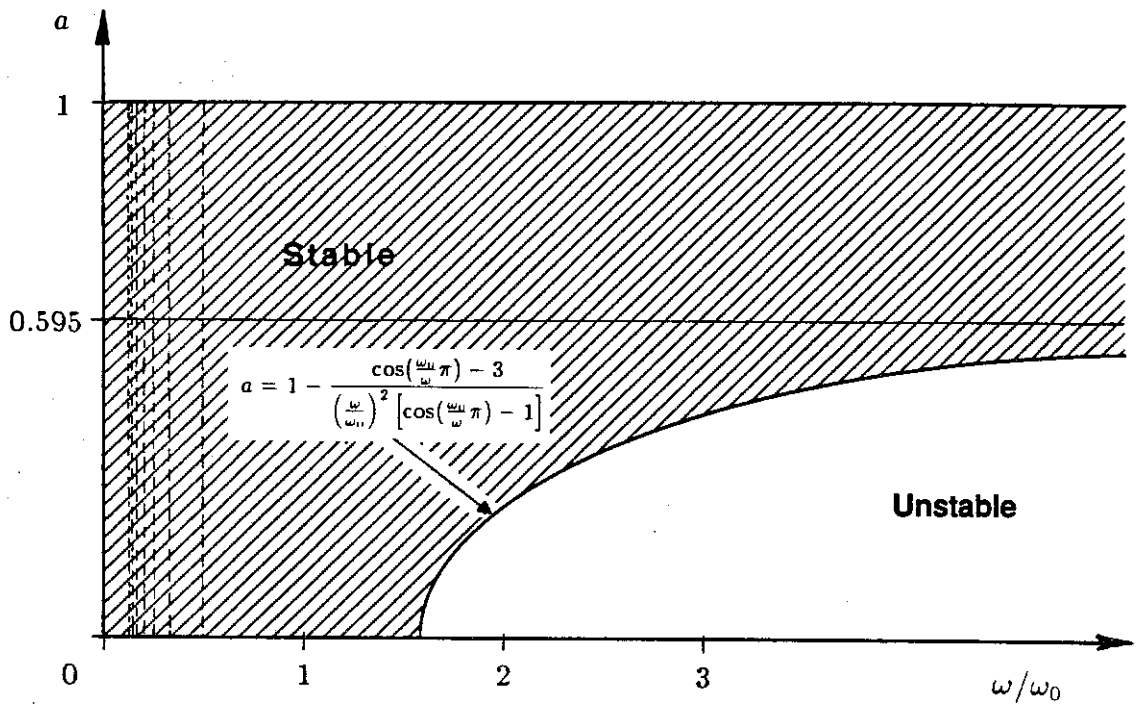

Figure 4.1: Stability diagram of symmetric solutions.

The magnitude of the largest eigenvalue is also plotted as a function of the frequency ratio in figures 4.2 and 4.3. The relative maxima in the region below resonance correspond to the singular frequency ratios $1/l$ and have value one. For the case $a = 0.7 > 0.595$ the magnitude is always less than one and all solutions are stable as expected.

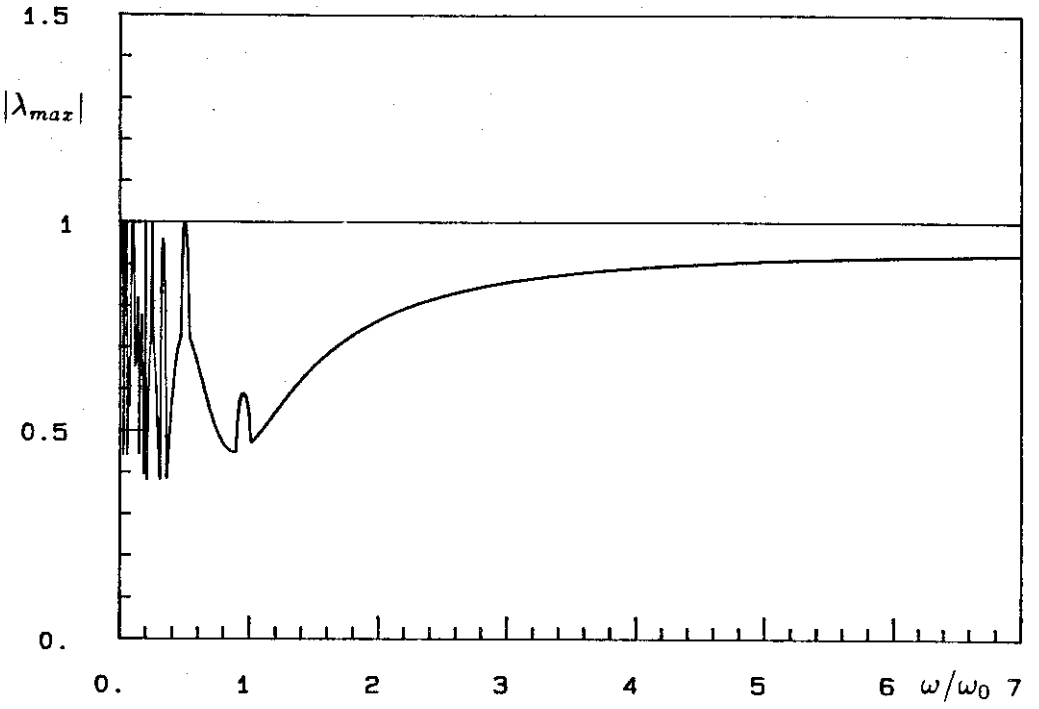

Figure 4.2: Magnitude of largest eigenvalue, $a = 0.7$.

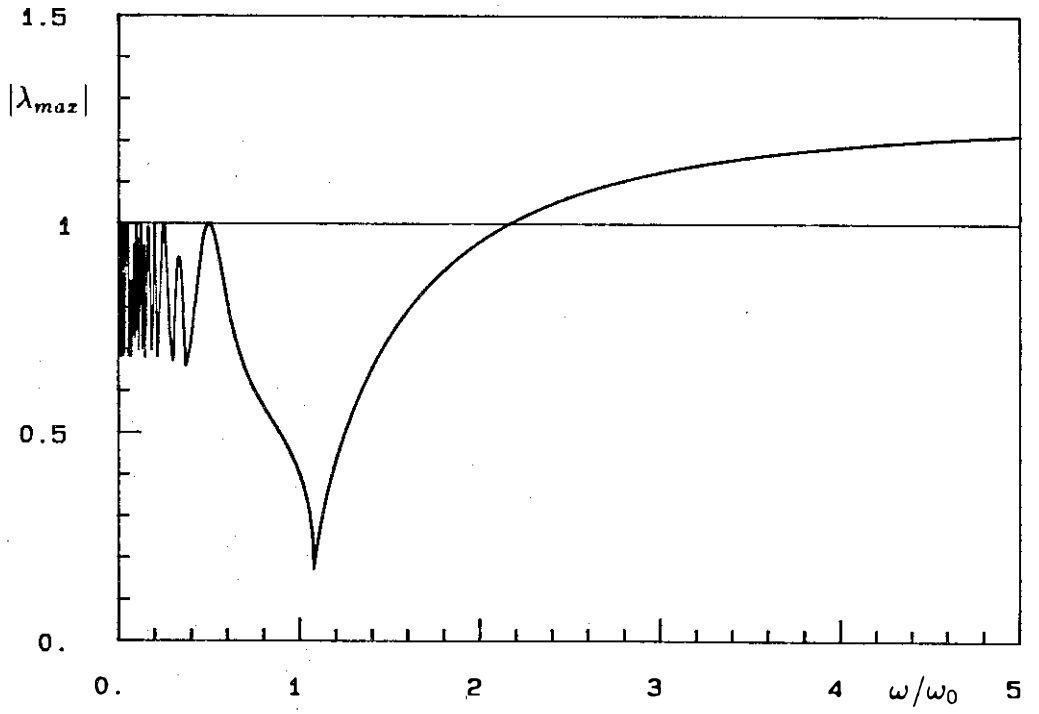

Figure 4.3: Magnitude of largest eigenvalue, $a = 0.3$.

4.2.2 Nonsymmetric Solutions

Due to lack of symmetry, the procedure is slightly different in this case. While in analyzing the symmetric type it is necessary to consider only half the cycle the other half being being identical, here we must consider both halves.

Recall that nonsymmetric solutions are characterized by

$$\frac{\omega_0}{\omega} = 2l,\ l = 1,2,\ldots; \qquad \theta_0 = -\frac{\pi}{2}; \qquad \dot{x}_0 \leq \frac{2Pa\omega}{\omega_0^2 - \omega^2} \tag{4.44}$$

and there are infinitely many. Because these solutions lie infinitely close to each other in phase space, it is evident that they must be neutrally stable. For, if one solution is perturbed slightly, the resulting motion will be on the orbit of a nearby solution and, therefore, stay there, the initial perturbation never decreasing.

More formally, this can be shown as follows. Let the perturbations in phase angle and velocity be as before. Because of (4.44), the zero-displacement condition (4.16) yields:

$$\Delta\theta_0' = \left[1 - \frac{1}{1 - \frac{\dot{x}_0(\omega_0^2 - \omega^2)}{2P\omega}}\right] \Delta\theta_0$$

Now, let $\gamma \in [0,1]$ and suppose

$$\dot{x}_0 = \gamma \frac{2Pa\omega}{\omega_0^2 - \omega^2}$$

Then

$$\Delta\theta_0' = \left[1 - \frac{1}{1 - \gamma a}\right] \Delta\theta_0 \tag{4.45}$$

Let $-\dot{x}_1$ be the initial velocity for the other arc. Then, we get

$$\Delta\theta_0'' = \left[1 - \frac{1}{1 - \frac{\dot{x}_1(\omega_0^2 - \omega^2)}{2P\omega}}\right] \Delta\theta_0'$$

But $\dot{x}_0 + \dot{x}_1 = \frac{2Pa\omega}{\omega_0^2 - \omega^2}$ and therefore

$$\dot{x}_1 = (1 - \gamma)\frac{2Pa\omega}{\omega_0^2 - \omega^2}$$

Substituting above for $\dot{x}_1$ we obtain

$$\Delta\theta_0'' = \left[1 - \frac{1}{1-(1-\gamma)a}\right]\Delta\theta_0' \tag{4.46}$$

For the complete cycle we then get

$$\Delta\theta_0'' = \left[1 - \frac{1}{1-\gamma a}\right]\left[1 - \frac{1}{1-(1-\gamma)a}\right]\Delta\theta_0$$

which reduces to

$$\Delta\theta_0'' = \frac{1}{1+\frac{(1-a)}{\gamma(1-\gamma)a^2}}\Delta\theta_0 \tag{4.47}$$

Now, $1-a > 0$ and $1-\gamma > 0 \Rightarrow \frac{(1-a)}{\gamma(1-\gamma)a^2} > 0$. Hence $\Delta\theta_0'' < \Delta\theta_0$ and these solutions are phase stable.

The impact condition (4.25) for the first arc yields

$$\frac{\Delta\dot{x}_1}{\omega_0} = -(a+b)\frac{\Delta\dot{x}_0}{\omega_0} = -\frac{\Delta\dot{x}_0}{\omega_0}$$

Similarly, for the other arc

$$\frac{\Delta\dot{x}_0'}{\omega_0} = -(a+b)\frac{\Delta\dot{x}_1}{\omega_0} = -\frac{\Delta\dot{x}_1}{\omega_0}$$

Hence $\frac{\Delta\dot{x}_0'}{\omega_0} = \frac{\Delta\dot{x}_0}{\omega_0}$ which confirms the earlier statement, namely that nonsymmetric solutions are *neutrally stable.*

4.2.3 Subharmonic Solutions

The solutions under consideration are only those special cases for which

$$\frac{\omega_0}{\omega} = \frac{1}{2l+1},\ l = 1,2,\ldots; \qquad \theta_0 = -\frac{\pi}{2}; \qquad \dot{x}_0 = x_0 = 0 \tag{4.48}$$

and are symmetric with 2 impacts/cycle. Because of the similarity of these subharmonic solutions to the harmonic orbits with $\frac{\omega_0}{\omega} = 2l+1$, one would expect similar stability characteristics, and, indeed, that is the case.

The stability analysis is identical to that of the harmonic case except that here impact occurs at $t_1 = \frac{\pi}{\omega_0} \Rightarrow \cos\omega_0 t_1 = -1,\ \sin\omega_0 t_1 = 0$. This results in perturbation equations which are the same as (4.36) and (4.37). Thus, subharmonic solutions of this type are *marginally* stable in phase and stable in the initial velocity.

5

Chaotic Motions

Having determined the periodic solutions and having established their stability characteristics, we turn now our attention to the region in parameter space where these solutions are unstable in order to determine the behavior of the system there.

One would expect other types of "regular" solutions such as subharmonic solutions to be stable there, but, as was pointed out in chapter 3, such solutions, if they exist, are unstable. With the exception of a few subharmonic motions discussed earlier, other such solutions cannot be found analytically because of the difficulty in solving the transcendental equations involved.

It turns out that in the region of instability of the harmonic solutions, motions are either quasiperiodic or chaotic. A typical time series is shown in figure 5.1 for $a = 0.3$ and $\omega/\omega_0 = 4$ where the motion of the system is recorded after 100 cycles of the excitation torque. Close observation reveals that there is no regularity of motion even though one would expect all transients to have died out.

It is generally believed today that chaotic motions of deterministic systems are the rule rather than the exception and are exhibited by even the simplest dynamical systems. As a result, even though evidence in the form of the irregular time series shown in figure 5.1 cannot be conclusive, we proceed in this chapter to describe and investigate the nature of chaotic motions exhibited by the impact damper. First we need a brief discussion on chaos in deterministic systems as well as the associated

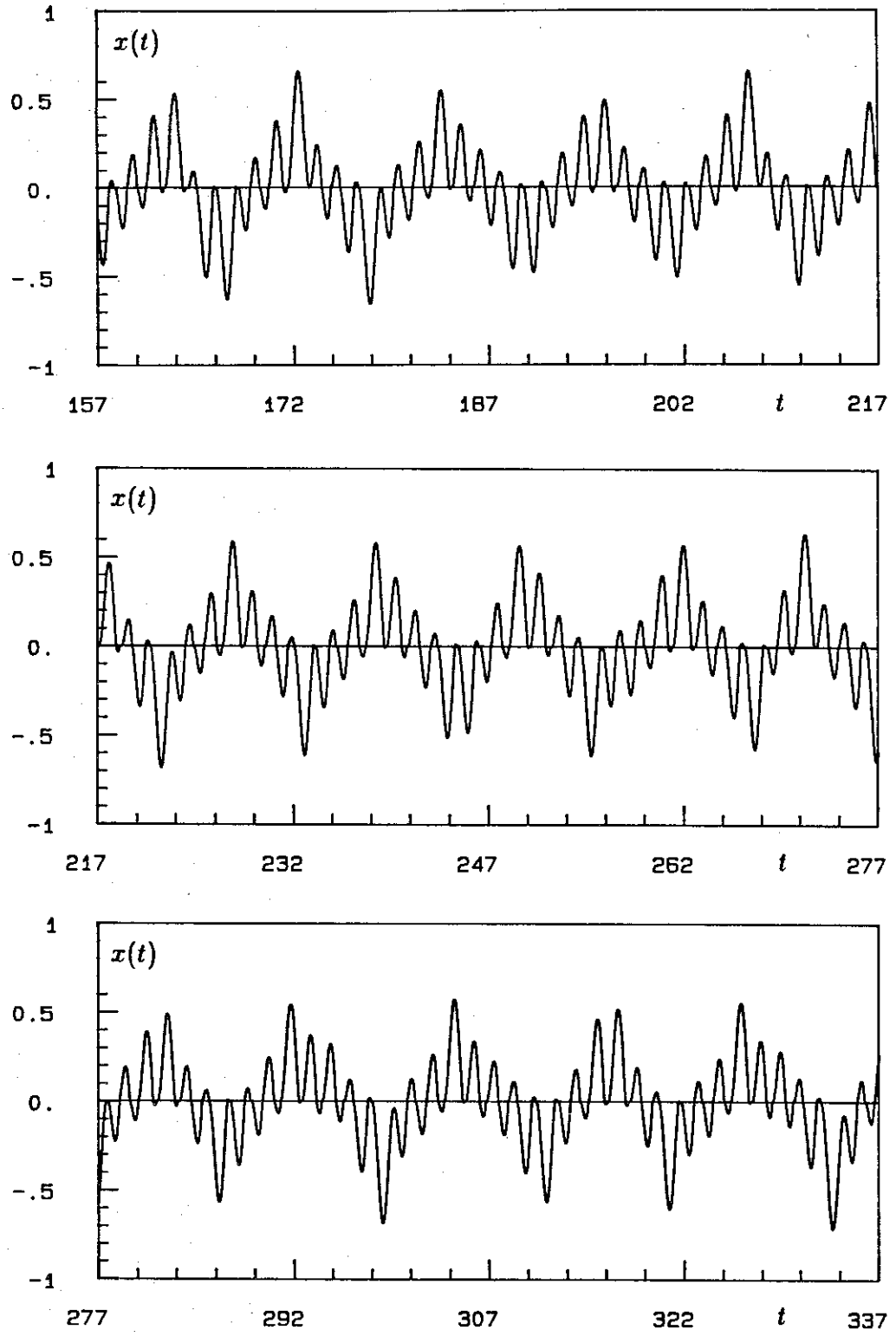

Figure 5.1: Solution plotted after 100 cycles, $a = 0.3$, $\frac{\omega}{\omega_n} = 4$.

methodology.

5.1 General Considerations

Since the purpose of the system under investigation is to provide damping, from the engineering point of view, the global results given in chapter 2 concerning the ultimate boundedness of solutions as well as the fact that even near resonance the amplitude of oscillations is relatively small, would be adequate. However, there has been growing interest in the steady state, nonperiodic response of dynamical systems for a number of reasons.

Besides the fact that these systems are interesting in their own right, such behavior, apparently chaotic motions from deterministic equations, is exhibited by systems from as diverse fields as electrical circuits, meteorology, elastic structures [3,5,10], biological systems [7] e.t.c.. Also, Shaw [11,12,13] has reported the existence of chaotic motions in impact dampers described by a second order system. In such problems, conventional methods of analysis such as perturbation methods clearly do not work and new approaches are needed.

Second, up until recently, such lack of regularity in the steady state response of a deterministic system was attributed to random inputs not measured, lack of accuracy in monitoring the response and/or the initial conditions as well as the random variation of some system parameter. Clearly, the existence of chaotic motions in a deterministic system indicates that not all such behavior is due to stochastic inputs but may well be an inherent system characteristic.

In such cases, the system motion is limited within a bounded region but does not involve what is considered "regular" motion, i.e., limit cycles, periodic solutions or motion near an equilibrium state. The term "strange attractor" is often used to classify bounded chaotic motions in contrast to the regular attractors mentioned above.

There is a variety of methods for determining whether a system is truly chaotic

or not and which provide useful information on the system characteristics: (a) Time histories, (b) Phase plane portraits, (c) Fourier transforms, (d) Poincaré maps and (e) computation of Lyapunov exponents. The first three are well known while the last two, although not new, have proven most useful in analyzing chaotic motions and have received considerable attention lately.

Put simply, the Poincaré map provides information on the state of the system at discrete instants in time, thereby causing possible motion regularity or pattern to surface. Of a more quantitative nature is the computation of Lyapunov exponents to be defined more precisely later. It is generaly accepted that a positive Lyapunov exponent is indicative of chaotic nature of a system and, therefore, provides a criterion for testing such behavior.

5.2 The Poincaré Map

Consider the dynamical system $\dot{\mathbf{x}} = \mathbf{f}(\mathbf{x})$, where $\mathbf{x}(t) \in \mathbb{R}^n$ and $\mathbf{f} : U \longrightarrow \mathbb{R}^n$, $U \subseteq \mathbb{R}^n$. We define [5] the flow ϕ_t associated with the system as a smooth function such that

$$\phi_t : U \longrightarrow \mathbb{R}^n, \quad \phi_t(\mathbf{x}) = \phi(\mathbf{x}, t); \quad \mathbf{x} \in U, \ t \in (a, b) \subseteq \mathbb{R}$$

with

$$\frac{d}{dt}(\phi(\mathbf{x}, t)) = \mathbf{f}(\phi(\mathbf{x}, t))$$

Clearly $\phi_{t+s} = \phi_t \circ \phi_s$ and if $\mathbf{x}(0) = \mathbf{x}_0$, then $\phi(\mathbf{x}_0, 0) = \mathbf{x}_0$. In this case, $\phi(\mathbf{x}_0, \cdot)$ defines a trajectory of the differential equation starting at $\mathbf{x}_0$.

Now, let Γ be a periodic orbit of ϕ_t in $\mathbb{R}^n$ and $\Sigma \subset \mathbb{R}^n$ be a local cross section of dimension $n - 1$ as shown in figure 5.2. The surface Σ must be chosen so that the flow is transverse to it. Let p be the point of intersection of Σ with Γ and let $V \subset \Sigma$ be some neighborhood of p. Then, the Poincaré map $\Pi : V \longrightarrow \Sigma$ is defined [5] for a point $q \in V$ by

$$\Pi(q) = \phi_\tau(q)$$

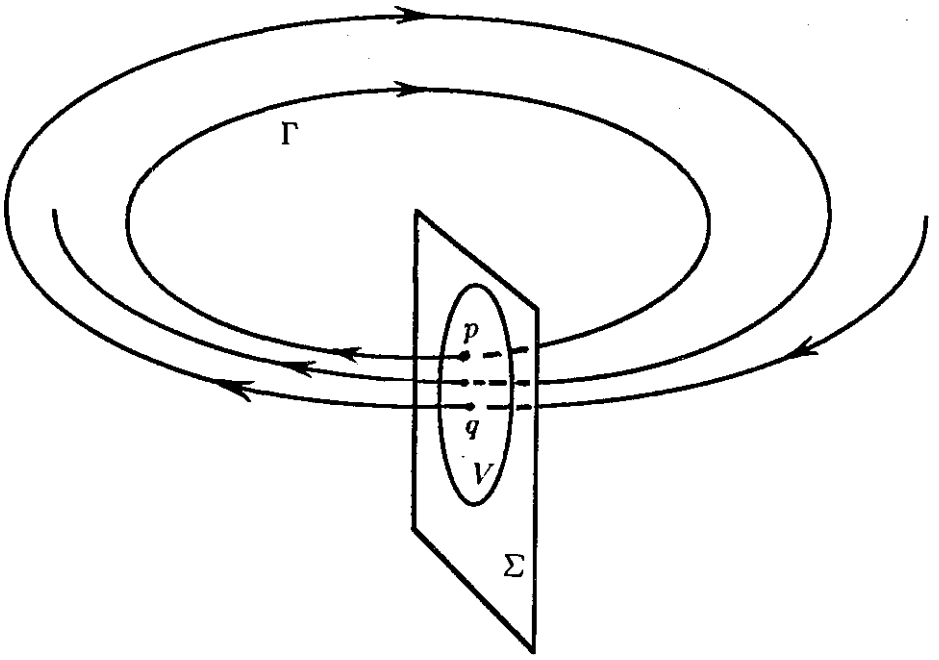

Figure 5.2: Poincaré map

where τ is the time taken for trajectory $\phi(q)$ starting at q to first return to Σ. Clearly p is a fixed point of $\mathbf{\Pi}$ and, if T is the period of Γ, then $\tau \longrightarrow T$ as $q \longrightarrow p$. Moreover, the stability characteristics of Γ are reflected on the stability characteristics of q.

Note that the choice of Σ is arbitrary and is made so as to best suit the problem. It can also be interpreted [3] as the occurrance of an event. In fact, in proving Lemma 2 of chapter 2, we have implicitly used the occurrance of an impact ($x = 0$) to monitor the distance of an arbitrary trajectory of the auxilliary system (2.8) from the limit cycle $\mathcal{L}(T, \beta)$. In that case, the implicit Poincaré section was

$$\Sigma = \left\{(x, u, v) \in \mathbb{R}^3 : \; x = 0, \; \dot{x} = u = v = \dot{y}\right\}$$

In the case of a periodically forced oscillation, the system is $\dot{\mathbf{x}} = \mathbf{f}(\mathbf{x}, t)$, $(\mathbf{x}, t) \in \mathbb{R}^n \times \mathbb{R}$ where $\mathbf{f}(\cdot, t) = \mathbf{f}(\cdot, t + T)$ is periodic in t with period T. Then, t may be included as an explicit state variable by defining $\vartheta = \omega t$, where $\omega = \frac{2\pi}{T}$ is

the frequency of the field vector $\mathbf{f}$. Therefore

$$\begin{aligned} \dot{\mathbf{x}} &= \mathbf{f}(\mathbf{x}, \vartheta) \\ \dot{\vartheta} &= \omega \end{aligned}$$

In this case, we can define a global cross section Σ as

$$\Sigma = \{(\mathbf{x}, \vartheta) \in \mathbb{R}^n \times S : \ \vartheta = \theta_0\}$$

where $S = [0, 2\pi)$. Here all solutions cross Σ transversely and the Poincaré map Π is defined globally. With Π defined as such, the state of the system is monitored at times $\theta_0 + k\frac{2\pi}{\omega}$, $k = 0, 1, 2, \ldots$ and the term "stroboscopic view" has often been used to describe the action of Π.

As in the case of the autonomous system, a periodic solution of $\dot{\mathbf{x}} = \mathbf{f}(\mathbf{x}, t)$ corresponds to a fixed point of Π and, if such a solution is stable, then so is the fixed point of Π. As a result, repeated iteration of Π on some initial point will generate a sequence of points on Σ which will converge to the fixed point. Similarly, the existence of a subharmonic solution will correspond to a finite number of points on Σ. If the solution is subharmonic of order m, then there will be m periodic points of Π in Σ.

It follows from the above that successive iteration of the Poincaré map which leads to an infinite number of points on Σ indicates that the behavior of the system is chaotic, never achieving any of the so called "regular" motions. Thus, a strange attractor of the dynamical system corresponds to a strange attractor of the Poincaré map Π.

In the case of the impact damper, the system is 4th order (including time) and therefore Σ is a surface in $\mathbb{R}^3$. Projections on the $x - \dot{x}$, $\dot{x} - v$ and $v - x$ planes of the points in the attracting set are shown in figures 5.3, 5.4 and 5.5 respectively for a test case with $a = 0.3$, $\omega_0 = 1$, $\omega = 5$ and $\theta_0 = -\pi/2$. There are 3000 points which have been recorded at half-period, giving two groups of points which

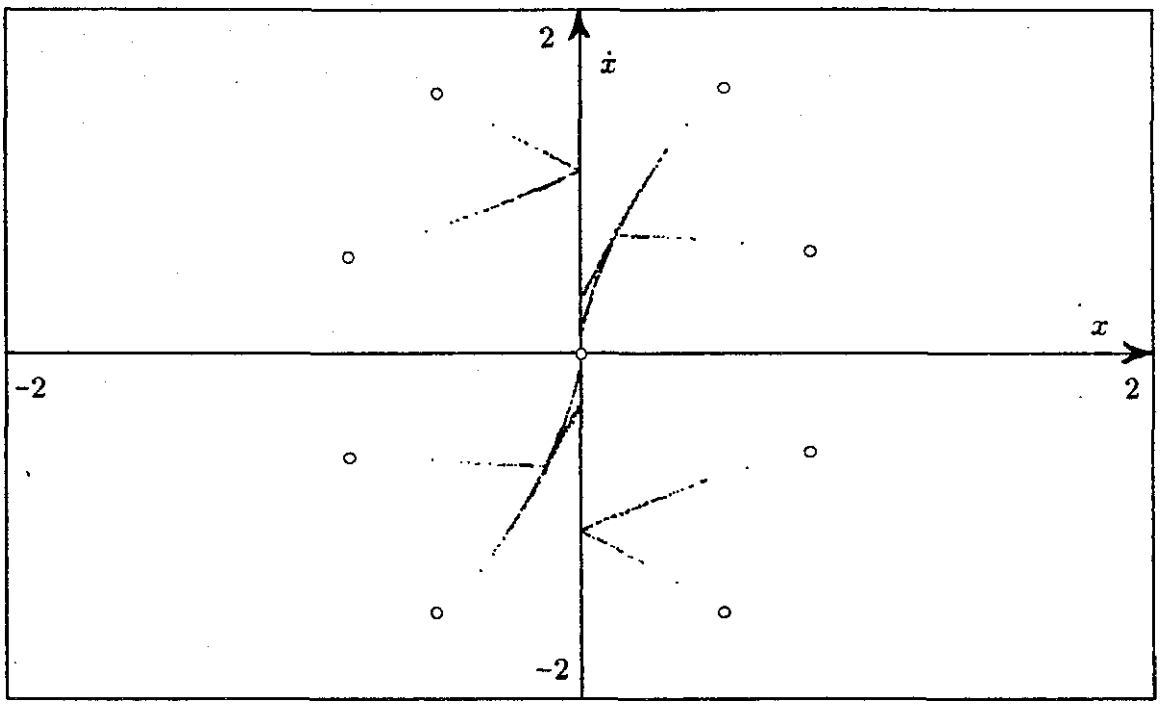

Figure 5.3: Poincaré map, $x - \dot{x}$ projection, 3000 points, $a = 0.3$, $\frac{\omega}{\omega_0} = 5$.

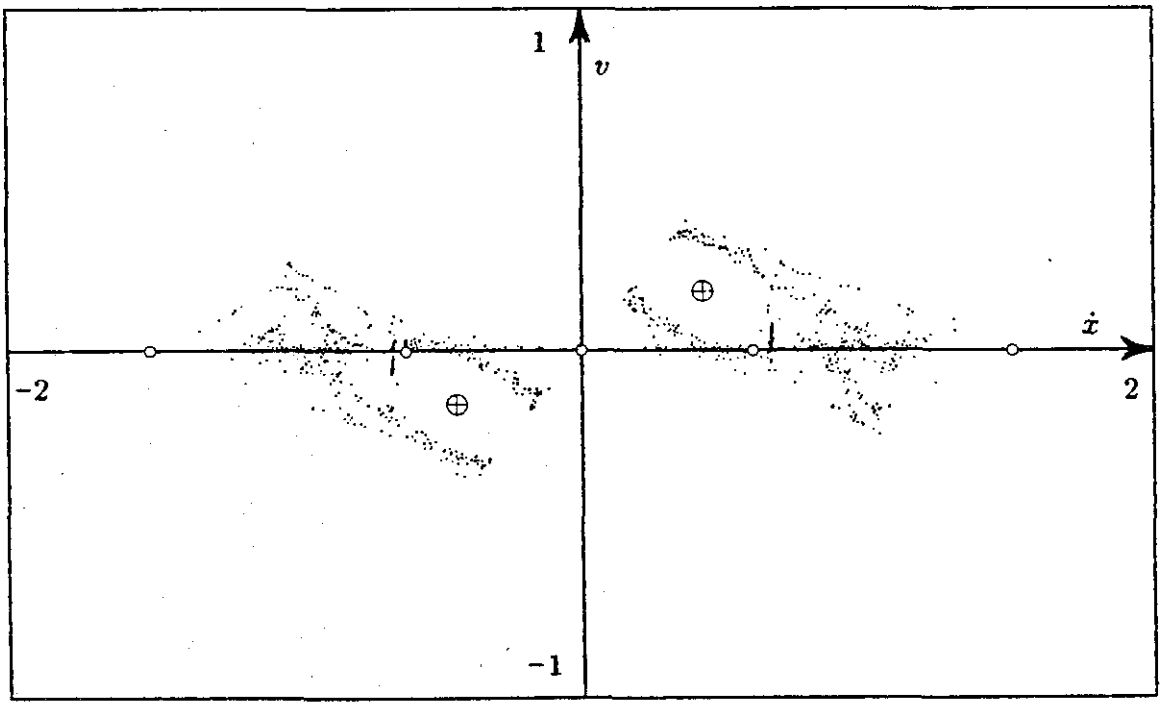

Figure 5.4: Poincaré map, $\dot{x} - v$ projection, 3000 points, $a = 0.3$, $\frac{\omega}{\omega_0} = 5$.

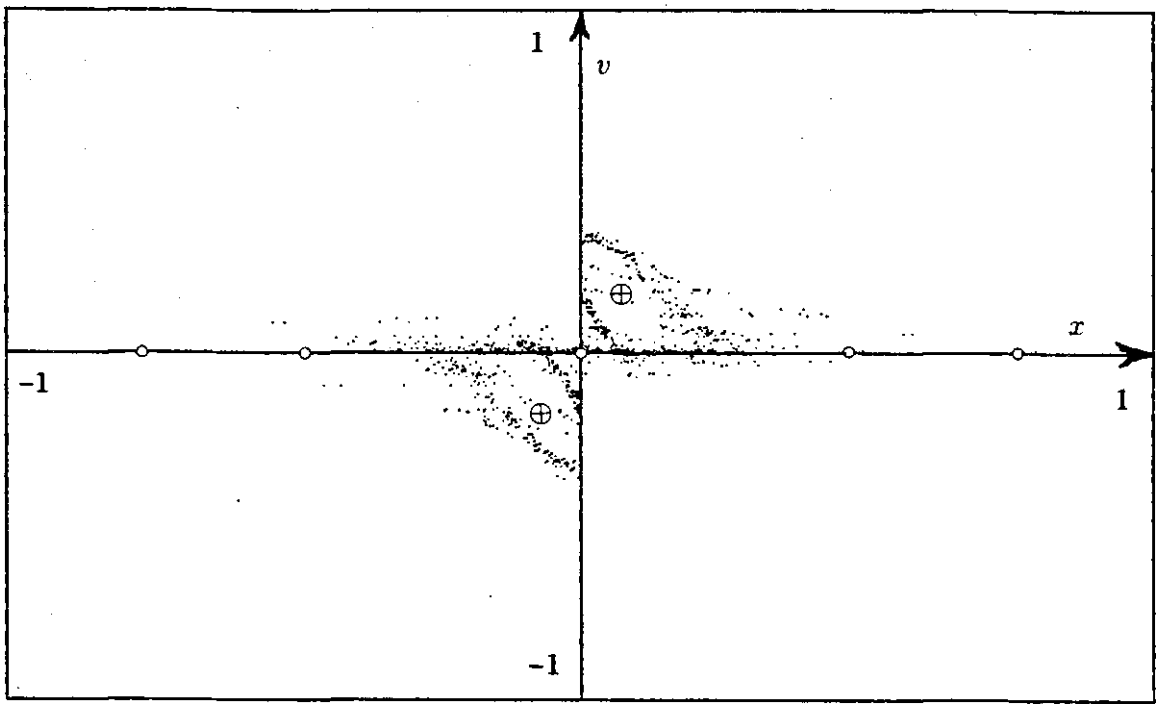

Figure 5.5: Poincaré map, $x - v$ projection, 3000 points, $a = 0.3$, $\frac{\omega}{\omega_0} = 5$.

are almost symmetric about the origin. The $x - \dot{x}$ projection consists of five distinct lines which intersect in pairs. They are relatively sharp and well defined which is atypical. The patterns in the other two projections are not so well defined with points appearing in clusters, and appear to be more typical of their kind. The periodic solution is also shown in these plots with a $\oplus$ while the points resulting from the subharmonic of order 5 are indicated with a circle. A three dimensional representation of the attractor is also shown in figure 5.6. Similar plots for $\frac{\omega}{\omega_0} = 3, 4$ also feature the sharp lines on the $x - \dot{x}$ plane except that in these cases there are three and four lines respectively.

Phase plane portraits of the chaotic trajectories are not very illuminating for two reasons. First, there is the difficulty of a two dimensional representation of three dimensional intersecting curves, which of course is not peculiar to this problem. This difficulty can be bypassed if the trajectories are smooth as is the case of the Lorentz

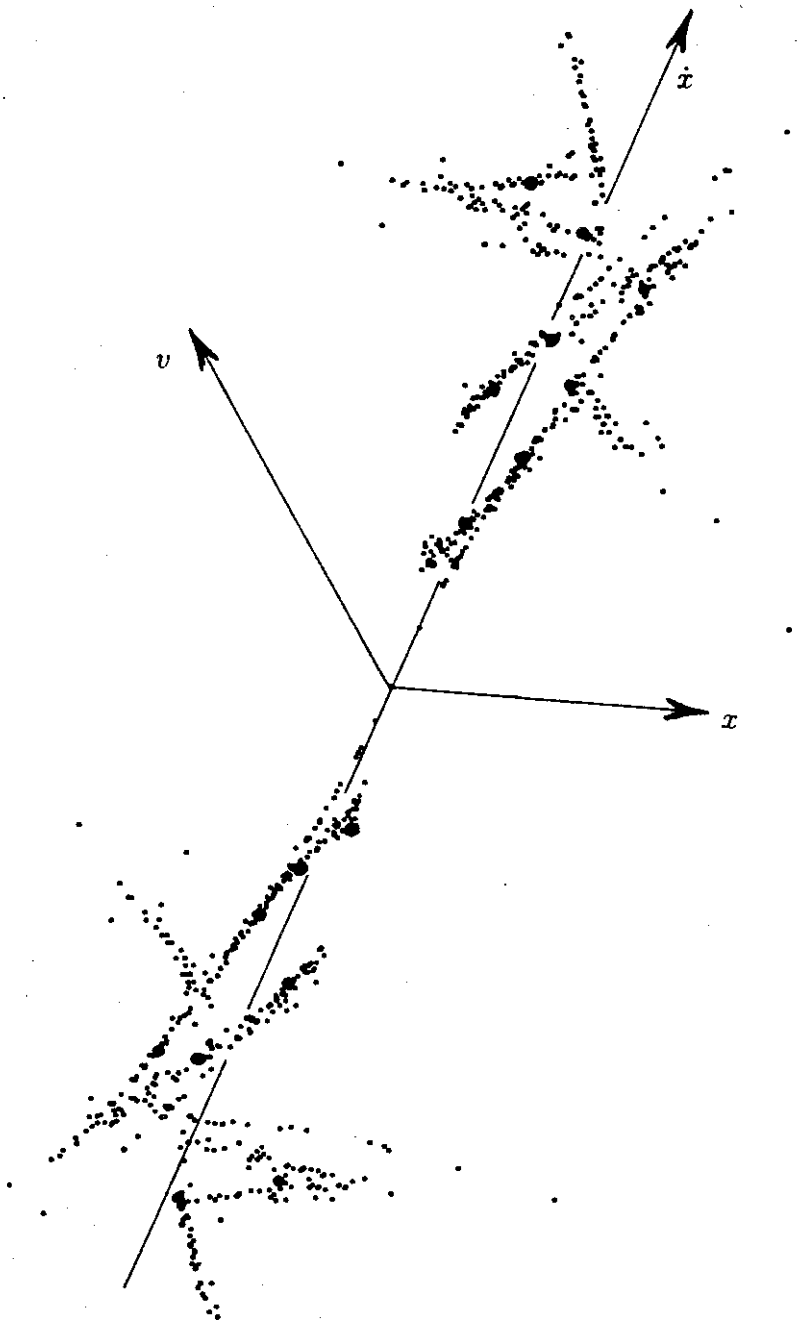

Figure 5.6: Three dimensional representation of the attractor, $a = 0.3$, $\frac{\omega}{\omega_0} = 5$.

and Roessler attractors. However, in the case of the impact damper, trajectories are discontinious and this, in fact, is the second source of complication.

Trajectories of periodic solutions shown so far are misleading in the sense that they only show jumps in the primary mass velocity $\dot{x}$ when $x = 0$. However, each arc of these orbits lies on a plane where the auxilliary mass velocity v is constant. These planes are perpendicular to the $v-$ axis and intersect it at $v = \pm\dot{x}_0$. Thus, every impact involves a discontinuity in $\dot{x}$ as well as a jump from one plane to another. In an arbitrary trajectory of course, v takes on many values and, therefore, jumps in v involve many planes. In the case of chaotic motions, the number of these planes is infinite. The result of transfers from plane to plane is to make the projection of the attractor on a two dimensional surface appear more complicated than it actually is.

The above features are are shown in figures 5.7abc where projections of a chaotic trajectory on the three coordinate planes are drawn for the test case $a = 0.5, \frac{\omega}{\omega_0} = 5$. Note that all motion is confined to a relatively small volume around the origin, in agreement with the theorem in chapter 2. Figure 5.7b shows a number of the planes involved and they are represented by horizontal lines perpendicular to the $v-$ axis. More informative is figure (c) where, lines parallel to the $\dot{x}-$axis represent trajectory arcs between impacts. All these lines originate from points along the line $\dot{x} = v$. Transfers to another $v = constant$ plane occur along straight lines all of which have the same slope. After each impact, the new $v = constant$ plane passes through the point where the transfer line first intersects the line $\dot{x} = v$.

The slope of the transfer lines depends only on the impact parameter a and can be found from

$$\text{slope} = s = \frac{\dot{x}(t^+) - \dot{x}(t^-)}{v(t^+) - v(t^-)}$$

where the usual notation is used for quantities before and after impact. Since $\dot{x}(t^+) = v(t^+) = a\dot{x}(t^-) + bv(t^-)$ we find

$$s = \frac{(a-1)\dot{x}(t^-) + bv(t^-)}{a\dot{x}(t^-) + (b-1)v(t^-)}$$

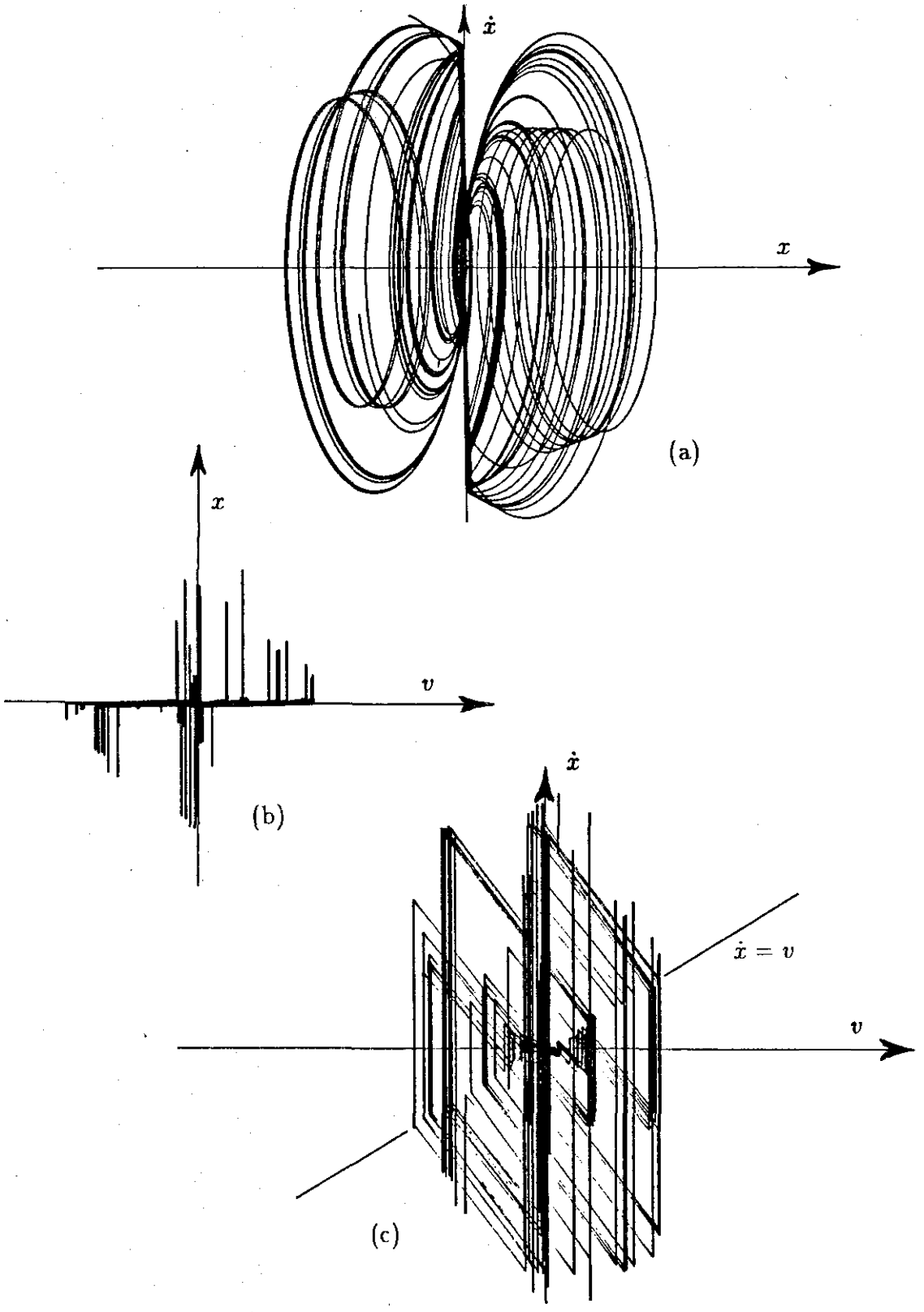

Figure 5.7: Projections of the phase plane portrait of a chaotic trajectory on the three coordinate planes. $a = 0.3$, $\frac{\omega}{\omega_n} = 5$.

Hence

$$s = \frac{-b\dot{x}(t^-) + bv(t^-)}{a\dot{x}(t^-) - av(t^-)} = -\frac{b}{a} = 1 - \frac{1}{a} < 0$$

Of more traditional nature is the computation of the steady state response spectrum. If the motion is periodic, the spectrum is discrete. On the other hand, a stochastic or chaotic signal will produce a continuous spectrum. Figures 5.8 and 5.9 show the 1024-point FFT for two impact parameters, $a = 0.9$ and $a = 0.3$ ($\omega/\omega_0 = 5$) respectively. The first case is well within the stability region of the periodic solutions, the response being periodic with frequency 5. This is confirmed in fig. 5.8 where a sharp peak is present at $\omega = 5$. In contrast, the spectrum for $a = 0.3$ is continuous with two dominant peaks at $\omega \approx 0.7$ and $\omega = 5$. The fact that the spectrum is continuous confirms the results obtained so far from the Poincaré map.

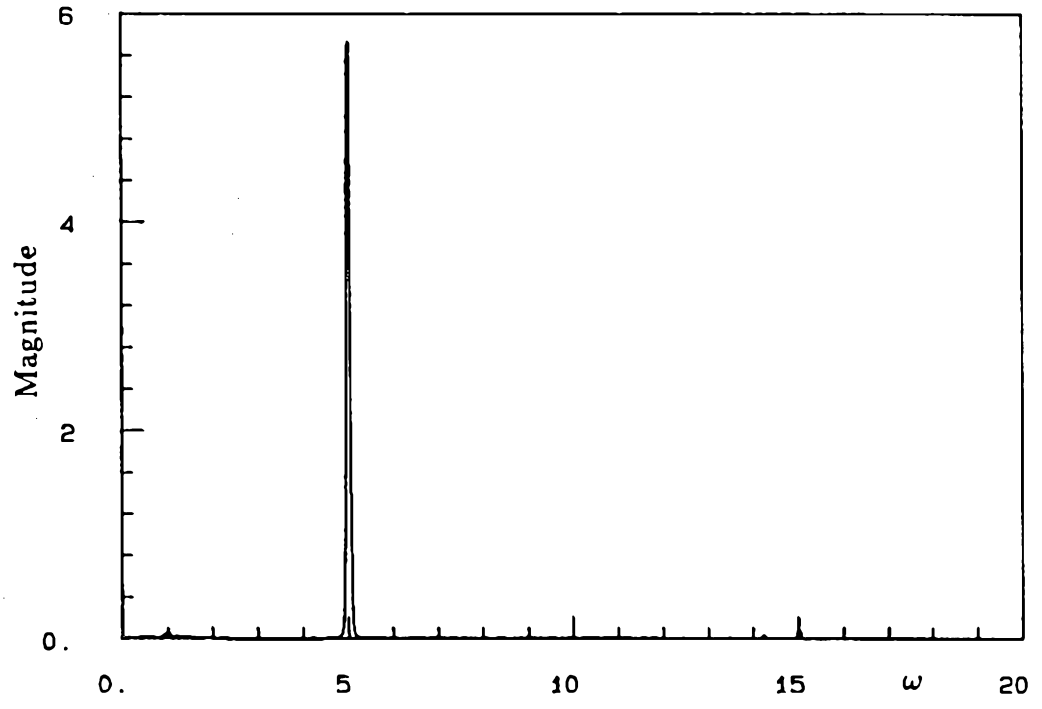

Figure 5.8: Response spectrum, $a = 0.9$, $\frac{\omega}{\omega_n} = 5$.

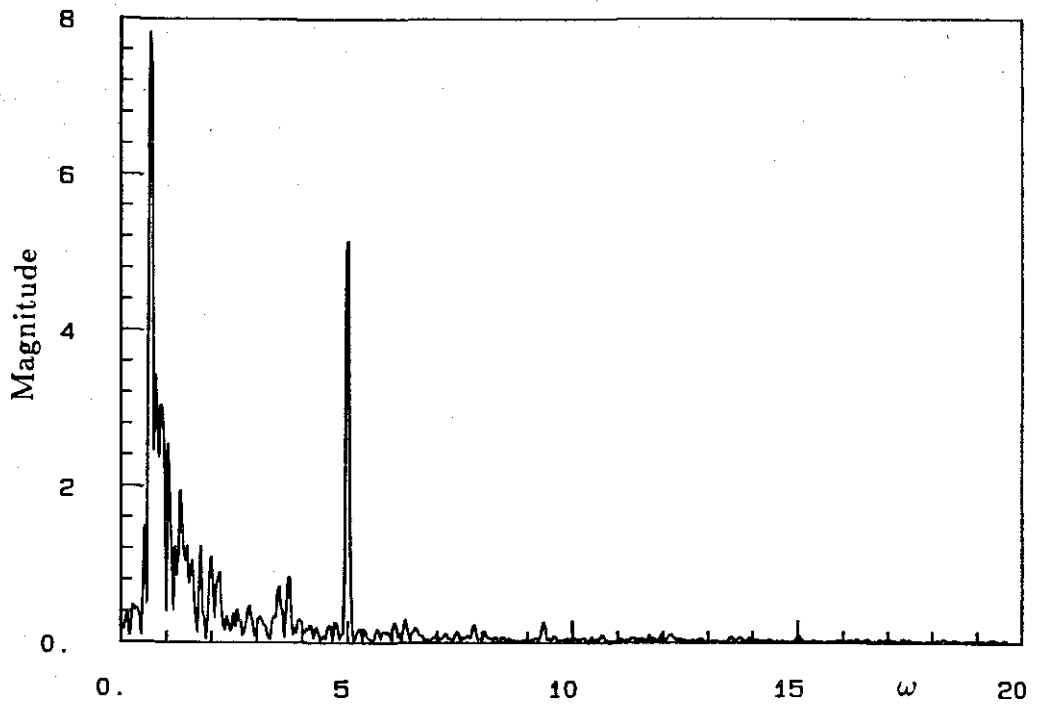

Figure 5.9: Response spectrum, $a = 0.3$, $\frac{\omega}{\omega_0} = 5$.

5.3 Lyapunov Exponents

The Lyapunov exponents can be used to quantify chaos in some sense, providing average exponential rates of divergence or convergence of nearby trajectories in phase space. Other similar measures are also defined but computational problems limit their range of applications. In fact, the computation of Lyapunov exponents is not free of problems either. Only in the simplest problems can they be computed analytically.

Following Wolf [14], we define the Lyapunov exponents in a manner which is most suitable for computation. Let the dimension of phase space be n, the flow be $\phi_t(\mathbf{x})$ and consider a sphere of infinitesimal radius ϵ centered at $\mathbf{x}_0 \in \mathbb{R}^n$. Under the action of $\phi_t(\mathbf{x})$, this sphere of initial conditions will translate and deform into an ellipsoid. Let $p_i(t)$, $i = 1, 2, \ldots, n$ be the lengths of the principal axes of the

ellipsoid. Then, the ith Lyapunov exponent μ_i is defined as

$$\mu_i = \lim_{t\to\infty} \frac{1}{t} \log_2 \frac{p_i(t)}{p_i(0)} \tag{5.1}$$

where the μ_i are ordered so that $\mu_1 > \mu_2 > \cdots > \mu_n$. The linear extent of the ellipsoid grows as $2^{\mu_1 t}$ but its orientation varies through the attractor in a complicated manner.

If all the Lyapunov exponents are negative, trajectories converge to an equilibrium point. Thus, motion is around a stable equilibrium point and therefore "regular". If the largest Lyapunov exponent is zero while the rest are less than zero the attractor is a limit cycle. In the case where $\mu_1 > 0$, the corresponding axis expands exponentially. If all solutions of the system are bounded, this exponential growth implies that some "folding" action forces separated trajectories to merge. This repeated "stretching" and "folding" gives rise to chaotic motions within the attractor. Note that the volume of the ellipsoid increases as $2^{\Sigma\mu_i t}$. Since solutions are bounded, it follows that the sum of Lyapunov exponents must be negative.

Thus, to detect chaotic motion, it is sufficient to compute the first Lyapunov exponent μ_1. Numerical computation of the limit (5.1) can only provide an estimate. Wolf [15] provides an algorithm and the program FET1 which computes a lower bound for μ_1 from a finite number of points in the attracting set. Clearly μ_1 depends on the system parameters. Various computations gave estimates of μ_1 ranging from 0.1 to 0.3. To put these numbers in perspective, using the same algorithm, Wolf [15] obtained estimates of μ_1 for the Lorentz attractor of 2.16, and for the Roessler attractor 0.13.

The values obtained are in agreement with the results from the Poincaré map, confirming the fact that these motions of the impact damper are indeed chaotic. Estimates of the other exponents can also be obtained using Wolf's algorithm, but the level of uncertainty in these numbers inreases rapidly rendering them meaningless.

5.4 Transition to Chaos

The stability boundary determined in the previous chapter separates the parameter space $a - \eta$, $\eta = \frac{\omega}{\omega_0}$ into two regions. We have seen from test cases that in the region of instability, chaotic behavior is exhibited by the system, and the question that arises is whether stable harmonic solutions and chaotic motions are the only possible steady state responses of the impact damper.

To answer this, as well as determine how loss of stability happens, we investigate the transition across the stability boundary as the impact parameter a varies. Recall that in analyzing the stability of the periodic solution, the initial conditions $\dot{x}(0) = \dot{x}_0$, $v(0) = v_0 = \dot{x}_0$, $\theta(0) = \theta_0$, $x(0) = 0$ were perturbed by amounts $\Delta\dot{x}_0 = \Delta v_0$, $\Delta\theta_0$ and the evolution of these quantities was monitored after every impact. Thus, we obtained equation (4.5) as

$$\xi_{m+1} = Q\xi_m + R(\xi_m) \tag{5.2}$$

where ξ_m is the perturbation vector, and the stability of the trivial solution of this difference equation was investigated in the first approximation. Loss of stability occurs on the boundary and further analysis of stable solutions requires knowledge of $R(\xi_m)$. Even though $R(\xi_m)$ is not known explicitly, it can be computed numerically and the stable steady state solution of (5.2) can be found by repeated iteration of the map (5.2). Thus, approximate values of the steady state perturbations $\Delta\dot{x}_0$ and $\Delta\theta_0$ may be obtained for a variety of values of a.

It was found in chapter 4 that on the stability boundary, the eigenvalues of the map (5.2) are complex conjugates and have modulus one. Thus, the trivial solution of the map becomes an ustable focus and the resulting Hopf bifurcation gives rise to a smooth invariant circle. As the parameter a continues to vary away from the stability boundary, the invariant circle grows and distorts[2] eventually becoming a strange attractor.

This phenomenon is depicted in figures 5.10, 5.11 and 5.12. Rather than plotting

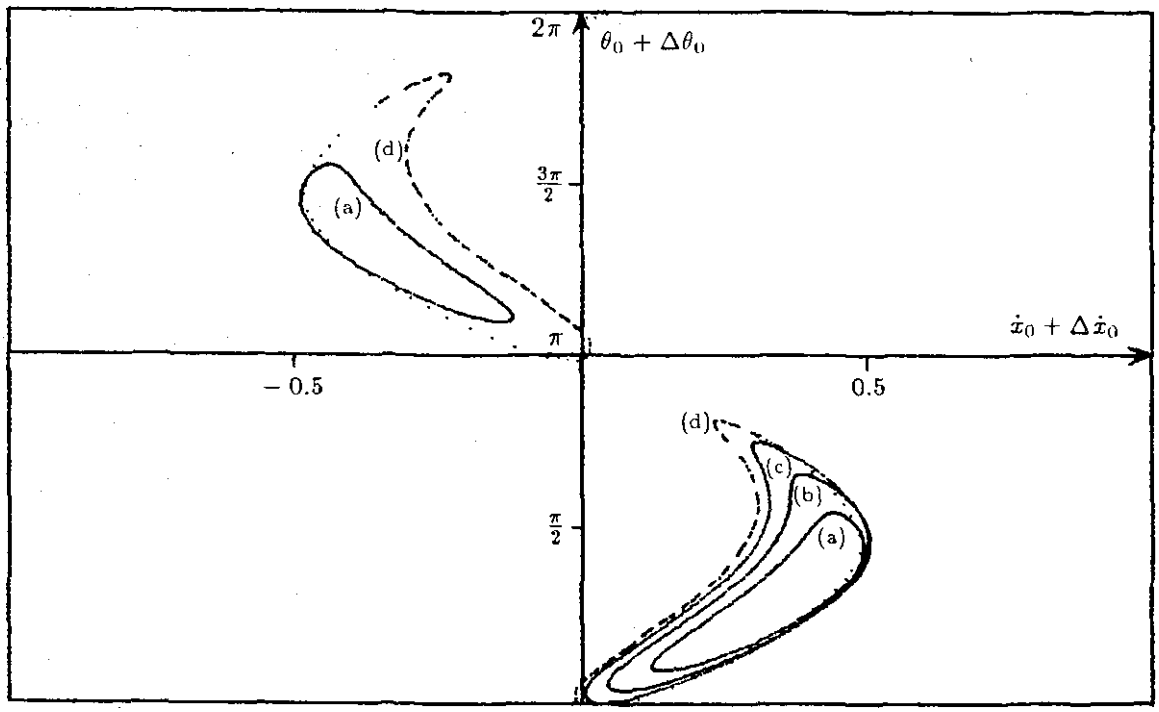

Figure 5.10: Invariant circles of map (5.2): (a) $a = 0.52$, (b) $a = 0.50$, (c) $a = 0.48$, (d) $a = 0.46$; $\eta = 5$.

the perturbations $\Delta\dot{x}_0$ and $\Delta\theta_0$, these graphs have been constructed by plotting $\dot{x} = \dot{x}_0 + \Delta\dot{x}_0$ and $\theta = \theta_0 + \Delta\theta_0$ which result every two impacts. In these plots there are two fixed points of (5.2), namely, $(\dot{x}_0, \theta_0)$ and $(-\dot{x}_0, \theta_0 + \pi)$.

The invariant circles are shown for $\frac{\omega}{\omega_0} = \eta = 5$ and $a = 0.52$, $a = 0.50$, $a = 0.48$. Note that on the stability boundary $a = a_s = 0.541114562$. For $a = 0.46$ the invariant circle does not exist any more. Rather, the solution wanders back and forth between the 2nd and 4th quadrants, and for $a = 0.3$ it has become a strange attractor. Figure 5.12 shows an enlargement of the portion of this attractor where its complicated structure is evident.

According to Aronson et. al. [2], the invariant circle is a circle in resonance, i.e., it contains saddle-node pairs. As the parameter of the problem varies, the stable and unstable manifolds of these pairs become entangled resulting in homoclinic tangency, and, as a result, "it is the approach to this homoclinic tangency which

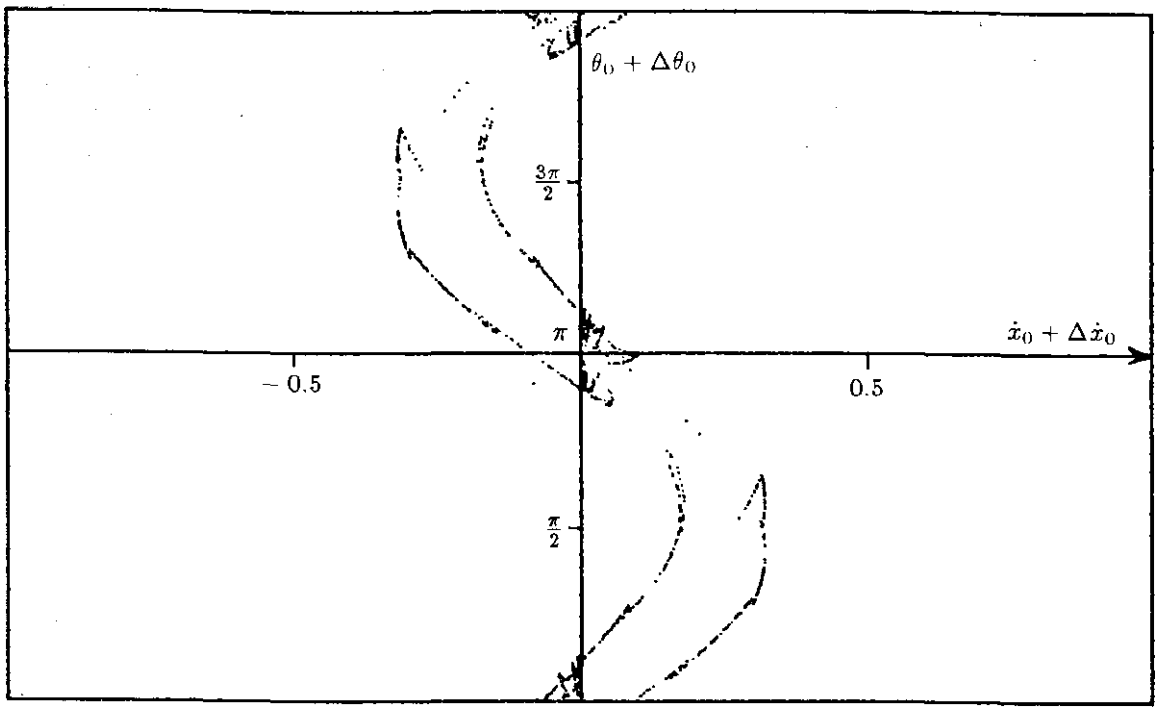

Figure 5.11: Breakdown of the invariant circle; $a = 0.3$, $\eta = 5$.

seems to govern the transformation of the smooth invariant circle into a strange attractor."[2]

The invariant circle in resonance present for some values of a represents quasiperiodic solutions of the impact damper while the strange attractor of the map (5.2) indicates that the system performs chaotic motions.

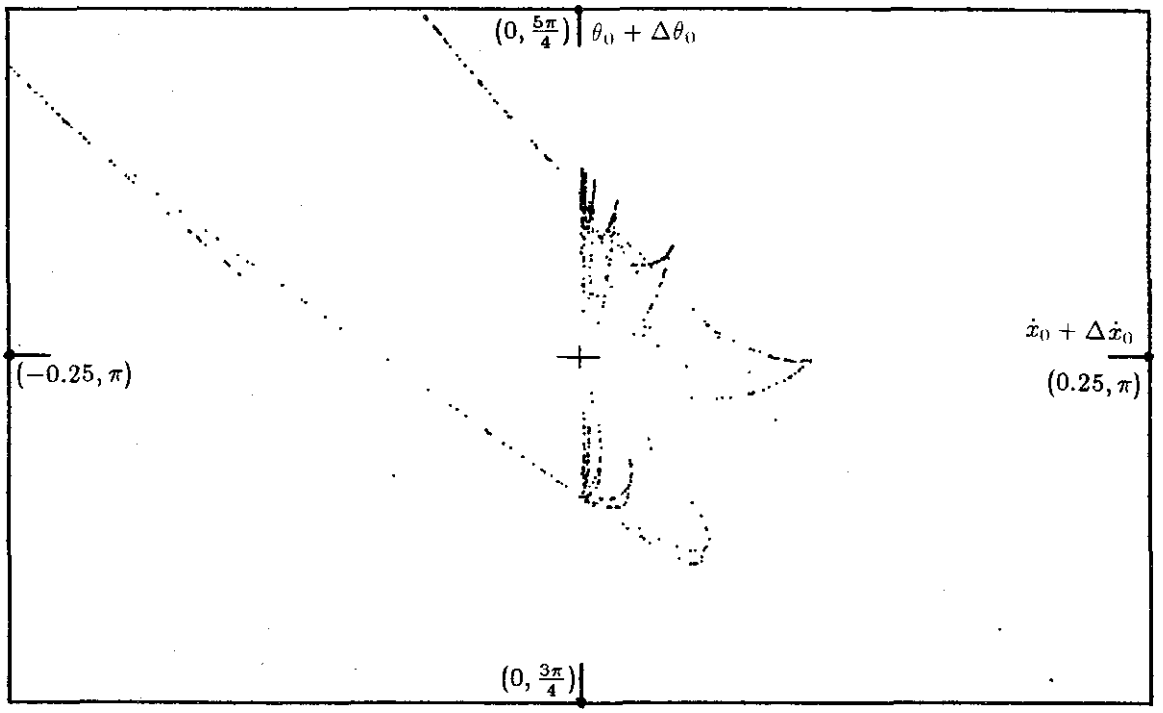

Figure 5.12: Enlargement of the region around $(0, \pi)$ of the attractor shown in fig. 5.11.

6

Overview and Concluding Remarks

The subject of this investigation is the dynamics of a semi-active impact damper consisting of an undamped forced torsional oscillator, a flywheel, and a clutch which engages at predetermined instants to lock the two instantaneously and for a very short time. Before clutch engagement, the two rotors move in opposite directions and, therefore, the locking action of the clutch is effectively that of an impact which slows down the primary system.

The most general result concerns the global behavior of the impact damper. It was shown that as long as the excitation torque is bounded, all solutions of the system are bounded, establishing thus that the system is an effective damping device limiting the amplitude of oscillations of the primary subsystem even at resonance.

Next, we characterized all 2 impacts/cycle periodic solutions by determining what the state of the system immediately after impact must be in order to perform periodic motion. It was found that while in most cases such solutions are symmetric about the origin when plotted in phase plane, there also exist nonsymmetric solutions if the frequency ratio is suitable. A small class of subharmonic solutions which involve no impacts was also found. Multiple-impact periodic solutions are either nonexistent or they are unstable.

The stability analysis was carried out by determining whether perturbations in the state of the system immediately after impact grow or decrease. The equations

of motion were effectively transformed into difference equations which describe the evolution of such perturbations after each impact. Using the linearized difference equations, the range of values of the impact parameter a and the frequency ratio η for which periodic solutions are stable was determined.

It was found that when periodic solutions are unstable, the system performs chaotic motions. This was verified by computing the largest Lyapunov exponent, and described using phase plane plots, the Poincaré map as well as the response spectrum of the system. Just outside the stability boundary, the fixed point of the map (5.2) associated with the impact damper undergoes Hopf bifurcation and the resulting invariant circle gives rise to a quasiperiodic solution. Further decrease of a results in breakdown of the structure of the invariant circle and the impact damper performs chaotic motions.

There are a number of points concerning the impact damper which require further research and study. First, the mechanism which governs the breakdown of the invariant circle must be investigated. If the invariant circle is a circle in resonance, the saddle-node pairs present represent multiple-impact subharmonic solutions of the impact damper. These solutions as well as the interaction of their stable and unstable manifolds must be determined.

The second point which needs further study concerns the practical applications of the system. As a quasi-static system, its damping effectiveness has been fully demonstrated by proving that all solutions are ultimately bounded. A more useful application however would be to damp perturbation oscillations of a flexible rotating shaft which carries a nominal torque T_0. In this case two questions of practical importance arise.

First is the question of sensing the equilibrium position $x = 0$ while the shaft is rotating in order to activate the clutch. Due to the difficulty in measuring position in a noninertial frame, another triggering mechanism must be used. Since measurements of velocity and acceleration are relatively easy, the activation mechanism

would have to be modified accordingly to utilize these signals.

The second question concerns the flexibility of the shaft, which, if included in the model, would lead to a multidegree of freedom primary system. In such a case, it is not obvious that all motions are well behaved and ultimate boundedness of solutions is not guaranteed. To test the behavior of a multidegree of freedom primary system, we consider the simplest possible, consisting of two lumped masses of equal moment of inertia I connected by torsional springs of equal stiffness k. Let the flywheel have moment of inertia J and suppose that the clutch is connected to the second mass and that it engages when this mass goes through its equlibrium position. Between impacts, the system is linear and the two equations of motion can be uncoupled. Let z_1, z_2 be the angular rotations of the two lumped masses measured from the equilibrium position and let x_1, x_2 be the generalized coordinates of the uncoupled system. While z_1 is continuous and only the second mass experiences direct impact, if x_1 and x_2 are used instead, the two equations are coupled at impact so that both x_1 and x_2 are discontinuous. For convenience we use x_1 and x_2 and have chosen the lowest system frequency $\omega_1 = 1$. With equal masses and springs this gives $\omega_2 \approx 2.618$. Let $a = I/(I+J)$, $b = J/(I+J)$ as before. Sample plots are shown in figures 6.1, 6.2 and 6.3.

The trajectories shown have been recorded after about 15 cycles of the excitation torque so that they are close to steady state. The response at resonance is shown in the first two figures. In these two cases the excitation torque is distributed evenly among the two masses, and $P_1 = P_2 = 0.1$, P_i being the torque amplitude acting on the ith mass. In the third figure, $P_1 = 0.1$, $P_2 = 0.2$ and $\omega = 2$. We observe that even though $a = 0.9$ (low damping) in all cases, the response of the system is bounded.

Clearly, the above are only indicative of what may be expected from a multidegree of freedom system and the three cases presented do not exhaust all the possibilities. More study is needed to derive results similar to those of chapter 2,

perhaps under some restrictions on the system configuration.

Finally, we note that an experimental investigation of the behavior of the system studied in this thesis would not only complement this work, but would also provide a basis for comparison of the theoretical results and help in assessing the practical feasibility of building such a device.

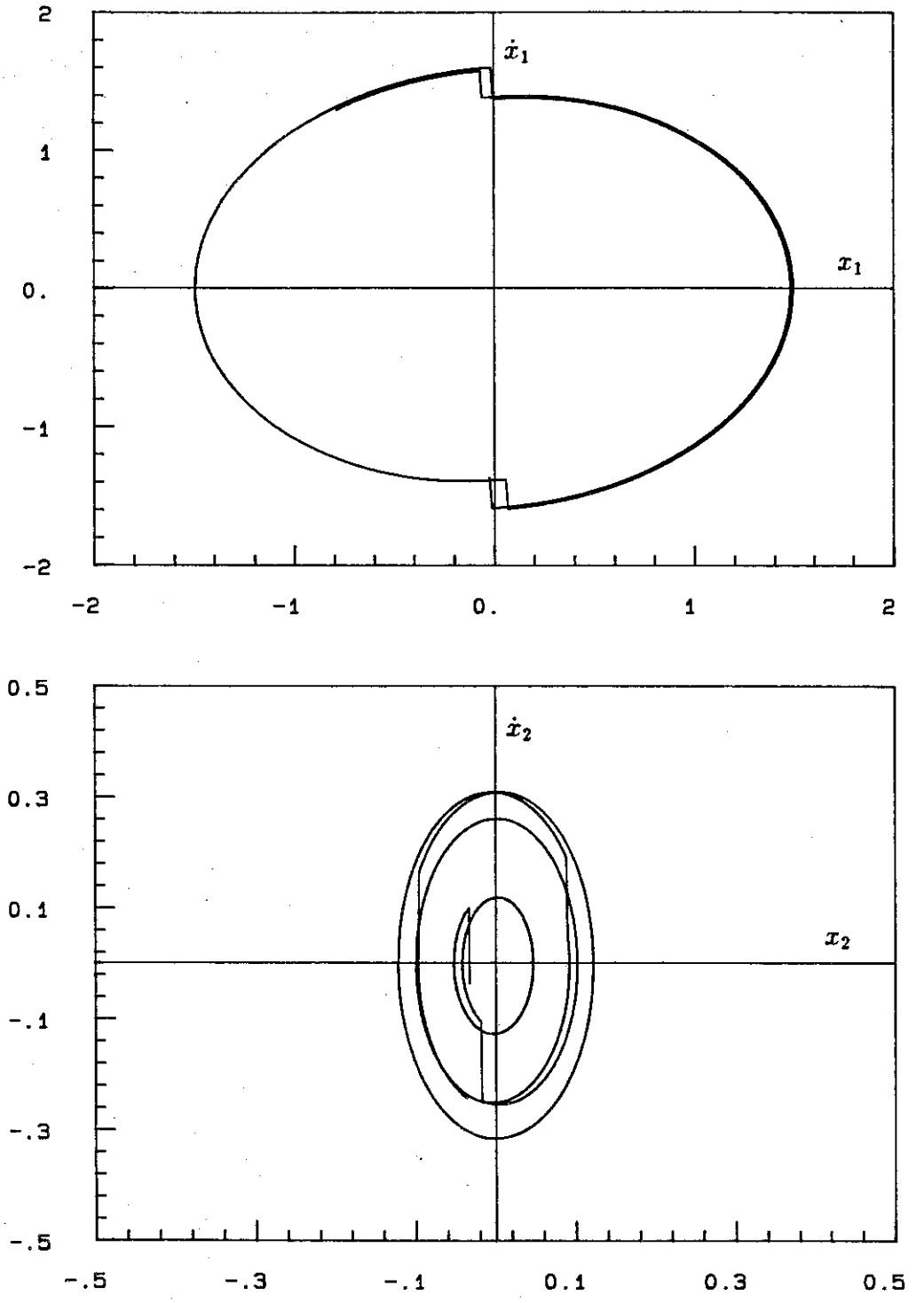

Figure 6.1: Steady state response at resonance, 2 d. o. f., $P_1 = P_2 = 0.1$, $a = 0.9$, $\omega = 1$.

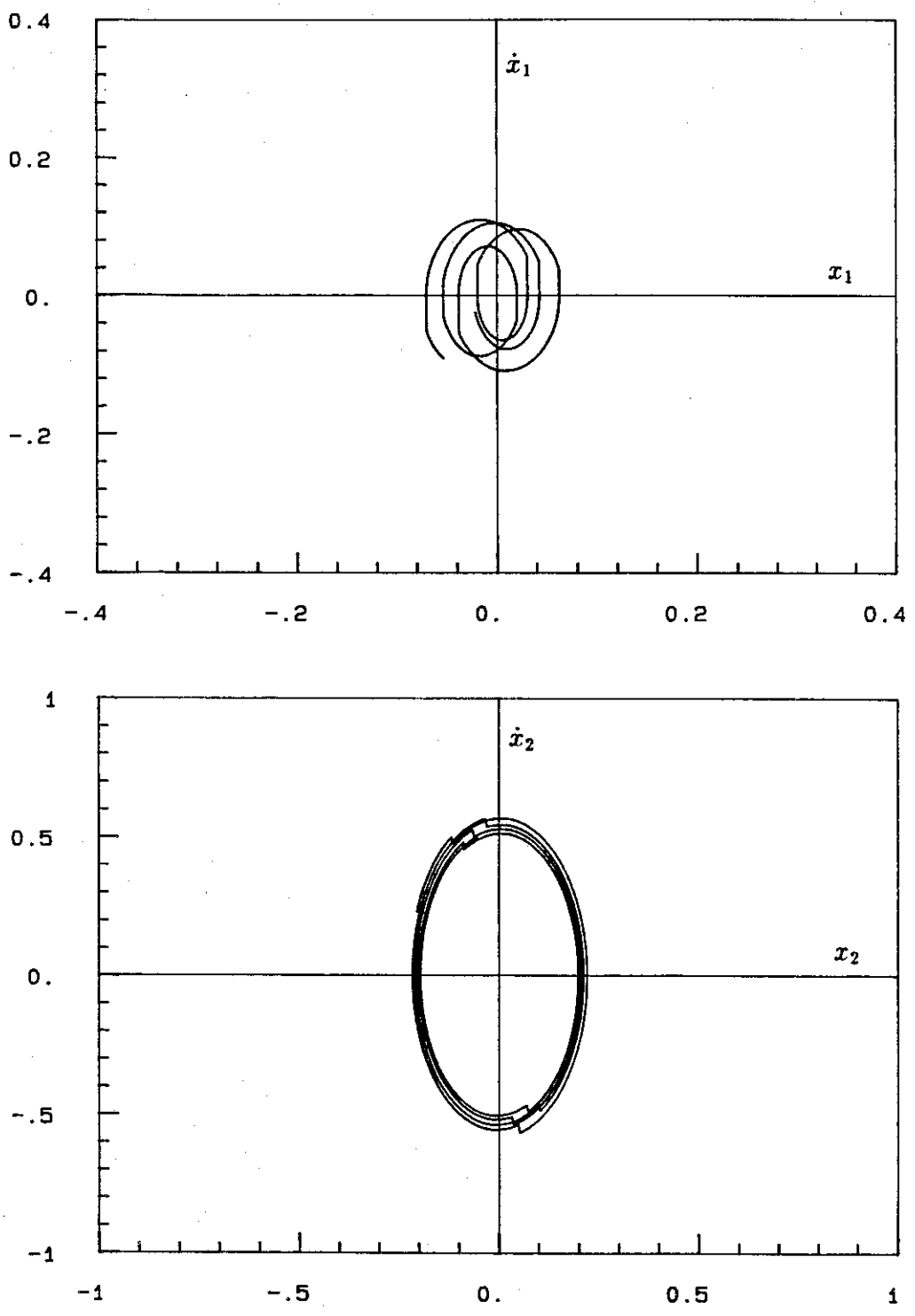

Figure 6.2: Steady state response at resonance, 2 d. o. f., $P_1 = P_2 = 0.1$, $a = 0.9$, $\omega = 2.618$.

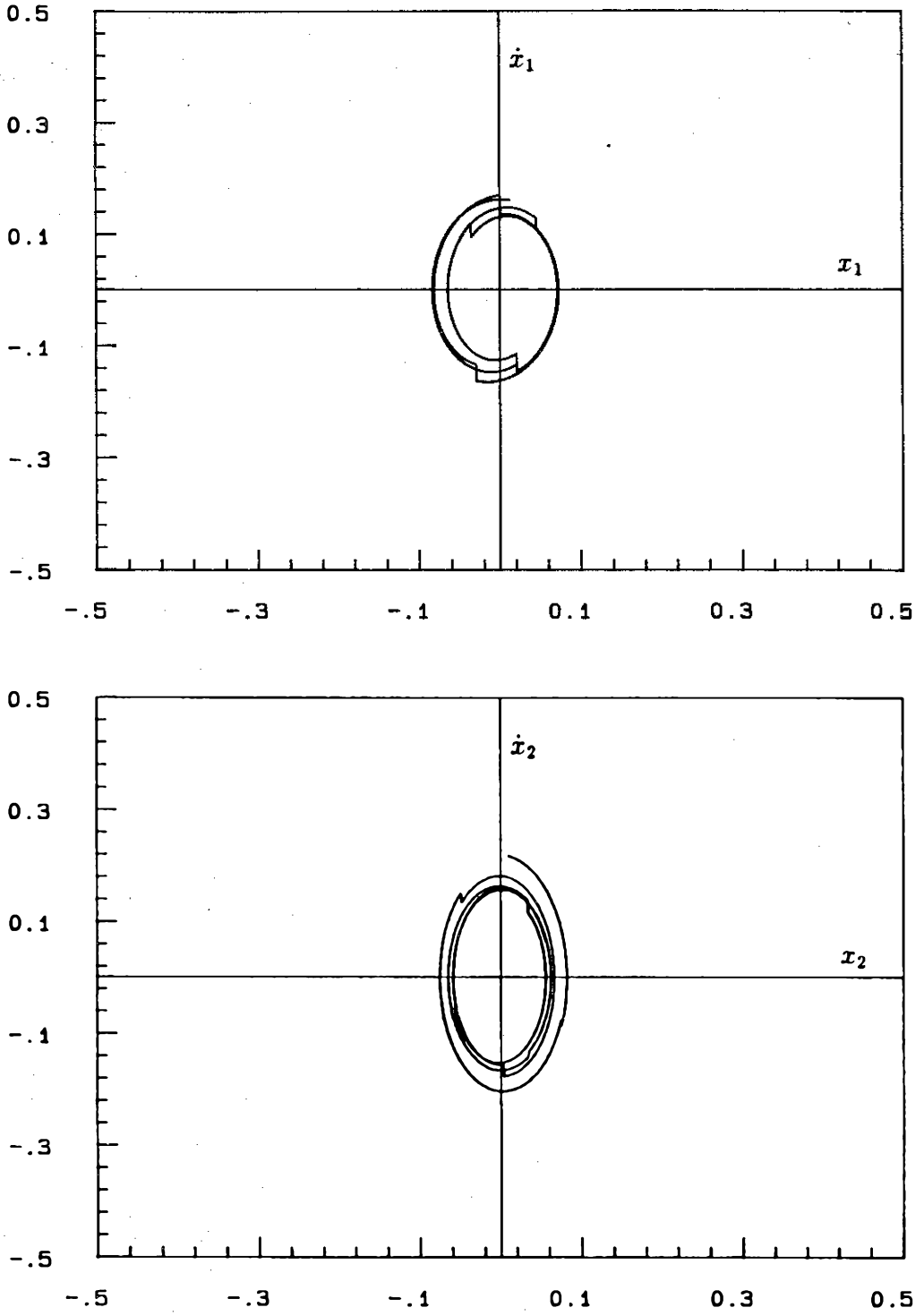

Figure 6.3: Steady state response, 2 d. o. f., $a = 0.9$, $P_1 = 0.1$, $P_2 = 0.2$, $\omega = 2$.

Appendix A

Solution of Equations (3.5) and (3.7).

CASE I: (Generic) $\cos(\frac{\omega_0}{\omega}\pi) \neq -1, \ \sin(\frac{\omega_0}{\omega}\pi) \neq 0.$

Equations (3.5) and (3.7) are identical to (3.8) and (3.9) as follows:

$$-\frac{\dot{x}_0}{\omega_0}\sin(\tfrac{\omega_0}{\omega}\pi) = \frac{P}{\omega^2-\omega_0^2}\left[1+\cos(\tfrac{\omega_0}{\omega}\pi)\right]\cos\theta_0 - \frac{P\left(\frac{\omega}{\omega_0}\right)}{\omega^2-\omega_0^2}\sin(\tfrac{\omega_0}{\omega}\pi)\sin\theta_0 \qquad (A.1)$$

$$\frac{\dot{x}_0}{\omega_0}\left[\frac{1+b}{a}+\cos(\tfrac{\omega_0}{\omega}\pi)\right] = \frac{P}{\omega^2-\omega_0^2}\sin(\tfrac{\omega_0}{\omega}\pi)\cos\theta_0 + \frac{P\left(\frac{\omega}{\omega_0}\right)}{\omega^2-\omega_0^2}\left[1+\cos(\tfrac{\omega_0}{\omega}\pi)\right]\sin\theta_0 \qquad (A.2)$$

Multiply (A.1) by $1+\cos(\frac{\omega_0}{\omega}\pi)$ and (A.2) by $\sin(\frac{\omega_0}{\omega}\pi)$:

$$-\frac{\dot{x}_0}{\omega_0}\sin(\tfrac{\omega_0}{\omega}\pi)\left[1+\cos(\tfrac{\omega_0}{\omega}\pi)\right] = \frac{P}{\omega^2-\omega_0^2}\left[1+\cos(\tfrac{\omega_0}{\omega}\pi)\right]^2\cos\theta_0 - \frac{P\left(\frac{\omega}{\omega_0}\right)}{\omega^2-\omega_0^2}\left[1+\cos(\tfrac{\omega_0}{\omega}\pi)\right]\sin(\tfrac{\omega_0}{\omega}\pi)\sin\theta_0$$

$$\frac{\dot{x}_0}{\omega_0}\left[\frac{1+b}{a}+\cos(\tfrac{\omega_0}{\omega}\pi)\right]\sin(\tfrac{\omega_0}{\omega}\pi) = \frac{P}{\omega^2-\omega_0^2}\sin^2(\tfrac{\omega_0}{\omega}\pi)\cos\theta_0 + \frac{P\left(\frac{\omega}{\omega_0}\right)}{\omega^2-\omega_0^2}\left[1+\cos(\tfrac{\omega_0}{\omega}\pi)\right]\sin(\tfrac{\omega_0}{\omega}\pi)\sin\theta_0$$

Adding and rearranging

$$\frac{\dot{x}_0}{\omega_0}\sin(\tfrac{\omega_0}{\omega}\pi)\left[\frac{1+b-a}{a}\right] = \frac{P}{\omega^2-\omega_0^2}\left[1+2\cos(\tfrac{\omega_0}{\omega}\pi)+\cos^2(\tfrac{\omega_0}{\omega}\pi)+\sin^2(\tfrac{\omega_0}{\omega}\pi)\right]\sin\theta_0 \tag{A.3}$$

Note that $1-a=b$. Substituting for a and solving for $\cos\theta_0$ we get

$$\cos\theta_0 = \frac{\frac{\dot{x}_0}{\omega_0}\left(\frac{b}{a}\right)\sin(\frac{\omega_0}{\omega}\pi)}{\frac{P}{\omega^2-\omega_0^2}\left[1+\cos(\frac{\omega_0}{\omega}\pi)\right]} \tag{A.4}$$

Multiply (A.1) by $-\sin(\frac{\omega_0}{\omega}\pi)$ and (A.2) by $1+\cos(\frac{\omega_0}{\omega}\pi)$ and add to get

$$\frac{\dot{x}_0}{\omega_0}\left[1+\cos(\tfrac{\omega_0}{\omega}\pi)\right]\left[1+\frac{1+b}{a}\right] = 2\frac{P\left(\frac{\omega}{\omega_0}\right)}{\omega^2-\omega_0^2}\left[1+\cos(\tfrac{\omega_0}{\omega}\pi)\right]\sin\theta_0 \tag{A.5}$$

Note that $1+\frac{1+b}{a}=\frac{2}{a}$. Substituting above and solving for $\sin\theta_0$ we get

$$\sin\theta_0 = \frac{\frac{\dot{x}_0}{\omega_0}\frac{1}{a}}{\frac{P\left(\frac{\omega}{\omega_0}\right)}{\omega^2-\omega_0^2}} \tag{A.6}$$

Then

$$\tan\theta_0 = \frac{1+\cos(\frac{\omega_0}{\omega}\pi)}{b\left(\frac{\omega}{\omega_0}\right)\sin(\frac{\omega_0}{\omega}\pi)} \tag{A.7}$$

Substituting for $\cos\theta_0$ and $\sin\theta_0$ in $\sin^2\theta_0+\cos^2\theta_0=1$ we find

$$\frac{\left(\frac{\dot{x}_0}{\omega_0}\right)^2\frac{1}{a^2}}{\left(\frac{P\left(\frac{\omega}{\omega_0}\right)}{\omega^2-\omega_0^2}\right)^2}\left[\frac{b^2\sin^2(\frac{\omega_0}{\omega}\pi)}{\left(\frac{\omega_0}{\omega}\right)^2\left[1+\cos(\frac{\omega_0}{\omega}\pi)\right]^2}+1\right] = 1 \tag{A.8}$$

which can be solved for $\dot{x}_0$ to give

$$\dot{x}_0 = \frac{Pa\omega}{|\omega^2-\omega_0^2|}\frac{1}{\sqrt{1+\frac{\left(\frac{\omega}{\omega_0}\right)^2 b^2\sin^2(\frac{\omega_0}{\omega}\pi)}{\left[1+\cos(\frac{\omega_0}{\omega}\pi)\right]^2}}} \tag{A.9}$$

CASE II: $\sin(\frac{\omega_0}{\omega}\pi) = 0, \quad \cos(\frac{\omega_0}{\omega}\pi) = 1 \iff \frac{\omega_0}{\omega} = 2l, \; l = 1, 2, \ldots$

In this case equations (A.1) and (A.2) reduce to

$$0 = 2\frac{P}{\omega^2 - \omega_0^2}\cos\theta_0 \tag{A.10}$$

$$\frac{\dot{x}_0}{\omega_0}\left[\frac{1+b}{a} + 1\right] = 2\frac{P\left(\frac{\omega}{\omega_0}\right)}{\omega^2 - \omega_0^2}\sin\theta_0 \tag{A.11}$$

From (A.10) we conclude that $\cos\theta_0 = 0 \Rightarrow \theta_0 = \pm\frac{\pi}{2}$. After simplification, (A.11) reduces to

$$\dot{x}_0 = \frac{Pa\omega}{\omega^2 - \omega_0^2}\sin\theta_0$$

Since in this case $\omega^2 - \omega_0^2 < 0$, it follows that for $\dot{x}_0 \geq 0$, $\sin\theta_0 = -1$. Hence

$$\theta_0 = -\frac{\pi}{2} \tag{A.12}$$

and

$$\dot{x}_0 = \frac{Pa\omega}{\omega_0^2 - \omega^2} \tag{A.13}$$

CASE III: $\sin(\frac{\omega_0}{\omega}\pi) = 0, \quad \cos(\frac{\omega_0}{\omega}\pi) = -1 \iff \frac{\omega_0}{\omega} = 2l + 1, \; l = 1, 2, \ldots$

Equation (A.1) is satisfied identically and (A.2) gives:

$$\frac{\dot{x}_0}{\omega_0}\left[\frac{1+b}{a} - 1\right] = 0 \Rightarrow \frac{\dot{x}_0}{\omega_0}\left[\frac{2b}{a}\right] = 0 \Rightarrow \dot{x}_0 = 0$$

However, θ_0 is still undetermined and therefore an additional constraint is required. To resolve this we note that for $0 < t < \frac{\pi}{\omega}$, $x(t) > 0$. The solution is given by

$$\begin{aligned} x(t) = {} & \frac{P}{\omega^2 - \omega_0^2}\cos\theta_0\cos\omega_0 t - \\ & - \frac{P\left(\frac{\omega}{\omega_0}\right)}{\omega^2 - \omega_0^2}\sin\theta_0\sin\omega_0 t - \\ & - \frac{P}{\omega^2 - \omega_0^2}\cos(\omega t + \theta_0) \end{aligned} \tag{A.14}$$

In view of $\omega^2 - \omega_0^2 < 0$ the condition for positive $x(t)$ reduces to the following expression:

$$\cos\theta_0 \cos\omega_0 t - \frac{\omega}{\omega_0}\sin\theta_0 \sin\omega_0 t - \cos(\omega t + \theta_0) < 0, \quad \forall t \in \left(0, \frac{\pi}{\omega}\right) \tag{A.15}$$

If $\theta_0 = -\frac{\pi}{2}$ then the condition above is satisfied. Thus the solution in this case is

$$\theta_0 = -\frac{\pi}{2} \tag{A.16}$$

$$\dot{x}_0 = 0 \tag{A.17}$$

CASE IV: (Resonance) $\omega = \omega_0$.

The solution in case of resonance is as follows:

$$x(t) = \left[\frac{\dot{x}_0}{\omega_0} - \frac{P}{2\omega_0^2}\sin\theta_0\right]\sin\omega_0 t + \frac{1}{2}P\frac{t}{\omega_0}\sin(\omega_0 t + \theta_0) \tag{A.18}$$

$$\dot{x}(t) = \omega_0\left[\frac{\dot{x}_0}{\omega_0} - \frac{P}{2\omega_0^2}\sin\theta_0\right]\cos\omega_0 t + \\ + \frac{1}{2}\frac{P}{\omega_0}\sin(\omega_0 t + \theta_0) + \frac{1}{2}Pt\cos(\omega_0 t + \theta_0) \tag{A.19}$$

Then, the condition for zero displacement at $t = \frac{\pi}{\omega_0}$ is

$$-\frac{P\pi}{2\omega_0^2}\sin\theta_0 = 0$$

Hence

$$\theta_0 = 0 \tag{A.20}$$

Using this value for the phase angle the expression for the velocity reduces to

$$\dot{x}(t) = \dot{x}_0\cos\omega_0 t + \frac{1}{2}\frac{P}{\omega_0}\sin\omega_0 t + \frac{1}{2}Pt\cos\omega_0 t$$

At $t = \frac{\pi}{\omega_0}^-$

$$\dot{x}\left(\frac{\pi}{\omega_0}^-\right) = \dot{x}_0\cos\pi + \frac{1}{2}P\frac{\pi}{\omega_0}\cos\pi \\ = -\dot{x}_0 - \frac{1}{2}\frac{P\pi}{\omega_0} \tag{A.21}$$

The impact condition and the requirement of symmetry result in

$$-\dot{x}_0 = a\left(-\dot{x}_0 - \frac{1}{2}\frac{P\pi}{\omega_0}\right) + b\dot{x}_0 \tag{A.22}$$

This gives the final expression for the initial velocity as

$$\dot{x}_0 = \left(\frac{a}{b}\right)\frac{P\pi}{4\omega_0} \tag{A.23}$$

Appendix B

Proof of Theorem 4.1

The proof of this theorem is found in [8] and repeated here for completeness.

Rewrite (4.9) as

$$\xi_m = Q^m \xi_0 + \sum_{i=1}^{m-1} Q^{m-1-i} R(\xi_i), \quad m \geq 1 \tag{B.1}$$

Since

$$\xi_{m+1} = Q^{m+1} \xi_0 \tag{B.2}$$

is asymptotically stable, it follows that

$$\|Q^m\| \leq Ce^{-\alpha m}$$

for some $C > 1$ and $\alpha > 0$. Hence

$$\|\xi_m\| \leq Ce^{-\alpha m}\|\xi_0\| + \sum_{i=0}^{m-1} Ce^{-\alpha(m-1-i)}\|R(\xi_i)\|$$

Making use of the assumptions of the theorem, $\exists \delta > 0$ such that, if $\|\xi\| < \delta$, then

$$\|R(\xi)\| \leq \frac{\alpha}{2C}\|\xi\|e^{-\alpha}$$

Therefore

$$e^{\alpha m}\|\xi_m\| \leq C\|\xi_0\| + \frac{\alpha}{2}\sum_{i=0}^{m-1} e^{\alpha i}\|\xi_i\| \tag{B.3}$$

Let $S_i = e^{\alpha i}\|\xi_i\|$ and $\delta = C\|\xi_0\|$. Then, from (B.3)

$$S_m \leq \delta + \frac{\alpha}{2}\sum_{i=0}^{m-1} S_i$$

$$\begin{aligned} \Longrightarrow S_i &\leq \delta + \frac{\alpha}{2} S_0 \\ &\leq \delta \left(1 + \frac{\alpha}{2}\right) \\ &\leq \delta e^{\frac{\alpha}{2}} \end{aligned}$$

and

$$\begin{aligned} S_2 &\leq \delta + \frac{\alpha}{2}(S_0 + S_1) \\ &\leq \delta \left[1 + 2\left(\frac{\alpha}{2}\right) + \left(\frac{\alpha}{2}\right)^2\right] \\ &\leq \delta e^{2\frac{\alpha}{2}} \end{aligned}$$

Similarly

$$S_m \leq \delta e^{m\frac{\alpha}{2}}$$

Hence

$$\begin{aligned} e^{\alpha m}\|\xi_m\| &\leq \delta e^{m\frac{\alpha}{2}} \\ \Longrightarrow \|\xi_m\| &\leq \delta e^{-\frac{\alpha m}{2}} \end{aligned}$$

from which we conclude that

$$\lim_{m\to\infty} \|\xi_m\| = 0. \qquad \blacksquare$$

Appendix C

Derivation of Matrix Q and Computation of Its Eigenvalues

C.1 Generic Case

For $\cos(\frac{\omega_0}{\omega}\pi) \neq \pm 1$ and $\sin(\frac{\omega_0}{\omega}\pi) \neq 0$ the coefficients c_i and d_i, $i = 1, 2, 3$ are:

$$c_1 = a\left[A_0\left(\frac{\omega_0}{\omega}\right)\cos(\tfrac{\omega_0}{\omega}\pi) + B_0\left(\frac{\omega_0}{\omega}\right)\sin(\tfrac{\omega_0}{\omega}\pi) + \frac{P\left(\frac{\omega}{\omega_0}\right)}{\omega^2 - \omega_0^2}\cos\theta_0\right] \quad \text{(C.1)}$$

$$c_2 = -\frac{Pa}{\omega^2 - \omega_0^2}\left[\sin(\tfrac{\omega_0}{\omega}\pi)\sin\theta_0 - \left(\frac{\omega}{\omega_0}\right)\cos(\tfrac{\omega_0}{\omega}\pi)\cos\theta_0 - \left(\frac{\omega}{\omega_0}\right)\cos\theta_0\right] \quad \text{(C.2)}$$

$$c_3 = -\left[a\cos(\tfrac{\omega_0}{\omega}\pi) + b\right] \quad \text{(C.3)}$$

$$d_1 = \frac{\omega_0}{\omega}\left[-A_0\sin(\tfrac{\omega_0}{\omega}\pi) + B_0\cos(\tfrac{\omega_0}{\omega}\pi) - \frac{P\left(\frac{\omega}{\omega_0}\right)}{\omega^2 - \omega_0^2}\sin\theta_0\right] \quad \text{(C.4)}$$

$$d_2 = -\frac{P}{\omega^2 - \omega_0^2}\left[\cos(\tfrac{\omega_0}{\omega}\pi)\sin\theta_0 + \left(\frac{\omega}{\omega_0}\right)\sin(\tfrac{\omega_0}{\omega}\pi)\cos\theta_0 + \sin\theta_0\right] \quad \text{(C.5)}$$

$$d_3 = \sin(\tfrac{\omega_0}{\omega}\pi) \quad \text{(C.6)}$$

Using the known solution for $\dot{x}_0$ from chapter 3 in (4.15), we obtain B_0 in terms of the phase angle θ_0 as follows:

$$B_0 = (a-1)\frac{P\left(\frac{\omega}{\omega_0}\right)}{\omega^2 - \omega_0^2}\sin\theta_0 \quad \text{(C.7)}$$

Thus B_0 and A_0 can be eliminated from the expressions for the coefficients c_i and d_i using (4.14) and (C.7). After simplification the results are

$$c_1 = Ga(1-a)\sin(\tfrac{\omega_0}{\omega}\pi)\left[\left(\frac{\omega}{\omega_0}\right)^2 - 1\right] \tag{C.8}$$

$$c_2 = Ga\sin(\tfrac{\omega_0}{\omega}\pi)\left[(1-a)\left(\frac{\omega}{\omega_0}\right)^2 - 1\right]\left[1+\cos(\tfrac{\omega_0}{\omega}\pi)\right] \tag{C.9}$$

$$c_3 = -\left[a\cos(\tfrac{\omega_0}{\omega}\pi) + b\right] \tag{C.10}$$

$$d_1 = G(a-2)\left[1+\cos(\tfrac{\omega_0}{\omega}\pi)\right] \tag{C.11}$$

$$d_2 = -G\left[\left[1+\cos(\tfrac{\omega_0}{\omega}\pi)\right]^2 + (1-a)\left(\frac{\omega}{\omega_0}\right)^2 \sin^2(\tfrac{\omega_0}{\omega}\pi)\right] \tag{C.12}$$

$$d_3 = \sin(\tfrac{\omega_0}{\omega}\pi) \tag{C.13}$$

$$\tag{C.14}$$

where

$$G = \frac{P}{\omega^2 - \omega_0^2}\frac{\sin(\frac{\omega_0}{\omega}\pi)}{1+\cos(\frac{\omega_0}{\omega}\pi)} \tag{C.15}$$

The transition matrix Q is

$$Q = \begin{bmatrix} 1 - \frac{d_2}{d_1} & -\frac{d_3}{d_1} \\ c_2 - c_1\frac{d_2}{d_1} & c_3 - c_1\frac{d_3}{d_1} \end{bmatrix} \tag{C.16}$$

and its characteristic polynomial is

$$\lambda^2 - \alpha_1\lambda + \alpha_0 \tag{C.17}$$

with

$$\begin{aligned} \alpha_1 &= 1 - \frac{d_2}{d_1} + c_3 - c_1\frac{d_3}{d_1} \\ &= \frac{1}{d_1}(d_1 - d_2 + c_3 d_1 - c_1 d_3) \end{aligned} \tag{C.18}$$

$$\begin{aligned} \alpha_0 &= (1 - \frac{d_2}{d_1})(c_3 - c_1\frac{d_3}{d_1}) + \frac{d_3}{d_1}(c_2 - c_1\frac{d_2}{d_1}) \\ &= \frac{1}{d_1}\left[c_3(d_1 - d_2) + d_3(c_2 - c_1)\right] \end{aligned} \tag{C.19}$$

Substituting for c_i and d_i from above and rearranging, we get equations (4.30) and (4.31).

C.2 Resonance

The solution is given by (3.10) and (3.11). At $\omega_0 t = (\pi + \Delta t_0')^+$, $x = 0$. Hence

$$0 = -\frac{\dot{x}_0 + \Delta\dot{x}_0}{\omega_0}\sin(\Delta T) - \frac{P}{\omega_0}\left(\frac{\Delta T + \pi}{\omega_0}\right)\sin(\theta_0 + \Delta\theta_0 + \Delta T) + \\ + \frac{P}{2\omega_0^2}\sin(\theta_0 + \Delta\theta_0)\sin(\Delta T) \tag{C.20}$$

To first order

$$\left(\frac{\dot{x}_0}{\omega_0} + \frac{P\pi}{2\omega_0^2}\right)\Delta T + \frac{P\pi}{2\omega_0^2}\Delta\theta_0 = 0 \tag{C.21}$$

Eliminating ΔT and using (3.21) we obtain (4.38).

The velocity prior to impact is

$$\dot{x}\left(\frac{\pi + \Delta t_0'}{\omega_0}\right) = (\dot{x}_0 + \Delta\dot{x}_0)\cos(\pi + \Delta t_0' - \Delta t_0) + \\ + \frac{1}{2}\frac{P}{\omega_0}\sin(\pi + \Delta t_0' - \Delta t_0 + \theta_0 + \Delta\theta_0) + \\ + \frac{1}{2}P\left(\frac{\pi + \Delta t_0' - \Delta t_0}{\omega_0}\right)\cos(\pi + \Delta t_0' - \Delta t_0 + \theta_0 + \Delta\theta_0) - \\ - \frac{P}{2\omega_0}\sin(\theta_0 + \Delta\theta_0)\cos(\pi + \Delta t_0' - \Delta t_0) \tag{C.22}$$

$$\approx -\left(\dot{x}_0 + \frac{P\pi}{2\omega_0}\right) - \Delta\dot{x}_0 + \frac{P}{\omega_0}\Delta T \tag{C.23}$$

Thus, at $\omega_0 t = (\pi + \Delta t_0')^+$

$$-\dot{x}_0 - \Delta\dot{x}_0' = a\left[-\left(\dot{x}_0 + \frac{P\pi}{2\omega_0}\right) - \Delta\dot{x}_0 + \frac{P}{\omega_0}\Delta T\right] + b(\dot{x}_0 + \Delta\dot{x}_0) \tag{C.24}$$

Using (A.22), (3.21) and (C.21) we get

$$\Delta\dot{x}_0' = (a - b)\Delta\dot{x}_0 + \frac{2Pab}{(1 + b)\omega_0}\Delta\theta_0 \tag{C.25}$$

Thus, Q is triangular and, therefore, the second eigenvalue is $\lambda_2 = (a - b)$.

Bibliography

[1] Andronov, A.A., Vitt, A.A. and Khaikin, S.E., *Theory of Oscillators,* Addison-Wesley, New York, 1966.

[2] Aronson, D.G., Chory, M.A., Hall, G.R. and McGehee, R.P., "Bifurcations from an Invariant Circle for Two-Parameter Families of Maps of the Plane: A Computer-Assisted Study," *Communications in Mathematical Physics,* Vol. 83, pp. 303–354, 1982.

[3] Dowell, E.H., "Observation and Evolution of Chaos for an Autonomous System," *Journal of Applied Mechanics,* Vol. 51, pp. 664–673, September 1984.

[4] Frederickson, P., Kaplan, J.L., Yorke, E.D. and Yorke, J.A., "The Lyapunov Dimension of Strange Attractors," *Journal of Differential Equations,* Vol. 49, pp. 185–207, 1983.

[5] Guckenheimer, J. and Holmes, P., *Nonlinear Oscillations, Dynamical Systems and Bifurcations of Vector Fields,* Springer-Verlag, New York, 1983.

[6] Hall, J.F., "An FFT Algorithm for Structural Dynamics," *Earthquake Engineering and Structural Dynamics,* Vol. 10, pp. 797–811, 1982.

[7] Holden, A.V. (ed.), *Chaos,* Princeton University Press, Princeton, New Jersey, 1986.

[8] Masri, S.F. and Caughey, T.K., "On the Stability of the Impact Damper," *Journal of Applied Mechanics,* pp. 586–592, September 1966.

[9] Masri, S.F., "Analytical and Experimental Studies of Impact Dampers," *Ph.D. Thesis,* California Institute of Technology, Pasadena, Calif., 1965.

[10] Moon, F.C., "Experiments on Chaotic Motions of a Forced Nonlinear Oscillator : Strange Attractors," *Journal of Applied Mechanics,* Vol. 47, pp. 638–644, September 1980.

[11] Shaw, S.W., "The Dynamics of a Harmonically Excited System Having Rigid Amplitude Constraints, Part 1: Subharmonic Motions and Local Bifurcations," *Journal of Applied Mechanics,* Vol. 52, pp. 453–458, June 1985.

[12] Shaw, S.W., "The Dynamics of a Harmonically Excited System Having Rigid Amplitude Constraints, Part 2: Chaotic Motions and Global Bifurcations," *Journal of Applied Mechanics,* Vol. 52, pp. 459–464, June 1985.

[13] Shaw, S.W. and Holmes, P.J., "A Periodically Forced Impact Oscillator with Large Dissipation," *Journal of Applied Mechanics,* Vol. 50, pp. 849–857, December 1983.

[14] Wolf, A., "Intermediate Length Scale Effects in Lyapunov Exponent Estimation," in Mayer-Kross, G. (ed.), *Proceedings of Los Alamos Conference on Dimensions and Entropies in Chaotic Systems,* Springer-Verlag, 1986.

[15] Wolf, A., Swift, J.B., Swinney, H.L. and Vastano, J.A., "Determining Lyapunov Exponents from a Time Series," *Physica,* Vol. 16D, pp. 285–317, 1985.